NTNU

Norwegian University of
Science and Technology

Depolymerisation and Characterisation of Xanthans

A study of rheological and structural
properties for Enhanced Oil Recovery

Christian Holmvik

Nanotechnology
Submission date: June 2018
Supervisor: Bjørn E. Christensen, IBT
Co-supervisor: Marianne Ø. Dalheim, IBT

Norwegian University of Science and Technology
Department of Biotechnology and Food Science

Abstract

Xanthan is a polysaccharide which is commonly used as a thickening agent in e.g. sauces and toothpastes due to its viscosifying properties. The same attributes make it applicable for Enhanced Oil Recovery (EOR). With today's increased focus on making a more environmentally friendly oil industry, xanthan has received renewed interest due to being non-hazardous and to some degree biodegradable. It has furthermore been shown that certain chemical substitutions can make it possible to improve xanthan's rheological properties and control its degradability. First, however, it is necessary to thoroughly characterise non-modified xanthans to create a basis for evaluating the effects of such modifications.

In this master's thesis, non-modified xanthans have been studied using various analytical methods. All samples originate from two separate industrial products. The first, called MX, has been purified directly from a fermentation broth produced by IRIS AS. The second xanthan was manufactured by CP Kelco under the name Kelzan XCD, and will hereafter be referred to as XCD. The master's project is a continuation of the work carried out during the preceding specialisation project of 2017, where the following main results were found: By thermogravimetric analysis (TGA), the moisture content of MX was shown to be $(10.43 \pm 0.05)\%$. A *Star Burst Mini* microfluidiser was further used to degrade MX and XCD by high pressure mechanical shear, yielding xanthan samples with different molecular weight distributions. Flow-through-times of all samples were measured by capillary viscometry in order to determine their intrinsic viscosities at a shear rate of $2500\,\mathrm{s}^{-1}$. For both MX and XCD, the results indicated that continued mechanical shear degradation would approach a lower limit for intrinsic viscosity of approx. $200\,\mathrm{mL/g}$ provided the conditions remained the same. Size exclusion chromatography combined with multi-angle laser light scattering (SEC-MALLS) indicated a corresponding limit for the weight average molecular weight of mechanically degraded MX to be about 400-500 kDa, while the results for XCD were too inaccurate for making such a prediction.

In the master's project, a *Kinexus ultra+* rotational rheometer was used to study the dependence of dynamic viscosity on shear rate for undegraded MX and XCD in alkaline solutions of various concentrations. Samples containing MX were found to have slightly higher viscosities than XCD under the same conditions. Structural analyses of the xanthans with proton nuclear magnetic resonance spectroscopy (^{1}H-NMR) were carried out for comparing samples that had been degraded either chemically with H_2O_2/NaOH or enzymatically using the cellulases BGI-30 and *Ecostone Goo*. Optimisation of the depolymerisation protocols was done by analyses using the bicinchoninic acid (BCA) reducing end assay and spectrophotometry. It was shown that degradation with H_2O_2/NaOH causes a high degree of deacetylation, while the amount of free acetate in samples depolymerised by cellulases were negligible. Ideal ^{1}H-NMR spectra were not obtained for any of the degraded MX samples, although the results indicated that MX is close to fully acetylated and pyruvated as the respective degree of substitutions were calculated to be $\mathrm{DS}_{\mathrm{Ac,\,MX}} = 1.48$ and $\mathrm{DS}_{\mathrm{Pyr,\,MX}} = 1.28$. On the other hand, XCD samples appeared to be sufficiently depolymerised for obtaining good spectra, resulting in $\mathrm{DS}_{\mathrm{Ac,\,XCD}} = 0.97$ and $\mathrm{DS}_{\mathrm{Pyr,\,XCD}} = 0.61$. This indicates that XCD has a significantly lower pyruvyl content compared to MX, which might have consequences for potential chemical modifications.

Sammendrag

Xantan er et polysakkarid som på grunn av sine viskositetsfremmende egenskaper ofte blir brukt som fortykningsmiddel i f.eks. sauser og tannkrem. De samme egenskapene utgjør basis for anvendelse av xantan for økt oljeutvinning (EOR). Med dagens økte fokus på en mer miljøvennlig oljeindustri, har xantan fått fornyet interesse siden det anses for å ikke være miljøskadelig og fordi det til en viss grad er biologisk nedbrytbart. Det har videre blitt vist at kjemisk substitusjon kan gjøre det mulig å forbedre xantanets reologiske egenskaper og kontrollere dets nedbrytbarhet. Det er derfor nødvendig å karakterisere ikke-modifiserte xantaner for å danne et sammenligningsgrunnlag før man kan evaluere effektene av slike modifikasjoner.

I denne masteroppgaven har ikke-modifiserte xantaner blitt studert ved hjelp av ulike analytiske metoder. Alle prøvene stammer fra to separate industriprodukter. Det første, kalt MX, har blitt renset direkte fra en fermenteringsvæske produsert av IRIS AS. Det andre xantanet ble produsert av CP Kelco under navnet Kelzan XCD, og vil heretter bli referert til som XCD. Masteroppgaven er en videreføring av et fordypningsprosjekt gjennomført høsten 2017, hvor følgende resultater ble funnet: Ved termogravimetrisk analyse (TGA) ble vanninnholdet i MX vist å være $(10,43 \pm 0,05)\%$. Et instrument ved navn *Star Burst Mini* ble videre brukt til å bryte ned MX og XCD ved høytrykksmekanisk skjær, noe som resulterte i xantanprøver med ulike molekylvektfordelinger. Gjennomstrømmingstider for alle prøvene ble målt ved kapillærviskometri for å bestemme egenviskositet ved en skjærhastighet på $2500\,\mathrm{s}^{-1}$. For både MX og XCD indikerte resultatene at egenviskositeten ved videre mekanisk nedbrytning ville flate ut ved omtrent 200 mL/g, forutsatt at betingelsene var de samme. Separasjon basert på gelfiltrering kombinert med deteksjon av flervinklet laserlysspredning (SEC-MALLS) indikerte en tilsvarende grense på 400-500 kDa for vektgjenomsnittlig molekylvekt av mekanisk nedbrutt MX, mens resultatene for XCD var for unøyaktige til å gjøre en tilsvarende prediksjon.

I løpet av masteroppgaven ble et roterende reometer av typen *Kinexus ultra+* brukt til å studere sammenhengen mellom dynamisk viskositet og skjærhastighet for ikke-nedbrutte prøver av MX og XCD i basisk løsning ved ulike konsentrasjoner. Prøver som inneholdt MX ble funnet til å ha vesentlig høyere viskositeter enn XCD under samme betingelser. Analyser av xantanene med kjernemagnetisk resonansspektroskopi (^{1}H-NMR) ble gjennomført for å sammenligne prøver som enten var brutt ned kjemisk med H_2O_2/NaOH eller enzymatisk ved bruk av cellulasene BGI-30 og *Ecostone Goo*. Optimering av nedbrytningsprotokollene ble utført ved å analysere konsentrasjonen av reduserende ender ved bruk av bicinchoninsyre (BCA) og spektrofotometri. Det ble vist at nedbrytning med H_2O_2/NaOH forårsaker en høy grad av deacetylering, mens mengden av fri acetat i prøver brutt ned av cellulaser var ubetydelig. Ingen av de nedbrutte MX-prøvene gav ideelle NMR-spektre. Likevel indikerte resultatene at MX er nær fullstendig substituert av pyruvat og acetat da de respektive substitusjonsgradene ble beregnet til å være $\mathrm{DS}_{\mathrm{Ac,\,MX}} = 1.48$ og $\mathrm{DS}_{\mathrm{Pyr,\,MX}} = 1.28$. XCD-prøvene viste seg derimot å være tilstrekkelig brutt ned for å fremskaffe gode spektre, noe som gav resultatene $\mathrm{DS}_{\mathrm{Ac,\,XCD}} = 0.97$ og $\mathrm{DS}_{\mathrm{Pyr,\,XCD}} = 0.61$. Dette indikerer at XCD har et betydelig lavere innhold av pyruvyl sammenlignet med MX, noe som kan ha konsekvenser for eventuelle kjemiske modifikasjoner.

Preface

This master's thesis is the combined product of a specialisation project and a master's project executed during the academic year of 2017-18. It will be clearly stated which experimental methods and results that have been adapted from the project thesis of 2017, and which content that is new as of the final master's project. The work has been carried out at the Department of Biotechnology and Food Science (IBT) of the Norwegian University of Science and Technology (NTNU) in Trondheim, Norway.

First of all, I would like to thank my main supervisor Professor Bjørn E. Christensen for granting me the opportunity to work with such an interesting topic; and for all his counsel regarding experimental issues, data analyses and other enlightening aspects during our discussions.

I am especially grateful to my co-supervisor Marianne Ø. Dalheim, PhD, who developed the protocol for purification of xanthan from the fermentation broth in addition to giving many detailed comments on earlier drafts of this thesis. I hope the results of my work will be of good use and wish her all luck with the further research on xanthan.

Senior Engineer Ann-Sissel T. Ulset has my deepest gratitude for performing SEC-MALLS analyses, and for taking on the role as my tutor during the experimental work in the laboratory. She taught me the practicalities I needed to know about most of the instruments and techniques that were used. I would further like to thank PhD Candidate Amalie Solberg for her assistance with the ^{1}H-NMR experiments, Staff Engineer Karin W. Dragsten from the Department of Chemical Engineering (IKP) for running the thermogravimetric analyses; and everyone working at the biopolymer laboratories for their helpful advice, demonstrations of instruments and for making me feel welcome.

Lastly, I want to thank my family for always supporting me when I need it the most; in particular my mother for her constant care and help in reviewing language and grammar of several unrefined sections.

This has been a demanding journey which has lasted nearly ten months; often involving long working days and late nights. It is with ambivalent feelings that I now conclude my five years of attending the Master Programme in Nanotechnology at NTNU.

Christian Holmvik

Trondheim, 25 June 2018

Dedicated to my grandfather, Andrzej J. Nowakowski,
for inspiring me to keep pursuing my academic goals.

Contents

List of Tables

List of Figures

Nomenclature

Acronyms and Initialisms

BCA	Bicinchoninic acid
DMSO	Dimethyl sulfoxide
DP	Degree of polymerisation
DS	Degree of substitution
EDTA	Ethylenediaminetetraacetic acid
EOR	Enhanced oil recovery
FDA	U.S. Food and Drug Administration
HPAM	Hydrolysed polyacrylamide
IPA	Isopropyl alcohol
LS	Light scattering
MALLS	Multi-angle laser light scattering
MHS	Mark-Houwink-Sakurada
NMR	Nuclear magnetic resonance
OD	Optical density (absorption)
ORD	Optical rotatory dispersion
RE	Reducing end of a saccharide
RF	Radio frequency
RMS	Root mean square
RU	Repeating unit of a polymer
SD	The corrected sample standard deviation
SE	Standard error
SEC	Size-exclusion chromatography
TGA	Thermogravimetric analysis
TMS	Tetramethylsilane

Symbols

α	Degree of chain scission	1
β	Coefficient in the Fuoss-Mead equation	1
$\boldsymbol{\mu}$	Magnetic moment	J/T
δ	Chemical shift	ppm
$\dot{\gamma}$	Shear rate	s^{-1}
ϵ	Molar absorbtivity	$\mathrm{M}^{-1}\,\mathrm{cm}^{-1}$
η	Dynamic (shear) viscosity	$\mathrm{Pa}\cdot\mathrm{s}$
η_r	Relative viscosity	1
η_sp	Specific viscosity	1
λ	Wavelength	nm
ν	Frequency of light	Hz
τ	Shear stress	Pa
θ	Scatter angle	rad
A	Area	m^2
a	Exponent in the Mark-Houwink-Sakurada equation	
A_2	Second virial coefficient	$\mathrm{mol}\cdot\mathrm{mL/g}^2$
C	Molar concentration	M
c	Mass concentration	g/L
E	Energy	J
F	Force	N
h	Planck's constant	$\mathrm{J}\cdot\mathrm{s}$
I	Nuclear spin	1
I	Power intensity of light	$\mathrm{W/m}^2$
J	Coupling constant	Hz
K	Coefficient in the Mark-Houwink-Sakurada equation	mL/g
k	*Pseudo* first order rate constant	h^{-1}
K_H	Hagenbach factor	s^3
k'	Huggins' constant	1
K^*	Optical constant	1
l	Length	m
m	Slope of the Fuoss-Mead linear regression line	$\mathrm{mL}^2/\mathrm{g}^2$
M_n	Number-average molecular weight	Da
M_w	Weight-average molecular weight	Da
n	Refractive index	1

n_0	Number of initial linkages at time 0	1
N_i	Number of chemical species i	1
n_i	Moles of chemical species i	mol
$n^{'}$	Number of cleaved linkages	1
P	Pressure	Pa
$P(\theta)$	Scattering function	1
r	Radius	m
R_w	Weight-average root mean square radius of gyration	nm
${R_\mathrm{G}}^2$	Mean square radius of gyration	nm^2
R_θ	Rayleigh factor	cm^{-1}
s	Slope of the Solomon-Ciuta linear regression line	$\mathrm{mL}^2/\mathrm{g}^2$
T	Temperature	°C
t	Flow-through-time	s
t_H	Hagenbach-corrected flow-through-time	s
U	Flow rate	m^3/s
V	Volume	m^3
v	Fluid speed	m/s
w	Weight (mass)	g
z	Position in the direction perpendicular to fluid flow	m
$[\eta]$	Intrinsic viscosity	mL/g
$\mathbf{B}$	Magnetic field	T

Chapter 1

Introduction

This chapter explains the background and motivation for studying the biopolymer xanthan in order to survey its most interesting properties for enhanced oil recovery applications.

1.1 Polymer Flooding for Enhanced Oil Recovery

Enhanced oil recovery, or EOR, is a collective term used to describe various techniques that can be implemented to increase the amount of crude oil extracted from a reservoir. With energy consumption and demand still expected to escalate for the next decades, it has become imperative to investigate methods for a more sustainable production from already existing oil fields[1]. As the industry will no longer be able to guarantee new discoveries that are easily accessible and inexpensive to produce from, these are necessary steps for securing the global transition from fossil fuels to renewable sources as the dominating supply of energy.

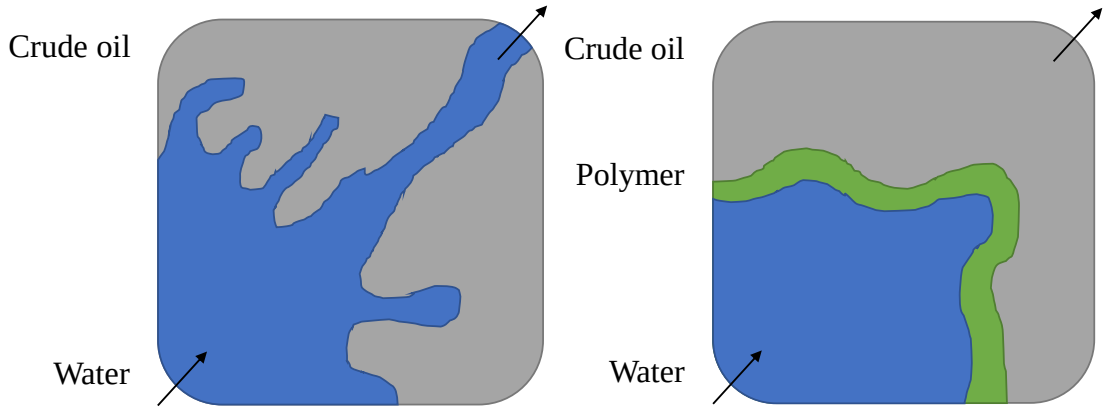

(a) Water flooding **(b)** Polymer flooding

Figure 1.1: Polymer flooding can lead to improved sweep efficiency by reducing the viscous fingering effect. (**a**) Water flooding causing viscous fingering. (**b**) Adding a polymer solution in the interface of water and oil improves the sweep efficiency. The illustration is based on a similar figure by Typhonix AS[2].

Polymer flooding is one of several existing EOR techniques. It involves the injection of long chained polymers in an aqueous solution for improving the *sweep efficiency* when the fluid drives the oil from the injection site towards the production well. The polymer

functions as a thickening agent and is therefore added in order to equalise the large difference in viscosity at the interface between water and oil. If only water were to be used to drive the oil directly, there would be an increased probability of *viscous fingering*. This is an unwanted effect where water channels through the reservoir with an uneven profile, thus bypassing volumes of oil which otherwise could be recovered with polymer flooding. An illustration of this effect is shown in Fig. 1.1. The viscous fingering effect results in a poor sweep efficiency, with the consequence of a negative economic impact since more water would have to be injected for a longer time in order to produce the same amount of oil[1].

1.2 Common Types of EOR Polymers

The most used polymer for reservoir injections is a synthetic single-chain macromolecule called HPAM, which is an abbreviation for *(partially) hydrolysed polyacrylamide*. Typically, 25-30% of amide groups in the polyacrylamide molecule are hydrolysed randomly in order to form negatively charged carboxylate groups[3]. This is done in order to reduce adsorption to mineral surfaces[1]. HPAM dominates for most EOR applications due to its unrivalled viscoelastic properties. However, there are some limitations associated with this polymer. As a polyelectrolyte with flexible linkages, it takes on the shape of a random coil in solution. Due to its many charged groups, the effective hydrodynamic volume will depend heavily on the ionic strength, i.e. salinity, of the solvent. At sufficiently high salt concentrations the molecule will collapse inwards, thereby reducing the viscosity[3].

Another challenge with HPAM is more related to how its use may impact the environment. Polyacrylamide has been shown to degrade slowly under natural conditions and will therefore eventually accumulate in terrestrial and aquatic ecosystems over time if not properly disposed[4]. Moreover, some studies show that commercial HPAM products can degrade into toxic acrylamide, potentially endangering both humans and animals[5].

An alternative to HPAM for polymer flooding is *xanthan*; a double-stranded, natural polysaccharide which also has been used for polymer flooding. As with HPAM, xanthan can be produced with high molecular weight and in large quantities, making it an excellent viscosifier. Moreover, it is relatively insensitive to changes in salinity due to its double-stranded structure, which provides an extreme chain stiffness[3]. There are some concerns within the oil industry regarding the use of biopolymers such as xanthan as they are generally perceived as *too* biodegradable. Microorganisms can potentially start digesting the polymers before or during oil field operation; a scenario which is far from optimal.

In order to make xanthan a more favourable competitor to HPAM and other EOR polymers, it may be possible to chemically modify the biopolymer so as to improve its rheological properties while simultaneously hindering enzymes from degrading it too fast[6]. Roy et al. (2014) developed such a procedure by using i.a. carbodiimide for grafting octylamine onto carboxyl groups of the xanthan side chains[7]. This method has later been applied to modify xanthan both under its ordered and disordered conformation[8]. Knowledge about the side chain composition is therefore important before attempting chemical modification of xanthan.

1.3 Scope of this Master's Thesis

This master's project was conducted during the Spring semester of 2018 and is a continuation of a specialisation project carried out during the Autumn semester of 2017[9]. The focus has been to characterise *non-modified* xanthans of various origins. The purpose of this work is to obtain data that can be compared with results from corresponding experiments on *modified* xanthan in the future. It is hoped that the contents of this thesis will contribute in showing the true potential of xanthan for enhanced oil recovery.

During the specialisation project, a range of samples with different molecular weight distributions were made by degradation with a Star Burst Mini microfluidiser. Analytic methods such as capillary viscometry and SEC-MALLS were then used to investigate the samples' viscous properties and molecular weights. The goal of the master's project has been to improve the characterisation of the xanthans based on the previous work from 2017. In particular, viscometry was repeated after improving the dissolution of undegraded xanthans by replacing the $NaNO_3$/EDTA solvent with $NaHCO_3$/NaOH. Rotational rheometry has further been used to study the relation between viscosity and shear rate for solutions at various concentrations. Another objective of the work was to investigate the molecular structures of various xanthans by ^{1}H-NMR. Prior to these analyses, however, depolymerisation protocols had to be optimised for obtaining spectra of suitable quality. This was achieved by comparing degradation using chemical reactants vs. digestive enzymes. The course of degradation in each of the methods has been assessed by the bicinchoninic acid (BCA) reducing end assay in combination with spectrophotometry.

Chapter 2

Theory

Theoretical concepts for understanding and describing features of the xanthan biopolymer are provided in this chapter. First, its chemical structure and properties will be presented; followed by an introduction to different degradation methods and ending with relevant explanations to the different characterisation techniques.

2.1 The Biopolymer Xanthan

Xanthan is an extracellular polysaccharide produced naturally by *Xanthomonas campestris*, a bacterium commonly found on e.g. cabbage plants. Due to its aggregating properties, it further has an important function in biofilm formation[10]. The biofilm is an extracellular matrix that protects the bacteria from environmental stresses and antimicrobial compounds[11]. Research from the early 1960s found xanthan to have exceptional rheological properties, and it has since 1969 been approved as a food additive by the U.S. Food and Drug Administration (FDA)[12]. Today, the biopolymer is produced through industrial fermentation processes, and it is applied as a thickening and stabilising agent in common products such as salad dressings and toothpastes. Moreover, xanthan gum has been an important ingredient in oil drilling fluids for suspension stabilisation under demanding conditions like e.g. high salt concentrations.

2.1.1 Chemical Structure

Native xanthan has a typical molecular weight M_w in the range $10^6 - 10^7$ Da[3, 13] The macromolecule is made up of a large number of repeating units (RUs) having the pentasaccharide structure as depicted in Fig. 2.1. Xanthan's backbone consists of β-1,4-linked D-glucose, where every second glucose has a trisaccharide side chain. This side chain is made up of a terminal β-1,4-D-mannose, a β-1,2-D-glucuronic acid and finally a α-1,3-D-mannose which is linked to the backbone. Between all saccharide units there are glycosidic C-O-C linkages.

As seen in Fig. 2.1, an O-acetyl group can be linked to C-6 on the mannose closest to the backbone, while a pyruvate ketal (pyruvyl) can be linked to C-4 and C-6 on the terminal mannose to form a diketal. Other studies have shown that the outer mannose can also be acetylated[14]. The substitution degrees depend on both bacteria strain and fermentation conditions[7]. The molecular weight of the RU can therefore vary. If there are

no pyruvyl nor acetyl groups, $M_{\mathrm{RU}} = 848$ Da[3]. With one of each of the two substituents the molecular weight would be 994 Da as $M_{\mathrm{Pyr}} = 87.054$ Da[15] and $M_{\mathrm{Ac}} = 59.044$ Da[16]. The avg. M_{RU} for any xanthan sample is therefore expected to be somewhere in between 848 Da and 994 Da. With the pyruvyl present, the side chain has a total of two carboxylic acid groups with $\mathrm{pK_a}$ close to 4.6[17]. The xanthan polymer will therefore have a net negative charge at pH levels above 4.6, making it a polyelectrolyte when dissolved in aqueous solutions with moderate to high pH.

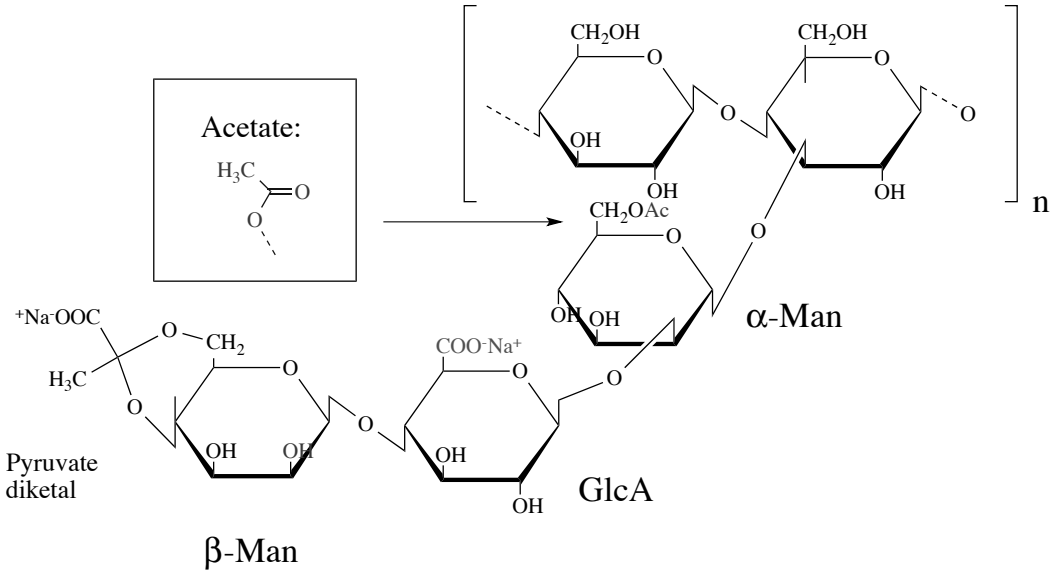

Figure 2.1: Structural formula of the repeating unit of a xanthan polymer. Substitution degrees of acetyl and pyruvyl of natural xanthan may vary depending on bacteria strain and fermentation conditions. Reproduced with permission from B.E. Christensen (2016): *Compendium TBT4135 Biopolymers*[3].

2.1.2 Properties of Xanthan

Being polyanionic for a large pH interval, xanthan is readily soluble in water below certain concentration limits. When dissolved it will make the solution markedly more viscous due to the high molecular weight and intramolecular electrostatic repulsion. Xanthan tends to form double-stranded helices when in a solution containing a sufficient concentration of salt[18]. This ordered conformation renders xanthan to be less susceptible to changes in ionic strength compared to single-stranded polyelectrolytes like e.g. HPAM[3]. Furthermore, it makes the polymer extremely stiff with a persistence length of 120 nm. For lower molecular weights, ordered xanthan molecules will therefore resemble rigid rods.

It is possible to induce a conformational transition to a single-stranded, disordered conformation by either lowering the *ionic strength* or by increasing the temperature past the conformational temperature T_{m}. The transition has been reported to occur around 60 °C[19], although this depends on factors such as the degrees of acetyl and pyruvyl, ionic strength and pH[7]. Thermal denaturation of native xanthan has been shown to be almost completely reversible, but it may induce local transitions which cannot be recovered during renaturation[20]. Xanthan in its disordered conformation will have a decreased persistence

length and becomes more flexible, thus behaving more like a random coil than a rigid rod. This impacts rheological characteristics because viscosity decreases as well.

Like many biopolymers, a xanthan solution is characterised as being a non-Newtonian fluid; meaning that the behaviour is *pseudoplastic* for increasing shear rates. This phenomena is also known as *shear thinning*. Viscosity will therefore decrease with higher rate of shearing deformation. These concepts will be elaborated in more detail in Section 2.4.

2.2 Degradation of Polymers

The following sections present the theory of three different methods for polymer degradation: mechanical, chemical and enzymatic.

2.2.1 Mechanical Shear Degradation

Depolymerisation of polymers having rod-like helical conformation, like e.g. xanthan and scleroglucan, can be achieved by forcing a polymer solution through a capillary at high shear rate[21]. Degradation of alginate from an initial M^{w} of over 500 kDa to under 100 kDa has further been performed by high pressure shear degradation using a Star Burst Mini HJP-25001H (Sugino Machine Ltd., Japan) wet pulverising system operating at a pressure of 245 MPa[22]. A schematic of its working principle is shown in Fig. 2.2.

The Star Burst Mini Wet Milling and Dispersing Device operates by extracting a solution volume into a chamber, where a plunger pressurises it at a set desired pressure (max. 245 MPa). The volume is then sent through a nozzle of 100 µm[22] to collide with a ceramic ball before exiting the machine to be collected. The throughput is reported by the manufacturer to be as large as 5-6 L/hour[23]. This method has therefore been claimed to overcome the disadvantages of e.g. low throughput efficiency and titanium ion contamination related to the method of ultrasonic depolymerisation[22, 24].

The mechanics behind high shear degradation of polymers do not follow a fully explained theory. Chain scission occurs supposedly as a result of molecular stress developed by hydrodynamic shear, but there is reason to suspect that additional effects such as adiabatic heating due to cavitation can further complicate such processes[25]. Observations have shown that mechanical degradation appears to follow a first-order rate law[22, 25]. In the case of mechanical degradation with the Star Burst Mini it should therefore become increasingly more difficult to break a polymer into shorter fragments with each subsequent degradation cycle. The native double-stranded conformation of the xanthan molecule should moreover not be affected substantially as long as the temperature does not exceed the conformational temperature T_{m} (B.E. Christensen, personal communication).

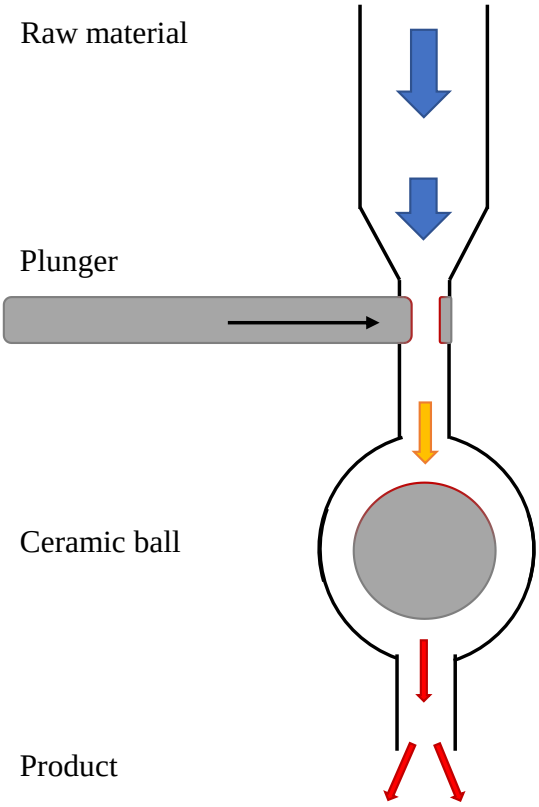

Figure 2.2: Schematic of the mechanism for high shear degradation with the Star Burst Mini. A plunger exerts high pressure up to 245 MPa on the raw material. The latter is sent to collide with a ceramic ball and exits the machine as a pulverised product. This figure is based on a similar illustration from the website of the company Sugino[23].

2.2.2 Chemical Degradation

Chemical reactants have proved effective in reducing the viscosity of xanthan solutions. One method involves adding hydrogen peroxide (H_2O_2) at an elevated pH level of minimum 8.0[26]. This method has been proven beneficial for oil production applications as no residuals are formed that can damage oil well formations; which is known to have been a problem with agents such as LiOCl and NaOCl. The pH can be adjusted by adding a caustic agent such as sodium hydroxide (NaOH) or potassium hydroxide (KOH). The benefit of increasing pH is that H_2O_2 becomes more effective at breaking down the polymer. By heating the solution the unstable O-O bonds of hydrogen peroxide will decompose at a faster rate, resulting in free radicals such as the hydroxyl radical[3]:

$$\mathrm{H{-}O{-}O{-}H} \longrightarrow \mathrm{HO^{\cdot}} + \mathrm{^{\cdot}OH}$$

These are highly reactive species that can attack a polymer by removing a hydrogen atom:

$$\mathrm{{-}CH{-}} + \mathrm{^{\cdot}OH} \longrightarrow \mathrm{{-}C^{\cdot}{-}} + \mathrm{H_2O}$$

Such oxidative damage creates unstable carbon radicals that can ultimately lead to bond cleavage through subsequent reactions.

2.2.3 Enzymatic Depolymerisation

In order to study and compare the primary structure of different xanthans by NMR, it is necessary to obtain oligomers where the molecular composition is kept intact. In other words, only glycosidic linkages of the backbone should be cleaved during degradation. Chemical degradation have proven to not be suitable due to concurrent side chain alterations[27]. An alternative is therefore to use cellulases, which has been shown to degrade xanthan when in its disordered conformation[28, 29]. A salt-free solution and an elevated temperature of 38 °C or higher are therefore usual prerequisites for enzymatic digestion, as free ions and lower temperature tend to stabilise the ordered conformation. The use of cellulases is furthermore a more appropriate model for simulating how degradation of xanthan by microorganisms can potentially occur during oil field operations.

2.3 TGA for Water Content Determination

Thermogravimetric analysis (TGA) is an experimental method which can be used for measuring mass change of a material with increasing temperature under a controlled atmosphere[30]. This technique has further been applied in food and pharmaceutical industries for accurate quantification of the water content of polymer particles[31]. TGA of polymer samples in normal air atmosphere by increasing temperature past the boiling point of water should yield a mass change related to the amount that has been vaporised. By assuming this mass change is only due to water evaporation, the initial water content of the sample can be estimated.

2.4 Viscosity of Polymer Solutions

The following subsections are about concepts in fluid mechanics which are important for understanding the purpose behind viscometric and rheological experiments of polymer solutions. All equations presented in subsections 2.4.1 - 2.4.3 and 2.4.5, except for Equation 2.7, have been acquired from p. 236-246 in B.E. Christensen (2016): *Compendium TBT4135 Biopolymers*[3].

2.4.1 Dynamic Viscosity of Non-Newtonian Fluids

The dynamic (shear) viscosity of a liquid is defined as:

$$\eta = \frac{\tau}{\dot{\gamma}} \tag{2.1}$$

τ denotes the *shear stress*, which is the ratio of force F and area A upon which the force acts:

$$\tau = \frac{F}{A} \tag{2.2}$$

$\dot{\gamma}$ is known as the *shear rate* and is defined as the derivative of the fluid speed v in the direction z perpendicular to the flow direction:

$$\dot{\gamma} = \frac{\mathrm{d}v}{\mathrm{d}z} \tag{2.3}$$

For non-Newtonian fluids like xanthan dissolved in an aqueous solution[12], τ will not increase proportionally with $\dot{\gamma}$ as opposed to the case for Newtonian fluids. Instead, the growth rate of τ declines with increasing shear rate; giving rise to the phenomena called shear thinning. Consequently, η will also decrease. The reason for this behaviour is that rod-like polymers, such as xanthan[32], will tend to align more with the flow direction as the shear rate increases.

2.4.2 Relating Flow-Through-Time to Viscosity

For a long cylindrical pipe like e.g. a viscometer capillary with constant and small enough cross-section for laminar flow to dominate, the flow rate U is given by the Poiseuille equation:

$$U = \frac{\mathrm{d}V}{\mathrm{d}t} = \frac{\pi r^4 \Delta P}{8\eta l} \tag{2.4}$$

V is the volume of liquid, t is the flow-through-time, ΔP is the pressure difference over the pipe, r is the pipe radius and l is the pipe length. By rearranging Eq. 2.4 and making it into an expression for η, it becomes clear that shear viscosity is directly proportional to flow-through-time t. Assuming all variables except t are constant, relative viscosity η_r and specific viscosity η_sp can be expressed as:

$$\eta_\mathrm{r} = \frac{\eta}{\eta_0} = \frac{t}{t_0} \tag{2.5}$$

$$\eta_\mathrm{sp} = \frac{\eta - \eta_0}{\eta_0} = \eta_\mathrm{r} - 1 = \frac{t}{t_0} - 1 \tag{2.6}$$

The subscript "0" is here used to denote variables related to the pure solvent. As a liquid enters and exits the contraction formed by the capillary inside a viscometer, there will be an excess pressure drop which is not accounted for in the Poiseuille equation. With the proper Hagenbach factor K_H this effect can be corrected for, yielding a more accurate flow-through-time t_H for the liquid flowing through the capillary. The following expression adapted from Eq. (4.19) in Wilke et al.[33] applies to capillaries with funnel-shaped ends:

$$t_\mathrm{H} = t - \frac{K_\mathrm{H}}{t^2} \tag{2.7}$$

Substituting the variables t and t_0 in Equations 2.5 and 2.6 with the Hagenbach-corrected variables t_H and $t_{0,\mathrm{H}}$ will therefore provide more definite results for η_r and η_sp.

2.4.3 Definition of Intrinsic Viscosity

Flow-through-times will decrease with lower concentrations of dissolved molecules, hence η_r and η_{sp} will also vary with change in concentration. However, the polymer/solvent system can be described without regard to concentration by a property called *intrinsic viscosity*, represented by the symbol $[\eta]$.

Intrinsic viscosity expresses the effective *hydrodynamic volume*, a property which depends on physical volume as well as shape. It is characteristic for a given polymer, and depends on its chain length as well as the type of solvent. The definition is given as:

$$[\eta] = \lim_{c \to 0} \left(\frac{\eta_{sp}}{c} \right) \tag{2.8}$$

Thus, the intrinsic viscosity is simply the limiting value of the ratio $\frac{\eta_{sp}}{c}$ as mass concentration c approaches 0.

2.4.4 Experimental Determination of Intrinsic Viscosity

Finding the value of $[\eta]$ directly from Eq. 2.8 would be difficult in practice. However, several empirical equations have been derived which can be used to arrive at an approximate estimation of the intrinsic viscosity based on experimental data. Four such models are presented below. The common feature between these is that linear regression analysis is applied to extrapolate a value for $[\eta]$ at $c = 0$.

Perhaps the most fundamental of the four models is the one known as Huggins' equation[34], which gives a linear relation between the ratio $\frac{\eta_{sp}}{c}$ and c:

$$\frac{\eta_{sp}}{c} = [\eta] + k'[\eta]^2 c \tag{2.9}$$

The coefficient k' is known as the Huggins constant. Its magnitude has been shown to be related to the hydrodynamic and thermodynamic interactions between polymer and solvent. A low value, typically around 0.3, indicates a good solvent while a high value suggests a poor one. For polyelectrolytes, k' will typically decrease as the ionic strength of the solution increases[35]. Molecular weight distribution and aggregation may also be of influence[36].

For a non-dilute solution where intrinsic viscosity is possibly very high, data plotted according to Eq. 2.9 may not follow a linear trend[24]. In such cases, a linear relation can still be achieved if one rather plots the base 10 logarithm of $\frac{\eta_{sp}}{c}$ for different concentrations. This yields a semi-logarithmic plot called a Hermann plot. Here, the base 10 logarithm of $[\eta]$ will be estimated as one extrapolates to $c = 0$:

$$\log_{10}[\eta] = \lim_{c \to 0} \left(\log_{10} \frac{\eta_{sp}}{c} \right) \tag{2.10}$$

A third model is represented by the Fuoss-Mead equation[37] (also known as the Kraemer equation[35]):

$$\ln \frac{\eta_r}{c} = [\eta] - \beta[\eta]^2 c \tag{2.11}$$

The coefficient β is related to the Huggins constant k' through the following equation[38]:

$$\beta = \frac{1}{2} - k' \tag{2.12}$$

In practice one can therefore find k' by knowing the slope $m = -\beta[\eta]^2$ of the regression line based on the Fuoss-Mead method:

$$k' = \frac{1}{2} + \frac{m}{[\eta]^2} \tag{2.13}$$

Under the constraints of Eq. 2.12, the Solomon-Ciuta equation can be derived by combining Equations 2.9 and 2.11[39]. This equation has in some instances been accredited to Billmeyer as well[24]:

$$[\eta] = \frac{2(\eta_{\mathrm{sp}} - \ln \eta_{\mathrm{r}})^{1/2}}{c} \tag{2.14}$$

Originally, this formula was established so as to determine $[\eta]$ from a single-point measure since the result has been found to be only weakly dependent on concentration within the dilute regime[35]. Eq. 2.14 is, strictly speaking, only valid for $k' = 1/3$, thus for high concentrations the Solomon-Ciuta model will still give a poor estimate of $[\eta]$ if the Huggins constant deviates too far from this value[38]. A safer option is also here to acquire data for several concentrations, fit a linear regression line to the data and eventually extrapolate a value for $[\eta]$ at $c = 0$.

Similar to the Fuoss-Mead model, the Huggins constant can be estimated if one knows the slope s of the Solomon-Ciuta regression line:

$$k' = \frac{1}{3} + \frac{s}{[\eta]^2} \tag{2.15}$$

As the value for k' is calculated differently than from Eq. 2.9 and 2.13, it will not necessarily be similar to the one obtained from neither Huggins nor Fuoss-Mead regression curves. This applies to the other models as well.

2.4.5 The Mark-Houwink-Sakurada Equation

Intrinsic viscosity of a polymer is related to its molecular weight M as given by the Mark-Houwink-Sakurada (MHS) equation:

$$[\eta] = KM^a \tag{2.16}$$

The coefficient K and exponent a are parameters which depend on the polymer-solvent system[3]. Moreover, the magnitude of a can reveal information about the shape of the polymer. For the three fundamental shapes a polymer can take when in solution, a will have the following specific values:

- Rigid rods: $a = 1.8$
- Random coils (assuming a good solvent): $a = 0.8$
- Spheres: $a = 0$

It is important to note that studies of macromolecular shape actually require measurements to be performed when $\dot{\gamma}$ approaches 0. Thus, Eq. 2.16 is mostly useful only when the shear rate is low enough to be within the Newtonian range.

Data of $[\eta]$ vs. M are often represented in a double-logarithmic plot. A power regression line fitted to the data will in that case appear as a line with a being the slope, since Eq. 2.16 can be equivalently written as:

$$\log[\eta] = \log K + a \log M \tag{2.17}$$

A linear regression of data where $\log[\eta]$ is plotted vs. $\log M$ will also provide a as the slope. For polymers of low M, the molecules will be expected to behave like short, rigid rods. As M increases, the long chains will gradually become more similar to flexible coils. This behaviour differs between type of polymers, however, as it also depends on their inherent stiffness.

2.5 SEC-MALLS

This section will explain theoretical concepts of size-exclusion chromatography combined with multi-angle laser light scattering (SEC-MALLS), and how this experimental method can be used to acquire the weight average molecular weight of a disperse polymer sample.

2.5.1 Definition of Weight Average Molecular Weight

The weight average molecular weight M_w is an estimate of the average molar mass, where the contribution of each individual molecule is weighted by its total weight (mass) w. The definition is given as:

$$M_\mathrm{w} = \frac{\sum_i w_\mathrm{i} M_\mathrm{i}}{\sum_i w_\mathrm{i}} \tag{2.18}$$

For disperse solutions, static light scattering experiments will give the weight average molecular weight[3].

2.5.2 Size-Exclusion Chromatography (SEC)

SEC is a method used to separate molecules of different hydrodynamic volumes in disperse solutions. This is required for obtaining a full description of the molar mass distribution for a given polymer sample. The principle of SEC is that a solution of macromolecules elutes through a column which contains stationary, porous gel or polymer particles. Molecules of smaller hydrodynamic volume will diffuse passively into these stationary particles to a greater extent than larger ones, thus becoming retained before diffusing out again. This means that larger macromolecules will elute first out from the column. An illustration is presented in Fig. 2.3.

Spectroscopic techniques can be used to measure the concentration of particles eluted at a given time during the SEC analysis. With an RI detector the variation in the measured refractive index n can be monitored as the concentration changes[3].

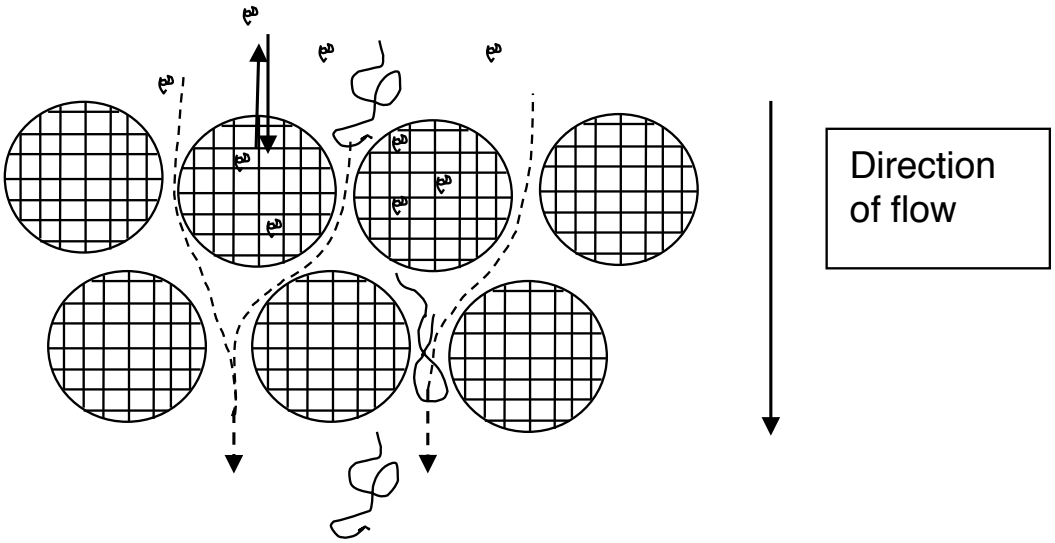

Figure 2.3: The principle of size-exclusion chromatography (SEC). Macromolecules of smaller hydrodynamic volume will diffuse passively through the pores of stationary particles inside the column. Molecules larger than the pore sizes will not be retained. Reproduced with permission from B.E. Christensen (2016): *Compendium TBT4135 Biopolymers*[3].

2.5.3 Multi-Angle Laser Light Scattering (MALLS)

MALLS is a technique where multiple detectors monitor how molecules in a solution scatter laser light at different angles from approx. 30° to 150°[3]. This can be used to determine both molecular weight M and the root-mean-square (RMS) radius R_{G}. When combined with SEC, software such as ASTRA can be used to record raw data for a large number of elution slices, thus providing distributions of M and R_{G} for the whole elution volume.

The relationship between scattered light, molecular weight M and mass concentration c can be approximated by the following equation which has been expanded to include the first power of c on the right hand side. The expression is adapted from *Eq. (13b)* from Zimm (1948)[40]:

$$\frac{R_\theta}{K^* c} = MP(\theta) - 2A_2 c M^2 P^2(\theta) + ... \tag{2.19}$$

K^* is an optical constant which depends on i.a. the square of the differential refractive index increment $\frac{\mathrm{d}n}{\mathrm{d}c}$ measured by the RI detector. R_θ, called the Rayleigh factor or the excess Rayleigh ratio, depends on i.a. the scattering angle θ. A_2 is known as the second virial coefficient, and its value is determined by the LS detectors. $P(\theta)$ is a theoretically-derived scattering function. *Eq. 6.2.16* from Christensen (2016)[3] gives an expression for the inverse of $P(\theta)$:

$$P(\theta)^{-1} = 1 + \frac{16\pi^2 {R_{\mathrm{G}}}^2}{3\lambda^2} \sin^2\left(\frac{\theta}{2}\right) + ... \tag{2.20}$$

${R_{\mathrm{G}}}^2$ is the mean square radius of gyration and λ is the light wavelength. As θ changes between the MALLS detectors, light scatter data are usually plotted against $\sin^2\left(\frac{\theta}{2}\right)$ on

the x-axis[3]. By expanding the square root of the reciprocal of Eq. 2.19 up to the first power of c, one obtains an expression called the Berry fit method as given by *Eq. 22* of the ASTRA user guide[41]:

$$\sqrt{\frac{K^*c}{R_\theta}} = \frac{1}{\sqrt{MP(\theta)}} + A_2c\sqrt{MP(\theta)} \tag{2.21}$$

When using the Berry fit method, ASTRA plots $\sqrt{\frac{K^*c}{R_\theta}}$ vs. $\sin^2\left(\frac{\theta}{2}\right)$ for the selected light scatter detectors for each elution slice. By choosing a certain fit degree, a polynomial regression curve of that order will be fitted to the data.

As θ approaches 0, $P(\theta)$ converges to unity[3]. One can thus obtain a reduced expression of which M can be estimated as long as A_2 is known. A simplified expression for M when $\theta = 0$ is here adapted from *Eq. 23* of the ASTRA user guide[41]:

$$M = \frac{4}{\left(\sqrt{\frac{K^*c}{R_{\theta=0}}} + \sqrt{\frac{K^*c}{R_{\theta=0}} - 4A_2c}\right)^2} \tag{2.22}$$

The Berry fit method is considered useful for molecules with RMS radii greater than 50 nm in combination with deleting high angle data[41]. An example is given in Fig. C.1, Appendix C of how the Berry fit method is used during ASTRA processing.

2.6 Spectrophotometry

The sections below will explain the fundamentals for how a reducing end assay can be used to obtain results for describing the course of polymer degradation.

2.6.1 The Bicinchoninic Acid (BCA) Assay

The BCA assay is commonly used for quantification of protein in a sample through the so-called *biuret reaction*[42], but it can also be used to assess the concentration of reducing ends (RE). Sugars containing a hemiacetal, i.e. the anomeric carbon of at least one end monosaccharide has an $-$OH group, can act as reducing agents[3]. This is a consequence of the said monosaccharide's ability to be in equilibrium between a cyclic and an open-chain aldehyde form (see Fig. 2.4); where the latter can be oxidised into a carboxylic acid. Reducing polysaccharides have generally one such reducing end; provided that any possible branches all have non-reducing ends. This includes xanthan as the D-glucose on one end is a hemiacetal, but the terminal D-mannose of the side chains are not (see Fig. 2.1 in Section 2.1.1).

The principle behind the BCA assay is that Cu^{2+} ions in an alkaline solution will be reduced to Cu^{+} by the RE. Bicinchoninic acid can then form a purple complex with the monovalent cupric ions [44]. The colour will be stronger and deeper as the concentration of reducing ends increases. An example is shown in Fig. 2.5 with D-glucose samples of different concentrations. Incubation at 75 °C for 30 min have been shown to accelerate the reaction within a suitable time frame without cleaving β-glucosidic bonds of cellodextrins, although higher temperatures can cause some degradation[45].

The correlation between colour and reducing ends can be described as the absorbance of monochromatic light is directly proportional to the RE concentration. A spectropho-

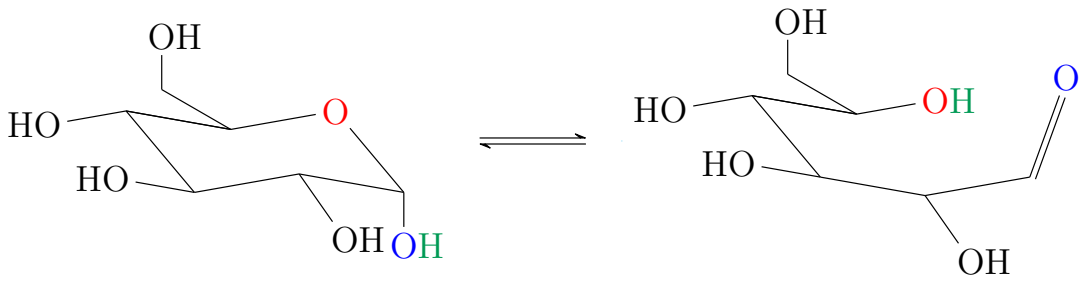

Figure 2.4: Equilibrium between cyclic α-D-glucose and the open-chain form. The illustration was made using the open-source *carbohydrates* LaTeX package[43].

tometer can therefore be used to quantify the absorbance for a range of different samples. This relation is known as the Beer-Lambert law, and it is given in Eq. 2.23[46].

$$\mathrm{OD}_\lambda = \log_{10}\left(\frac{I_0}{I}\right) = \epsilon l C \tag{2.23}$$

OD_λ is the optical density, i.e. the absorbance, of a specific wavelength λ. I is the power intensity of the light after passing through the sample cell, while I_0 is the initial intensity. The ratio I_0/I is further known as the inverse of the transmittance. The constant ϵ is sometimes referred to as molar absorbtivity, l is the length of the light path through the sample and C denotes molar concentration.

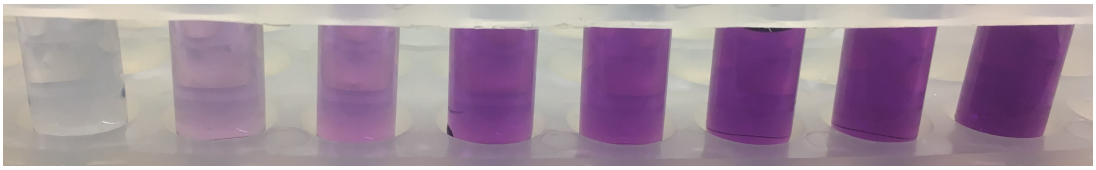

Figure 2.5: Change in colour with reducing end concentration of D-glucose samples during a BCA assay experiment. Concentrations from left to right: 0 to 7 µg/mL with 1 µg/mL increments.

2.6.2 Quantities from Polymer Degradation

In order to describe the course of depolymerisation, it becomes useful to introduce some quantities for describing how polymers change when cleaved into shorter fragments. The following equations and theory have been acquired from p. 126-131 and 219 in B.E. Christensen (2016)[3]; except for Eq. 2.25.

The *number average molecular weight* is defined as the arithmetic mean of the molecular weight of individual macromolecules. It can be expressed as follows:

$$M_\mathrm{n} = \frac{\sum_i N_\mathrm{i} M_\mathrm{i}}{\sum_i N_\mathrm{i}} = \frac{\sum_i c_\mathrm{i}}{\sum_i \frac{c_\mathrm{i}}{M_\mathrm{i}}} \tag{2.24}$$

$\mathrm{N_i}$ is the number of molecules, while $\mathrm{M_i}$ and $\mathrm{c_i}$ are the molecular weight and mass concentration of each polymer, respectively. Similarly, the fraction $\mathrm{c_i/M_i}$ can be interpreted as the separate molecules' molar concentration $\mathrm{C_i}$.

As each xanthan polymer strand has only one reducing end, the molar concentration of RE is furthermore equal to the total molar concentration of individual polymers. M_n can therefore be expressed as

$$M_n = \frac{c}{C_{RE}} \tag{2.25}$$

Eq. 2.25 is the key for using spectrophotometry data to calculate M_n and all following quantities for polymer samples. By knowing M_n, the *number average degree of polymerisation* can be calculated from Eq. 2.26.

$$DP_n = \frac{M_n}{M_{RU}} \tag{2.26}$$

M_{RU} is the molecular weight of the repeating unit, which will vary depending on the substitution degrees of acetyl and pyruvyl. DP_n denotes therefore the average number of RUs in the polymer chain of a disperse sample. As a polymer is being degraded, the DP_n will be lowered due to cleaving of linkages between the monomers. The *degree of chain scission*, or fraction of broken linkages, is directly related to DP_n by Eq. 2.27.

$$\alpha = \frac{n'}{n_0} = \frac{1}{DP_n} \tag{2.27}$$

The variables n' and n_0 refer to the number of cleaved and initial linkages, respectively. Strictly speaking, the equation does not hold for the $DP_{n,0}$ at time 0 before degradation as α by definition is then equal to 0. Even so, for polymers of long chains the inverse of DP_n will anyways be approximately 0.

Random depolymerisation of linear (unbranched) polymers follows a first order reaction. During the early stages of degradation when $\alpha < 0.02$, the following equation applies:

$$\frac{1}{DP_n} = \frac{1}{DP_{n,0}} + kt \tag{2.28}$$

Here, $DP_{n,0}$ is the degree of polymerisation at time 0 and t is the time. The coefficient k is known as the *pseudo* first order rate constant; where *pseudo* indicates that it is influenced by changes in factors such as temperature, buffer and pH.

Xanthan and other multi-stranded polymers display in reality a more complex behaviour during degradation compared to linear polymers. The reason for this is that non-covalent bonds between the strands can continue to stabilise the macromolecular structure when α is low. As new reducing ends will always form when glycosidic linkages are broken, however, the use of a reducing end assay should still give results that coincide with Eq. 2.28.

2.7 ^{1}H-NMR Spectroscopy

This section serves to explain the fundamentals of ^{1}H-NMR Spectroscopy and how this technique can be used to study variations of acetate and pyruvate substituents of xanthan. Most of the theory of this section has been obtained from W. Reusch (2013): Nuclear Magnetic Resonance Spectroscopy[47].

2.7.1 Basic Principles

Nuclear magnetic resonance (NMR) spectroscopy is a non-destructive technique that is widely used for determining the structure of organic compounds. ^{1}H-NMR, or proton NMR, is a subcategory where the signals of interest stem from the ^{1}H isotope. The protons has a characteristic nuclear spin of $I = \frac{1}{2}$. As it is a spinning charged particle, it will generate a magnetic field with a magnetic moment $\boldsymbol{\mu}$. In the presence of an external magnetic field $\mathbf{B_0}$, ^{1}H is permitted to exist in one of two spin states with $\boldsymbol{\mu}$ being either aligned with or opposed to the applied field. The former, referred to as the $+\frac{1}{2}$ or α state, has lower energy and is more populated. The latter is of higher energy and is known as the $-\frac{1}{2}$ or β state. The energy difference ΔE between the α and β states depends on the strength of the magnetic field as shown in Eq. 2.29.

$$\Delta E = \frac{\mu_{\mathrm{z}} B_{0\mathrm{z}}}{I} \tag{2.29}$$

Here z denotes the direction parallel to the magnetic field. NMR spectrometers use high field magnets to separate the spin states. Radio frequency (RF) radiation is then used to flip the alignment of the spins[48]. The energy required for the excitation can be expressed in terms of frequency ν as a consequence of the Planck-Einstein relation $E = h\nu$, where the Planck constant h has an approximate value of $6.63 \times 10^{-34}\,\mathrm{J\,s}$. One obtains thus the following expression:

$$\nu = \frac{\mu_{\mathrm{z}} B_{0\mathrm{z}}}{Ih} \tag{2.30}$$

^{1}H in a molecule are surrounded by electrons that shield the nuclei from the magnetic field. Consequently, the field strength must be increased in order for a shielded proton to absorb the same amount of RF energy. If the magnetic field is fixed, the frequency of the electromagnetic radiation must be lowered instead. As the electron density varies with type and quantity of neighbouring atoms and ions, the shielding effect is different depending on where the protons are located. The ^{1}H will therefore resonate and absorb the photon energy for different frequencies. These resonance signals can be detected, thus giving rise to a spectrum where individual resonance peaks can be separated according to frequency differences. As the latter will depend on the magnetic field strength, one usually reports a signal's *chemical shift* δ with respect to a reference compound defined to be at 0 ppm. This standard is usually tetramethylsilane (TMS). The formula is given in Eq. 2.31.

$$\delta = \frac{(\nu_{\mathrm{s}} - \nu_{\mathrm{ref}}) \cdot 10^6}{\nu_{\mathrm{ref}}} \tag{2.31}$$

The difference ν_s-ν_{ref} is in the order of Hz and refers to the frequency difference between a particular resonance signal and the reference. By dividing with ν_{ref} one achieves a numerical locator that does not depend on the magnetic field. As the denominator is in the order of MHz, the fraction is multiplied with 10^6 and expressed as parts per million (ppm). Resonance signals from most organic compounds are detected in a range of 0-12 ppm.

Some resonance signals in a ^{1}H-NMR spectrum exhibit a first order symmetric splitting pattern (multiplet) due to spin coupling interactions with e.g. *vicinal* hydrogens of different chemical shifts. These are nuclei that are separated by three separate covalent bonds. Protons separated by two bonds, i.e. attached to the same atom, can also interact. This is called *geminal* coupling. Splitting will not occur for *isochronous* hydrogens having the same chemical shift, which is a common case for geminal protons. However, splitting can occur if they are e.g. locked into different environments and thus no longer chemically equivalent.

The number of peaks in a first order splitting pattern follows the $N+1$ rule, where N denotes the number of neighbouring spin-coupled nuclei with a similar *coupling constant* J. This constant has the unit Hz and can be quantified as the separation between two peaks in a multiplet. A proton with a single vicinal neighbour that is not chemically equivalent will thus appear as a symmetric doublet in the spectrum, with the peaks separated by a characteristic coupling constant (see the upper part of Fig. 2.6). Three-bond vicinal coupling is commonly written as ^3J. The separation is the same between all signals in a multiplet and is independent of the external magnetic field strength. Even so, second order coupling effects can perturb the symmetry if the coupled nuclei have similar, but not equal, chemical shifts (see the lower part of Fig. 2.6).

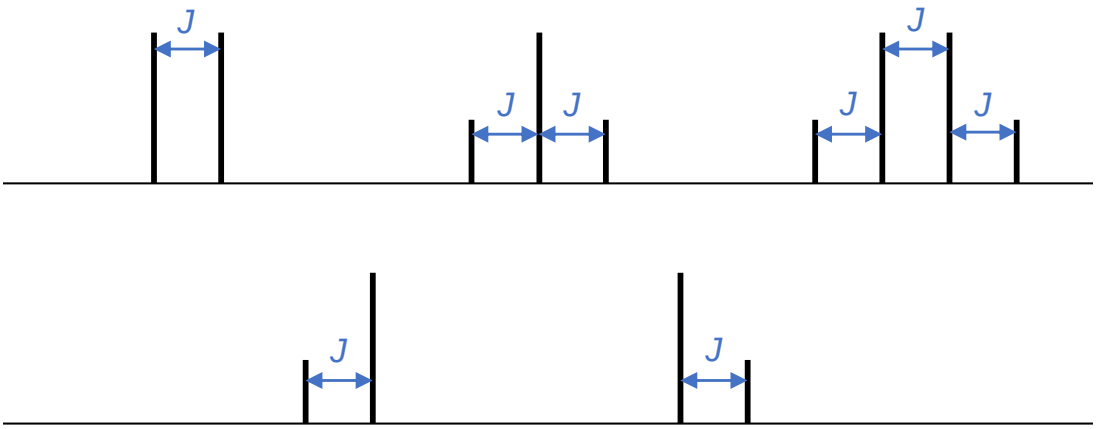

Figure 2.6: Illustrations of splitting patterns and how coupling constants are measured. Top: A clean doublet, triplet and quartet experiencing only first order coupling effects. Bottom: Example of non-symmetric doublets corresponding to two geminal protons which are not chemically equivalent.

2.7.2 Xanthan Substituents

As mentioned in Section 2.1.1, xanthans are acetylated and pyruvated to varying degrees as a result of factors such as bacteria strain and fermentation conditions. Certain proton resonances from these groups are easily distinguished in a ^{1}H-NMR spectrum of xanthan when using D_2O as solvent and acquiring data at 80 °C[7, 8]. These arise from the CH_3 group of each substituent, resulting in peaks around 1.5 ppm for pyruvyl and 2.2 ppm for acetyl. A resonance around 1.9 ppm will also occur for any free acetate that has been cleaved off. Additionally, a more deshielded signal at about 5.2 ppm have been shown to originate from the anomeric proton of the inner mannopyranosic unit, referred to as H-1 α-D-man[49].

The *degree of substitution* (DS) of substituent i on a polymer can be defined as the ratio of moles of substituent n_i to moles of repeating units n_RU. From a ^{1}H-NMR spectrum this proportion can be calculated by integrating peaks that correspond to signals from the substituent and an internal reference that is always present in the RU. The integrals I_i and I_ref must each further be divided by the number of chemically equivalent hydrogens, $N_\mathrm{H,i}$ or $N_\mathrm{H,ref}$, that constitute these signals. This whole procedure can been compressed into the following equation:

$$\mathrm{DS_i} = \frac{n_\mathrm{i}}{n_\mathrm{RU}} = \frac{N_\mathrm{H,ref} I_\mathrm{i}}{N_\mathrm{H,i} I_\mathrm{ref}} \tag{2.32}$$

With Eq. 2.32 the amount of acetyl, pyruvyl and free acetate relative to H-1 α-D-man can be calculated from a proton NMR spectrum of a xanthan sample as long as the spectrum is of sufficient resolution[49].

2.8 Statistics

Equations for fundamental statistical analysis are given below. These were used when computing averages and uncertainties for some of the results presented in Chapter 4.

The formula for computing the sample mean is given in Eq. 2.33.

$$\bar{x} = \frac{1}{n}\sum_{\mathrm{i}=1}^{n} x_{\mathrm{i}} \tag{2.33}$$

For all three equations x_{i} is the value for sample i and n corresponds to the number of samples.

Eq. 2.34 shows the formula for computing the corrected sample standard deviation.

$$\mathrm{SD} = \sqrt{\frac{\sum_{\mathrm{i}=1}^{n}(x_{\mathrm{i}} - \bar{x})^2}{n-1}} \tag{2.34}$$

The use of the denominator $n-1$ instead of n is commonly known as *Bessel's correction* for limiting the bias of this estimator[50]. SD is used for stating how scattered the data is around the sample mean[51] and should therefore be interpreted as a way of describing the data population itself.

Eq. 2.35 gives the formula for computing the standard error.

$$\mathrm{SE} = \frac{\mathrm{SD}}{\sqrt{n}} \tag{2.35}$$

SE indicates "the uncertainty around the estimate of the mean measurement"(Altman and Bland, 2005)[51]. It expresses how close the calculated sample mean is to the true average of the population.

Chapter 3

Materials and Methods

Experimental methods performed during the master's project are described in this chapter together with lists of materials and instruments that were used. This includes also how the xanthan samples were acquired and prepared before each experiment. Sections 3.1, 3.3, 3.4, 3.5.1, 3.6.1 and 3.6.2 have been adapted from the project thesis (C. Holmvik, 2017)[9].

3.1 Xanthan Samples

Mainly two different types of xanthan were studied during this project:

- Xanthan purified and precipitated directly from a fermentation broth (IRIS AS - the International Research Institute of Stavanger), hereafter referred to as MX.
- KELZAN XCD Xanthan Gum powder (CP Kelco), hereafter referred to as XCD.

MX was precipitated and purified from a fermentation broth following the protocol described in Section 3.3. This broth was acquired from IRIS AS and contained no added formalin. KELZAN XCD Xanthan Gum is a commercial product in powder form produced by CP Kelco. It was provided by the NTNU Biopolymer Laboratory. A duplicate of the cover picture showing MX and XCD can be found in Fig. 3.1.

Additionally, two other xanthan samples were included in some of the experiments for comparison with the main samples. These are listed below.

- xan0614-3: Purified KELZAN XCD. Sonicated for 30 min.
- XCDp: Purified KELZAN XCD. Not sonicated.

Both originate from the KELZAN XCD Xanthan Gum and were prepared by Ina Beate Jenssen during her master thesis work in 2013/14[24]. Her sample preparation procedure involved centrifugation at 10 000 rpm for 60 min, filtration through 0.45 µm filters and dialysis against 150 mM $NaNO_3$ and 10 mM EDTA. The samples were furthermore freeze-dried and stored in a freezer.

Figure 3.1: The xanthans MX (left) and XCD (right) in their solid form (top) and when dissolved in MQ water (bottom) at 10 mg/mL concentrations. This image is the same as the picture on the book cover.

3.2 Overview of Experimental Pathways

A flow chart has been included in Fig. 3.2 as an overview of the main experimental methods and for which samples these were applied to.

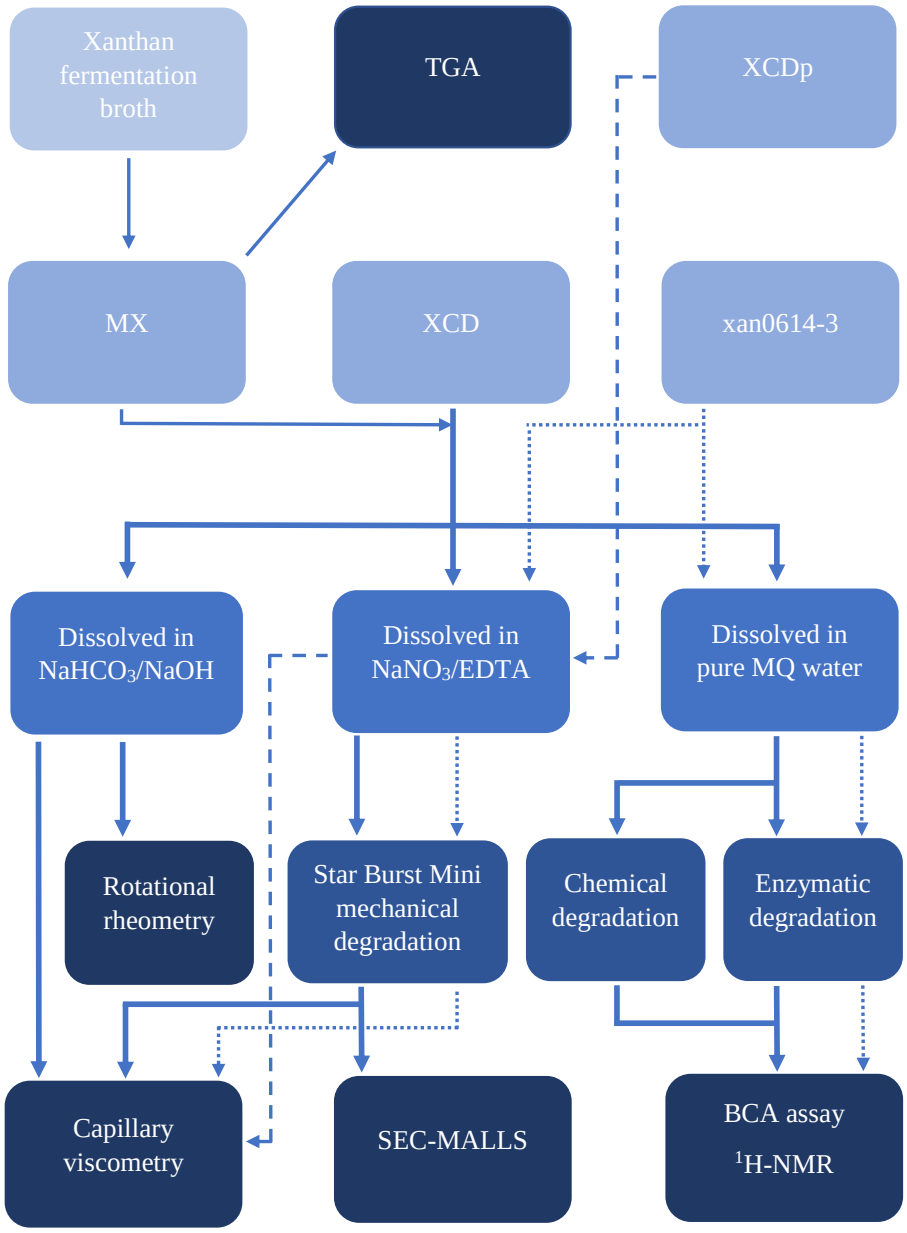

Figure 3.2: Flowchart showing the experimental pathways for the different xanthans. MX - Precipitated from fermentation broth; XCD - KELZAN XCD Xanthan Gum; xan0614-3 - Purified XCD, sonicated for 30 min; XCDp - Purified XCD, not sonicated.

3.3 Preparation of Xanthan MX

A specific protocol developed by Marianne Ø. Dalheim, PhD, was followed in order to isolate MX from the fermentation broth. Fig. 3.3 presents an overview of this process in a flowchart. All initial MX samples were prepared according to this protocol during the project in 2017[9].

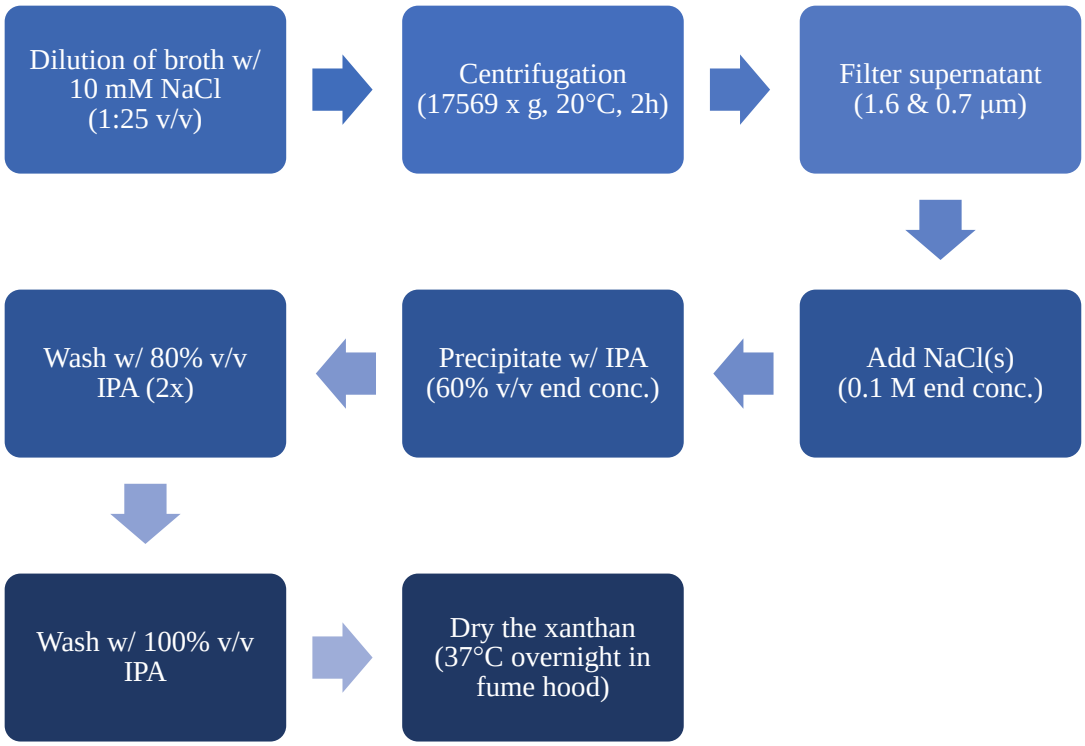

Figure 3.3: Flowchart of the isolation protocol for obtaining MX from the fermentation broth. IPA: isopropyl alcohol.

Materials used for isolation of MX can be found in the two following lists. All equipment that was in contact with the fermentation broth was autoclaved before and after use to remove possible biological contamination. Two different autoclaves were used as listed below. Glassware used for precipitation with isopropyl alcohol (IPA) did not have to be autoclaved.

Materials for autoclavation

- Centrifuge buckets (1 L) with aluminium screw caps
- Erlenmeyer flasks (5 L)
- 10 mM NaCl in DI water
- Flasks w/ screw caps (5 and 10 L)
- Graduated cylinder (1 L)
- Büchner filtering flask and funnel
- ASTELL 95-135 litre top loading autoclave
- MATACHANA S1000 autoclave (Thune Produkter AS)

Other materials used for purification of MX

- Fermentation broth
- Isopropyl alcohol (IPA), 100%
- DI water
- NaCl(s)
- Centrifuge: Sorvall Lynx 6000 Thermo Scientific
- Centrifuge rotor: Fiberlite™ F9-6 x 1000 LEX (Thermo Scientific)
- Vacuum pump
- Large funnels
- Petri dishes
- Glass rod
- Whatman glass microfibre filter GF/A 1.6 µm (GE Healthcare)
- Whatman glass microfibre filter GF/F 0.7 µm (GE Healthcare)
- Lab spoons
- Tweezers
- Laboratory weight
- Drying oven

7.5 L of 10 mM NaCl in DI water was prepared and distributed evenly into three Erlenmeyer flasks. The flasks were covered with aluminium foil and autoclaved. After autoclavation, 300 mL of broth was mixed with 7.2 L 10 mM NaCl and thus diluted 1:25.

The diluted fermentate was distributed evenly into the centrifuge buckets and centrifuged for 2 hours at 17568 x g and 20 °C. Thereafter, the supernatant was poured over into autoclaved 5 L flasks for temporary storage. Filtration was performed using a Büchner filtering flask connected to a vacuum pump and a two-part funnel containing a sintered glass disc. Disposable filters of 1.6 µm and 0.7 µm pore size were used in combination with this setup.

NaCl(s) was added to the filtrate to an end concentration of 0.1 M as this would induce a "salt shock" condition for easier precipitate extraction. Pure 100% v/v IPA was then added to an end concentration of 60% v/v. Precipitate was extracted using a glass rod and washed twice with 80% v/v IPA in separate Petri dishes before a final wash with 100% v/v IPA. Tweezers and spoons were used continuously for proper washing. MX xanthan precipitate was finally placed inside a drying oven at 37 °C overnight.

3.4 Thermogravimetric Analysis of MX

Materials

- Desiccator with SICAPENT drying agent
- DSC/TG alumina pans
- Laboratory weight
- Tweezers
- Thermogravimetric analyser, STA 449 C Jupiter (Netzsch-Gerätebau GmbH)

Thermogravimetric analysis (TGA) was performed on MX with the purpose of estimating its bound water content. Staff Engineer Karin W. Dragsten (Department of Chemical Engineering, NTNU) performed the measurements with a STA 449 C Jupiter thermogravimetric analyser during the project in 2017[9].

30.5 mg xanthan was first weighed out and placed in a desiccator the previous day in order to have an excess amount of nearly dried material. From this amount, two separate

samples of 5.4 mg and 5.3 mg were weighed out and placed into two separate disposable alumina pans.

Using an empty alumina pan, the thermogravimetric analyser was reset and calibrated. Mass change with increasing temperature over time was then measured for both samples. Temperature range was set to 32-140 °C with a temperature change rate of 5 °C/min. The temperature did, however, increase to almost 150 °C during the experiment as seen in Fig. A.1 in Appendix A. Data was recorded every 15 seconds until an end time of 30.5 min, and all measurements were performed in air.

3.5 Depolymerisation Methods

Three different methods were applied to degrade xanthan while dissolved in aqueous solutions. Samples that were depolymerised through mechanical shear at high pressure (Section 3.5.1) were later characterised with capillary viscometry and SEC-MALLS (Sections 3.6.1 and 3.6.2). Chemically and enzymatically degraded samples (Sections 3.5.2 and 3.5.3) were analysed with the BCA assay and ^{1}H-NMR (Sections 3.6.4 and 3.6.5).

3.5.1 Mechanical Shear Degradation

Materials

- Dry samples: MX, XCD and xan0614-3
- MQ water
- Ice for cooling
- Beakers
- Flasks w/ screw caps
- Laboratory weight
- Centrifuge tubes, 50 mL (VWR)
- Rocking shaker
- VDI 12 homogeniser (VWR)
- $NaNO_3$(300 mM)/EDTA(20 mM)
- $NaNO_3$(150 mM)/EDTA(10 mM)
- Star Burst Mini Wet Milling and Dispersing Device, model no. HJP-25001CE (Sugino)

Mechanical degradation using the Star Burst Mini was performed during the project in 2017[9]. All xanthan samples were dissolved in MQ water in separate centrifuge tubes to a concentration of 10 mg/mL. The solution with XCD was further blended with a VDI 12 homogeniser for approx. 5 min. The other samples were placed in a rocking shaker overnight for mixing.

A 2x buffer of $NaNO_3$(300 mM)/EDTA(20 mM) was added to all samples in order to reduce the xanthan concentration to 5 mg/mL. This was followed by an addition of 1x buffer of $NaNO_3$(150 mM)/EDTA(10 mM) to dilute the solutions further down to 1 mg/mL. The XCD solution was mixed for an additional 15 min using the VDI 12 homogeniser.

The Star Burst Mini was warmed up before operation with MQ water for several minutes at increasing pressure intervals. Operational pressure for degradation was set to 240 MPa (actual jet pressure was approx. 210 MPa).

Three different sample solutions were degraded with the Star Burst Mini: MX, XCD and xan0614-3. Each of these were processed separately by continuously pouring the

available volume into the material tank. This process was repeated 10 times for each sample (10 pulverising cycles).

About 30 mL from each solution was extracted from the total volume after a certain number of pulverising cycles. This resulted in series of up to 7 samples each. For MX and XCD the samples were extracted prior to degradation (pulverising cycle 0), after each of the cycles 1 to 4, 6 and finally cycle 10. Due to a limited amount of xan0614-3, only samples after pulverising cycles 0 and 10 were obtained.

3.5.2 Chemical Degradation with H_2O_2/NaOH

Materials

- Dry samples: MX and XCD
- H_2O_2, 10% (w/w)
- NaOH, 1.0 M
- OLS 200 water bath (Grant)
- Ice bath
- Beta 1-8 LDplus freeze-dryer (CHRIST)
- Dialysis bags, 14.3 mm diameter, cutoff 12-14 kDa (Medicell International LTD)
- MQ water

MX and XCD were dissolved separately in MQ water to a concentration of 6.0 mg/mL, resulting in two solutions with a volume of 10 mL each. 1.0 M NaOH and 10% (w/w) H_2O_2 were added to end concentrations of 4.8 mM and 54.3 mM, respectively. After mixing, the samples were placed in a water bath for 1 hour at 80 °C. The degraded samples were then immediately placed in an ice bath and stored in a refrigerator for rapid cooling.

The depolymerised samples were split in two equal parts and one part was further diluted to 1 mg/mL. The diluted samples were then distributed into dialysis bags (two for each xanthan type as a fail-safe measure) before being placed in a 7 L MQ water bath at RT for dialysis. The water was changed two times with time intervals of minimum 4 hours. All dialysed samples were recovered and eventually freeze-dried.

3.5.3 Enzymatic Depolymerisation with Cellulases

Materials

- Dry samples: MX, XCD and xan0614-3
- Ecostone Goo (EG), FCH-A5
- BGI-30 (BGI), FCH-A45
- OLS 200 water bath (Grant)
- Ice bath
- Digital thermometer
- MQ water
- Beta 1-8 LDplus freeze-dryer (CHRIST)

Cellulases Ecostone Goo (EG) and BGI-30 (BGI) were provided by colleagues of Prof. Christensen in the Netherlands, but with unknown stock concentrations. MX and XCD were dissolved in MQ water to a concentration of 1.0 mg/mL. Three samples with volumes of 50 mL were then prepared from each of the xanthans. Samples of cellulases EG and BGI were diluted 1:1000 with MQ water, with an additional sample of BGI being diluted

1:100. A 1:100 dilution of EG was not prepared due to the small amount of stock solution available.

500 µL of one of the diluted enzymes was added to each of the MX and XCD solutions. Thus, for both xanthan types, each sample contained 10 µL diluted enzyme per mg xanthan of either EG (1:1000), BGI (1:1000) or BGI (1:100). The numbers in parentheses denote the dilution from stock concentrations. The same procedure was done with xan0614-3, although only BGI (1:100) was used in this case.

5-10 mL starting point samples after addition of enzyme (0 hours) were extracted before placing the solutions in a water bath at 60 °C. A digital thermometer inserted in a flask with MQ water was included to observe when the solutions would reach the target temperature, indicating when the timer was to be started. The warm-up period lasted around 10 min. Samples (5-15 mL) were taken out at 1, 3, 24 and 48 hours (the last being at 44 hours for xan0614-3).

All MX and XCD samples were freeze-dried after enzymatic depolymerisation. This was only done with xan0614-3 samples that were to be used for ^{1}H-NMR.

3.6 Characterisation Techniques

Several instruments and methods were used to characterise the degraded as well as the initial xanthan samples. The samples have been specified for each of the methods below.

3.6.1 Capillary Viscometry

Materials

- Series of samples: MXm, XCDm and xan0614-3m
- Dry samples: MX, XCD and XCDp
- Buffer 1: $NaNO_3$(150 mM)/EDTA(10 mM)
- Buffer 2: $NaHCO_3$(25 mM)/NaOH(19.1 mM)
- DECONEX (10% v/v)
- MQ water
- Acetone
- Rubber bulb
- N_2 gas supply
- Pipette (2-10 mL)
- AVS 310 (Schott Gerate)
- AVS measuring stand
- ABU91 Autoburette (Radiometer Copenhagen)
- Water bath
- Magnetic stirrer
- Stir bar
- Acrodisc 5 µm syringe filters (PALL Life Sciences)
- Syringes, 20 mL
- Ubbelohde dilution viscometer, no. 531 01/0a (Schott Gerate)

Capillary viscometry was performed on the series of MX, XCD and xan0614-3 dissolved in Buffer 1 (see the list above), as obtained from mechanical shear degradation with the Star Burst Mini (see Section 3.5.1). Additionally, a solution of 1 mg/mL non-degraded XCDp was prepared in Buffer 1. These mentioned samples were analysed during the project in

2017[9]. Later, in the master's project, 0.5 mg/mL solutions of non-degraded MX and XCD were also dissolved in Buffer 2 (see the list above) and analysed.

Some of the sample solutions had to be diluted with their respective buffers to concentrations less than 1 mg/mL due to being too viscous for performing measurements. Starting concentrations for each sample can be found in the reports included in Appendix B. The samples were furthermore filtered through 5 µm filters using syringes to exclude any larger impurities or aggregates prior to analysis.

The rest of the procedure applies to all experiments unless specified differently. An Ubbelohde dilution viscometer was rinsed using 10% v/v DECONEX, MQ water and acetone before complete drying with N_2 gas. This process was repeated before every new measurement.

For experiments during the project in 2017, 14 mL of pure Buffer 1 was pipetted into the Ubbelohde before the viscometer was submerged and fastened to an AVS measuring stand inside a water bath 20.0 °C. The flow-through-time was measured five times with a Schott Gerate AVS 310, and the average time t_0 was calculated based on these data. The process was repeated with Buffer 2 during the master's project, but with a temperature of 25.0 °C.

Samples were added individually to the Ubbelohde in the same manner as with the buffers. A magnetic bar was included to stir the contents at 130 rpm during the course of each experiment. A Radiometer Copenhagen ABU91 Autoburette was used to automatically dilute the sample. For samples dissolved in Buffer 1 the temperature was 20.0 °C, while it was 25.0 °C for those in Buffer 2.

The computer programs *ViscControl* and *ViscRun* were used to set up and control the experiments. For each sample, flow-through-times were recorded four times for five different concentrations and were automatically saved in a .doc file together with Hagenbach-corrected values. Corrected mean flow-through-times for each concentration were furthermore saved in a .xls file.

Senior Engineer Ann-Sissel T. Ulset (Department of Biotechnology and Food Science, NTNU) provided a pre-made Excel file template for calculation of intrinsic viscosities which was used for data analyses.

3.6.2 SEC-MALLS

The list below shows the materials used to prepare xanthan samples for SEC-MALLS analyses. All experiments were performed during the project in 2017[9]. Information about the main parts of the complete SEC-MALLS instrument is given in Table 3.1.

Materials

- Series of samples: MXm and XCDm
- Mixing containers, 10 mL
- Screw top vials, 4 mL (Supelco)
- PTFE/silicone septa (Supelco)
- Syringe filters, 0.45 µm (VWR)
- Syringes, 5 mL
- Software:
  ASTRA (Wyatt Technology)
- $NaNO_3$(150 mM)/EDTA(10 mM)

Table 3.1: Overview of SEC-MALLS equipment parts

Part	Producer	Model
Autoinjector	Shimadzu	SCL - 10A VP
Pump	Shimadzu	LC - 10AD
Column 1	Toso Haas	TSK G6000 + G5000 PWXL
Column 2	Toso Haas	TSK G6000PW
Degasser	Biotech	Degassi Classic
LS-detector	WTC*	Dawn Heleos II
RI-detector	WTC*	Optilab R-rEX

* WTC: Wyatt Technology Corporation

Undegraded and mechanically degraded MX and XCD (series of MXm and XCDm samples) were prepared for SEC-MALLS injections as described below. The samples were originally dissolved in $NaNO_3$(150 mM)/EDTA(10 mM) to a concentration of 1 mg/mL. However, most of the samples had to be further diluted using the same buffer due to high viscosities. After dilution and mixing, approx. 4 mL of each sample was extracted with a syringe and pushed through 0.45 µm filters into a screw top vial.

All SEC-MALLS experiments were performed by Senior Engineer Ann-Sissel T. Ulset (Department of Biotechnology and Food Science, NTNU). Data obtained from SEC-MALLS measurements were processed using the ASTRA 6.1 software (Wyatt Technology Corporation). Procedures for baselines, peaks and regression models were modified individually for each sample with assistance from Prof. Bjørn E. Christensen and Ann-Sissel T. Ulset.

3.6.3 Rotational Rheometry

Materials

- Dry samples: MX and XCD
- $NaHCO_3$ (25 mM)/NaOH (19.1 mM)
- Kinexus ultra+ rotational rheometer (Malvern Panalytical)
- Cone: CP4/40 SR1869 SS
- Plate: PLS61 S11556 SS
- Software: rSpace for Kinexus
- Pipettes (3 mL)

Xanthan solutions were prepared by dissolving MX and XCD directly in $NaHCO_3$ (25 mM)/NaOH (19.1 mM) to 4.0 mg/mL. Further dilutions with the same buffer resulted in samples with concentrations 3.0, 2.0, 1.5, 1.0 mg/mL, and 500, 250, 125, 62.5 µg/mL. The rheometer was equipped with the geometries specified in the list above. Approx. 3 mL of sample was applied onto the plate before each measurement.

The experiment parameters were set using the accompanying software *rSpace*. All experiments were carried out at 25 °C. For xanthan concentrations of 1.0 mg/mL and below, data was collected between shear rates of 10^{-2} and $10^{3}\,s^{-1}$ at ten points per decade. For the higher concentrations the lower shear rate limit was changed to $10^{-3}\,s^{-1}$. The measurements were performed for a total of four parallels per sample.

3.6.4 BCA Assay & Spectrophotometry

Materials

- Samples: MX, XCD and xan0614-3
- D-Glucose, 1 mg/mL (Sigma Life Science)
- Unicam Heλios ϵ Spectrophotometer
- Cuvettes, polystyrene semi-micro, 1.5 - 3.0 mL, 10 mm light path (VWR)
- OLS 200 water bath (Grant)
- Assay reagent A
- Assay reagent B
- MQ water
- Test tubes w/ marbles
- Test tube racks

The reducing end concentrations of non-degraded and chemically/enzymatically degraded MX, XCD and xan0614-3 were determined using the modified BCA assay method as described by Zhang and Lynd (2005)[45].

Reagent A was prepared by dissolving 971 mg bicinchoninic acid (BCA), 27.14 g Na_2CO_3 and 12.1 g $NaHCO_3$ in 500 mL MQ water. For reagent B, 624 mg $CuSO_4{\cdot}5H_2O$ and 631 mg L-serine were added to a separate 500 mL of MQ. 1 volume of reagent A was mixed with 1 volume of reagent B prior to analysis.

Standard solutions were prepared by diluting 1 mg/mL D-Glucose with MQ water to 14, 12, 10, 8, 6, 4 and 2 µg/mL. A final standard of 0 µg/mL (pure MQ) was included. Xanthan samples were dissolved in MQ water and diluted depending on the amount of time they had been in water baths at elevated temperatures during degradation (see Sections 3.5.2 and 3.5.3). Exact concentrations after adding the BCA mix can be found in Section E.2 in Appendix E.

Three parallels à 1 mL of standards and xanthan samples, and several parallels (6-18) of pure MQ for the blank mixtures, were pipetted into separate test tubes. 1 volume of A+B reagent mix was added to 1 volume of the contents in the test tubes. Marbles were placed on top to limit water evaporation. All tubes were placed in a water bath at 75 °C for 30 min and then cooled to room temperature.

The blanks were mixed and approx. 2.5 mL was extracted and used to zero the spectrophotometer at a wavelength of 560 nm. The absorbance of all standards and samples were then measured and recorded. Any sample or standard displaying an optical density significantly above 1.000 was diluted with the blank mix before measuring again. Optical densities for diluted samples were multiplied with the respective dilution factor before being recorded.

3.6.5 ^{1}H-NMR

Materials

- MX, XCD and xan0614-3
- Beta 1-8 LDplus freeze-dryer (CHRIST)
- D_2O, 99.9 atom % D (Sigma-Aldrich)
- NMR tubes w/caps (Wilmad LabGlass)
- Sension+ MM 374 pH meter (Hach)
- U402-M3-S7/200 Extra long pH micro electrode (Mettler Toledo)
- Avance III HD 400 MHz w/ 5 mm SmartProbe (Bruker)
- Software: TopSpin 3.5pI7 (Bruker)

Selected samples of chemically and enzymatically degraded xanthans were freeze-dried and dissolved in D_2O before characterisation with ^{1}H-NMR spectroscopy. Concentrations ranged from 3.3 to 16.4 mg/mL depending on the available amount and need for dilution due to high viscosities. All samples were analysed at a frequency of 400 MHz and a temperature of 80 °C. Analyses were performed with assistance from PhD Candidate Amalie Solberg (Department of Biotechnology and Food Science). A micro electrode was further used to measure the pH of the samples while still in the NMR tubes. For a complete list of samples and related parameters, see Table F.1 in Appendix F.

Chapter 4

Results and Discussion

The results obtained during the master's project will be presented and discussed simultaneously in this chapter. These can be found in Sections 4.3 and 4.4 (with subsections). The most important results from the project in 2017[9], which have been adapted for this thesis, can be found in Sections 4.1 and 4.2 (with subsections). However, Section 4.2.1.3 includes new results that were obtained in February 2018. For an overview of experimental pathways for the different xanthan samples, see Fig. 3.2 in Section 3.2.

4.1 Estimation of Water Content by TGA

Thermogravimetric analyses (TGA) were conducted for two separate parallels of MX, i.e. the xanthan precipitated from the fermentation broth, in order to determine its moisture content. This was done during the project in 2017[9]. The starting mass for each parallel was approx. 5 mg and the percentage of original mass was recorded every 15 seconds with a temperature increase of 5 °C/min in the range 35-150°C. At starting point, $t = 0$, the percentage of original mass was set to 100%. During the analyses, the system temperature increased continuously up to approx. 150 °C before decreasing towards 140 °C for the final measurements. Data from both parallels can be found in Fig. 4.1 as plots of percentage of original mass vs. temperature.

A sudden decrease in mass of about 2-3% happened during the first 3.5 min of measurements before the temperature started to increase. Due to the temperature decreasing towards 140 °C for the final measurements, more data were also obtained for the temperature interval 140-150 °C. For raw data and diagrams visualising percentage of original mass and temperature plotted separately as functions of time, see Table A.1 and Fig. A.1 in Appendix A.

The reduction in mass percentage for the two parallels proceeded almost identically. One notable difference is that there was a larger decrease in the beginning for parallel 1 compared with parallel 2. A reason for this might be the difference in starting temperature at $t = 0$ ($T_{0,1} = 36.2$ °C for P1 and $T_{0,2} = 35.4$ °C for P2).

The avg. lowest percentage of original mass was calculated based on a selected population of data where the percentage of original mass had stabilised ($t > 24$ min, 54 data points). By assuming that the loss in mass was only due to complete evaporation of bound water, the avg. water mass percentage was obtained by subtracting this value from 100%. The water mass content of desiccated MX was thus found to be (10.43 ± 0.05)%

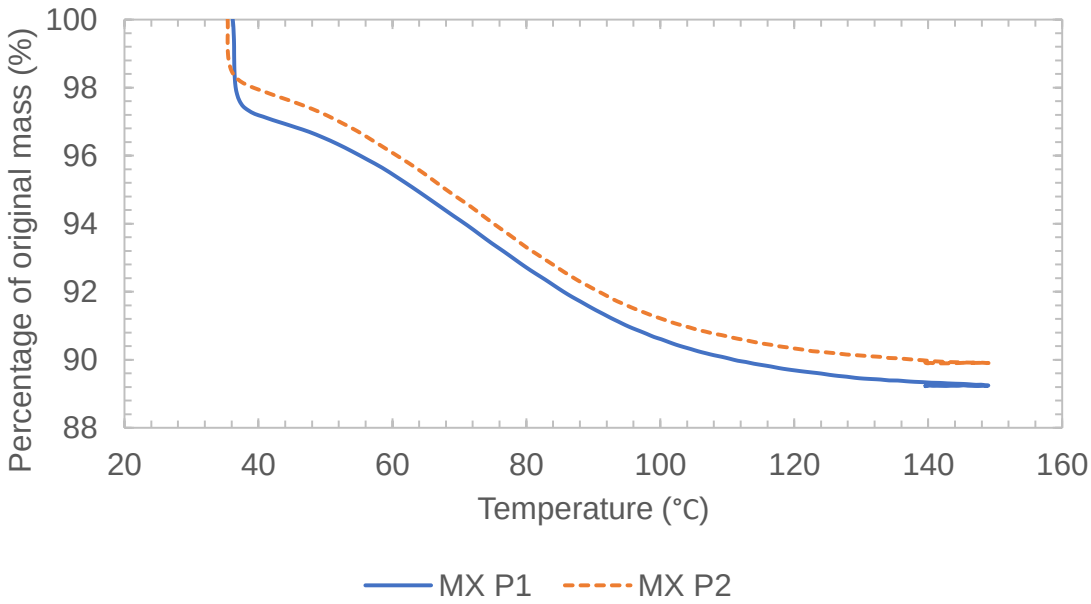

Figure 4.1: Percentage of original mass vs. temperature during thermogravimetric analyses of two xanthan MX parallels.

when exposed to normal air atmosphere at room temperature (Table 4.1). By knowing this, solutions containing MX could be prepared with more accurate concentrations. In comparison, Roy et al. (2014) reported a moisture content of 10.8% for their xanthan sample[7], while Fantou et al. measured 10.1%[8]. Both were determined by TGA.

Table 4.1: Estimated water content of MX by thermogravimetric analysis.

Lowest mass (%)	Water mass (%)
89.57 ± 0.05	10.43 ± 0.05

Values are means ± SE, given as percentages of the original mass of MX at starting point.

4.2 Mechanical Degradation of Xanthan

Mechanically degraded xanthan samples were analysed by capillary viscometry and SEC-MALLS during the project in 2017[9]. The purpose of this was to study how intrinsic viscosity and weight average molecular weight changes throughout degradation. It was furthermore attempted to determine the molecular shape of xanthan MX by combining the results from both experimental methods (Section 4.2.3).

4.2.1 Intrinsic Viscosities from Capillary Viscometry

The purpose of capillary viscometry was to estimate the intrinsic viscosities of xanthan samples in order to assess how this characteristic changed with the number of degradation cycles during mechanical degradation with the Star Burst Mini.

Flow-through-times of xanthan samples dissolved in either $NaNO_3$ (150 mM)/EDTA (10 mM) or $NaHCO_3$ (25 mM)/NaOH (19.1 mM) were measured using a Schott Gerate Ubbelohde dilution viscometer, type no. 531 01/0a. The average shear rate $\dot{\gamma}$ inside the Ubbelohde capillary was $2500\,s^{-1}$.

Relative and specific viscosity, η_r and η_{sp}, were calculated based on the average Hagenbach-corrected flow-through-time for each of the six different concentrations obtained per sample. The Hagenbach factor was given as $K_H = 30\ 800$ for this particular viscometer. η_r and η_{sp} were used to calculate and plot data according to four linear regression models: Huggins, Hermann, Fuoss-Mead and Solomon-Ciuta. By linear regression and extrapolation towards concentration $c = 0$, a value for $[\eta]$ was estimated from each of the models. The average intrinsic viscosity $[\eta]_{avg}$, as well as the average Huggins constant k'_{avg}, were then calculated for each sample. Note that a value for k' was not obtained from the Hermann model.

For some of the samples, the values obtained from the Huggins model was excluded from the calculation of averages. The reason was that this model often estimated a markedly lower value for $[\eta]$ and a higher value for k' than the other three methods, especially for the least degraded samples. See the notes below each of the respective Tables 4.2-4.5 for which samples this applies to. All values in the mentioned tables are given with corrected sample standard deviations (SD) calculated from the population used to estimate $[\eta]_{avg}$ and k'_{avg}. SD has been reported instead of standard error (SE) due to the results being obtained from different regression models.

4.2.1.1 Mechanically Degraded MX and XCD

During the project work in 2017[9], viscometry was performed on the series of mechanically degraded samples originating from MX, i.e. the fermentation broth precipitate, and the xanthan gum product Kelzan XCD. The obtained results are listed in Tables 4.2 and 4.3 according to the number of cycles each sample has been degraded using the Star Burst Mini. In general, $[\eta]_{avg}$ decreased with the amount of pulverisation cycles as expected. Samples were dissolved in $NaNO_3$ (150 mM)/EDTA (10 mM) and all measurements were performed at 20 °C. For raw data and regression plots, see Sections B.1 and B.2 in Appendix B.

For all MX samples (Table 4.2), the estimated $[\eta]$ and k' from the regression analysis with the Huggins model were excluded when calculating average values and SD, as

Table 4.2: Viscometry results for mechanically degraded MX samples dissolved in $NaNO_3$/EDTA. T =20 °C.

Sample	**Pulverising cycles**	$[\eta]_{\mathbf{avg}}$ **(mL/g)**	$k'_{\mathbf{avg}}$
MXm0[†]	0	2649 ± 11	0.48 ± 0.02
MXm1	1	1026 ± 4	0.49 ± 0.02
MXm2	2	731.7 ± 0.3	0.42 ± 0.00
MXm3	3	569.6 ± 0.2	0.46 ± 0.00
MXm4	4	487.7 ± 0.6	0.52 ± 0.01
MXm6	6	405.1 ± 0.1	0.46 ± 0.00
MXm10	10	316.4 ± 0.3	0.60 ± 0.01

Values are means ± SD. Results from Huggins' model were neglected for all samples.
[†] 2402 ± 5 mL/g with another buffer (see Table 4.5).

previously explained in Section 4.2.1. For the XCD samples (Table 4.3), $[\eta]$ and k' from Huggins were mostly close to those obtained with the other models, i.e. Fuoss-Mead, Solomon-Ciuta and Herman. Results acquired with Huggins have therefore been included when calculating the mean for all samples originating from XCD, except for the one that was pulverised for a single cycle (XCDm1).

Table 4.3: Viscometry results for mechanically degraded XCD samples dissolved in $NaNO_3$/EDTA. T =20 °C.

Sample	**Pulverising cycles**	$[\eta]_{\mathbf{avg}}$ **(mL/g)**	$k'_{\mathbf{avg}}$
XCDm0[†]	0	191.6 ± 0.0	0.19 ± 0.01
XCDm1[‡]	1	592.5 ± 0.6	0.40 ± 0.00
XCDm2	2	474.9 ± 0.9	0.32 ± 0.01
XCDm3	3	391.4 ± 0.4	0.37 ± 0.01
XCDm4	4	346.2 ± 0.3	0.37 ± 0.01
XCDm6	6	300.5 ± 0.3	0.31 ± 0.01
XCDm10	10	225.2 ± 0.5	0.69 ± 0.05

Values are means ± SD.
[†] 1743 ± 5 mL/g with another buffer (see Table 4.5).
[‡] Results from Huggins were not included in the calculations only for this sample.

One sample that distinguishes itself from the others is XCDm0. Its intrinsic viscosity was expected to be much higher than the obtained result of 191.6 mL/g. The reason seemed to be that undegraded XCD did not dissolve properly in the $NaNO_3$/EDTA buffer, further making the solution difficult to refine with 5 µm filters before measurements. Mixing with the VDI 12 homogeniser was therefore attempted, but this made little to no improvement. Although different starting concentrations were tried, from 62.5 µg/mL to 500 µg/mL,

all the estimated $[\eta]_{avg}$ were around 200 mL/g. The result reported in Table 4.3 was obtained using an initial concentration of 500 µg/mL. Trials without filtering first were also attempted, but the solution was then either too viscous or it contained particles large enough to block the capillary so that flow-through-times could not be recorded. Similar challenges were reported by Ina Beate Jenssen for her non-purified, sonicated XCD test sample[24]. It is therefore believed that the results for XCDm0 in Table 4.3 do not give a correct representation of the sample. Experiments with other samples were therefore tried to find a better estimate of the intrinsic viscosity (see Sections 4.2.1.2 and 4.2.1.3).

$[\eta]_{avg}$ for XCD are lower than for corresponding MX samples degraded with the same number of pulverising cycles. This implies that the original, non degraded MX sample is of higher molecular weight than XCD (see Section 4.2.2). The values for k'_{avg} for XCD are also generally lower than those for MX. This might indicate a more narrow molecular weight distribution[36]. Otherwise, the degradation of XCD seems to have followed a similar trend to that of MX.

The changes in intrinsic viscosity for both MX and XCD throughout mechanical degradation have been plotted in Fig. 4.2. Power trendlines have also been used here as guides to the eye and for approximately predicting the outcome of continued degradation up till 20 pulverising cycles. The undegraded samples have not been included for better visualisation. Both trendlines seem to level off around 200 mL/g, thus indicating an approximate limit for how low intrinsic viscosity, measured at $\dot{\gamma} = 2500\,s^{-1}$, can be achieved with a jet pressure of 210 MPa.

Further literature investigations during the master's project revealed that mechanical degradation by sonication of polystyrene is markedly faster at lower concentrations[52]. The suggested explanation was that polymer chains would then overlap less and become more susceptible to hydrodynamic forces. It would therefore be interesting to see if a similar concentration dependency could be observed when degrading xanthan with the Star Burst Mini.

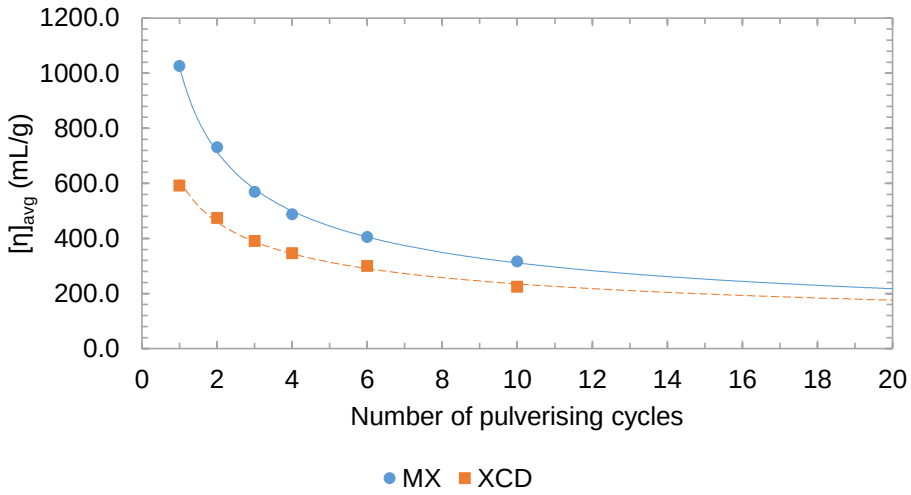

Figure 4.2: Decrease in intrinsic viscosity of MX and XCD degraded by a wet pulverising system at a chamber pressure of 210 MPa. Results for MXm0 and XCDm0 have not been included. Power trendlines (R^2 = 0.998 for MX and R^2 = 0.991 for XCD) were used as guides to the eye and for approximately predicting the outcome of continued degradation with this method. Data were obtained at shear rate $\dot{\gamma}$=2500 s^{-1}.

4.2.1.2 XCDp and xan0614-3

Table 4.4 shows viscometry results for two additional xanthan samples, XCDp and xan0614-3, that were also acquired during the project in 2017[9]. These originate from Kelzan XCD xanthan gum and were obtained from the master's project of Ina Beate Jenssen[24]. Xan0614-3 was first sonicated for 30 min, but both XCDp and xan0614-3 had been purified and freeze dried. The purification procedure involved centrifugation at 10 000 rpm for 60 min, filtration through 0.45 µm filters and dialysis against $NaNO_3$ (150 mM)/EDTA (10 mM). Results from the Huggins model were not included for any of the samples except for xan0614-3 (10 pulverising cycles). For raw data and regression plots, see Section B.3 in Appendix B.

Table 4.4: Viscometry results for XCDp and xan0614-3 dissolved in $NaNO_3$/EDTA. $T = 20\,°C$.

Sample	**Pulverising cycles**	$[\eta]_{\mathbf{avg}}$ **(mL/g)**	$k'_{\mathbf{avg}}$
XCDp-m0	0	964 ± 6	0.84 ± 0.07
xan0614-3m0	0	786 ± 2	0.49 ± 0.01
xan0614-3m10†	10	156.6 ± 0.3	0.93 ± 0.07

Values are means ± SD.
† Results from Huggins' model were included, but only for this sample.

As expected, xan0614-3m0 had a lower $[\eta]_{avg}$ than XCDp, as the former was already degraded by sonication for 30 min[24]. The obtained intrinsic viscosity of 786 ± 2 mL/g was, however, considerably higher than the result of 385 mL/g reported for the sample *xan30* in Table 3.1.4, Section 3.1.3 of I.B. Jenssen (2014). Xan30 was stated to be Kelzan XCD that had been sonicated for 30 min, and it was therefore expected that this sample and xan0614-3m0 would have similar intrinsic viscosities. The solvent used for xan30 was 100 mM NaCl instead of $NaNO_3$ (150 mM)/EDTA (10 mM), but the equipment and temperature (20 °C) were the same as here for xan0614-3m0. The use of another solvent is likely not the full reason for the intrinsic viscosities being this different. Even so, it has not been confirmed if there are other dissimilarities between xan0614-3m0 and xan30.

Further degradation of xan0614-3 by 10 cycles of pulverisation at 210 MPa resulted in an intrinsic viscosity of 156.6 ± 0.3 ($\dot{\gamma}$=2500 s^{-1}). This is the lowest achieved for any of the mechanically degraded samples in this study. Flow-through-times of the different concentrations of xan0614-3m10 did not all yield data that fitted well on a straight line. Two data points were rejected when doing the regression analysis, although this did not alter $[\eta]_{avg}$ substantially.

Due to the difficulties of achieving proper measurements for XCDm0 in $NaNO_3$/EDTA (see Table 4.3), XCDp-m0 was included in the measurements in order to get a better estimate of the true intrinsic viscosity of undegraded Kelzan XCD Xanthan Gum. However, since the sample preparation involved mixing with a blender[24], the purified XCDp-m0 sample could have possibly been degraded to some extent and therefore have a lower $[\eta]_{avg}$ relative to the non-purified XCD of which it originated from. It was therefore decided to try improving the dissolution of XCD instead by changing the solvent.

4.2.1.3 Comparing MX and XCD in Different Solvents

Dissolution of XCD in $NaHCO_3$ (25 mM)/NaOH (19.1 mM) proved to be much more successful than with $NaNO_3$ (150 mM)/EDTA (10 mM). Viscometry experiments was therefore repeated during the master's project for both undegraded XCD and MX samples (XCDm0 and MXm0) in the new buffer (Table 4.5). Analyses in $NaHCO_3$/NaOH were performed at 25.0 °C and not 20.0 °C as previously. The reason for this temperature change was in case the results would be compared with data from rheometry experiments which were performed at 25.0 °C (Section 4.3). $[\eta]_{avg}$ for XCDm0 was found to be 1743 mL/g in the new buffer, which is much higher than what was obtained for XCDm0 in $NaNO_3$/EDTA (192 mL/g), as well as for all the degraded XCD samples (Table 4.3). The intrinsic viscosity for the original XCD sample is also markedly higher than for XCDp, suggesting that some degradation indeed did occur during the purification by I.B. Jenssen[24]. The $[\eta]_{avg}$ for MX in $NaHCO_3$/NaOH was, however, a little lower than for the corresponding sample in $NaNO_3$/EDTA (2402 mL/g vs. 2649 mL/g). This could be a result of the change in analysis temperature from 20.0 °C to 25.0 °C, as intrinsic viscosity decreases with higher temperature[53]. Nevertheless, the result for solvent $NaHCO_3$/NaOH is considered to be a more representative result for XCDm0 than those previously shown for XCDm0 in Table 4.3 and XCDp in Table 4.4.

Table 4.5: Viscometry results for MX and XCD in different solvents.

Sample	**Solvent**	T (°C)	$[\eta]_{\mathbf{avg}}$ **(mL/g)**	$k'_{\mathbf{avg}}$
XCDm0	$NaHCO_3$/NaOH	25	1743 ± 5	0.50 ± 0.02
XCDm0*	$NaNO_3$/EDTA	20	192 ± 0	0.19 ± 0.01
MXm0	$NaHCO_3$/NaOH	25	2402 ± 5	0.47 ± 0.01
MXm0†	$NaNO_3$/EDTA	20	2649 ± 11	0.48 ± 0.02

Values are means ± SD.

* Same as in Table 4.3. Results from the Huggins model were only used for this sample.

† Same sample and results as in Table 4.2.

4.2.2 SEC-MALLS Analyses

Results obtained from SEC-MALLS analyses during the project in 2017[9] are presented and discussed in the following sections. As such analyses provide a lot of information, the main focus have been to obtain and analyse data regarding weight-average molecular weight M_w. Supplementary data and results can be found in Appendix C. Procedures for selecting the appropriate light scattering baseline, peak and data model had to be adjusted manually for all experiments.

The Berry model (Eq. 2.21 in Section 2.5.3) with fit degree 2 was used for all samples as better fits could then be obtained for all samples. Calibrated values for the differential refractive index increment and the second virial coefficient were set to $\frac{dn}{dc} = 0.1500$ mL/g and $A_2 = 1.000 \times 10^{-4}\,\text{mol} \cdot \text{mL/g}^2$, respectively.

4.2.2.1 Mechanically Degraded MX

All seven samples originating from the mechanically degraded MX (MXm0-MXm10) were analysed with SEC-MALLS. Two injections were performed per sample using 150 mM $NaNO_3$/10 mM EDTA as the buffer solvent. The two injections are from here distinguished by the letters *a* and *b*. E.g. MXm0a corresponds to the first injection and MXm0b to the second injection of MX after 0 pulverisation cycles.
A selection of chromatograms and molecular weight distributions are presented in Fig. 4.3. For results from all injections, see Fig. C.2 in Appendix C. Dashed lines indicate concentration profiles determined by the differential refractive index (dRI). The red chromatogram of MXm0a in Fig. 4.3 is noticeably narrower than the others due to the injected mass being half of that of the other three. Otherwise, all dRI signal curves seem to be smooth and having broad, singular peaks. All samples can thus be interpreted as being disperse, but still normally distributed. The chromatograms are shifted more towards higher elution volumes with the number of pulverising cycles. This is as expected from SEC theory as the least degraded polymers should elute first from the columns.

The molecular weight distributions are not as readily explained. Ideally, these curves should overlap and only decrease with elution volume if the samples really were suitable for the TSK G6000 + G5000 PWXL columns. It seems that the high molecular weights make this difficult. This especially applies to the undegraded MXm0a as seen in Fig. 4.3, but all samples are showing irregularities towards larger elution volumes. Further investigation is therefore needed to optimise column separation.

One can further see that the molecular weight even starts to increase towards the end of elution for some of the samples, suggesting that agglomeration has occurred. It seems that this effect increases in magnitude the more degraded the sample is, as e.g. some data points of the distribution for MXm10b (pink) are of even larger molecular weights than MXm0a (red) between 12.7 and 13.7 mL. However, this only concerns a small percentage of the xanthan polymers of MXm10b as it occurs far to the left from its dRI peak at approx. 16 mL.

Weight-average molecular weights, with uncertainties, for mechanically degraded MX samples are presented in Table 4.6. These are averages of the two separate SEC-MALLS injections. Molecular weights have further been plotted vs. number of pulverisation cycles in Fig. 4.4.

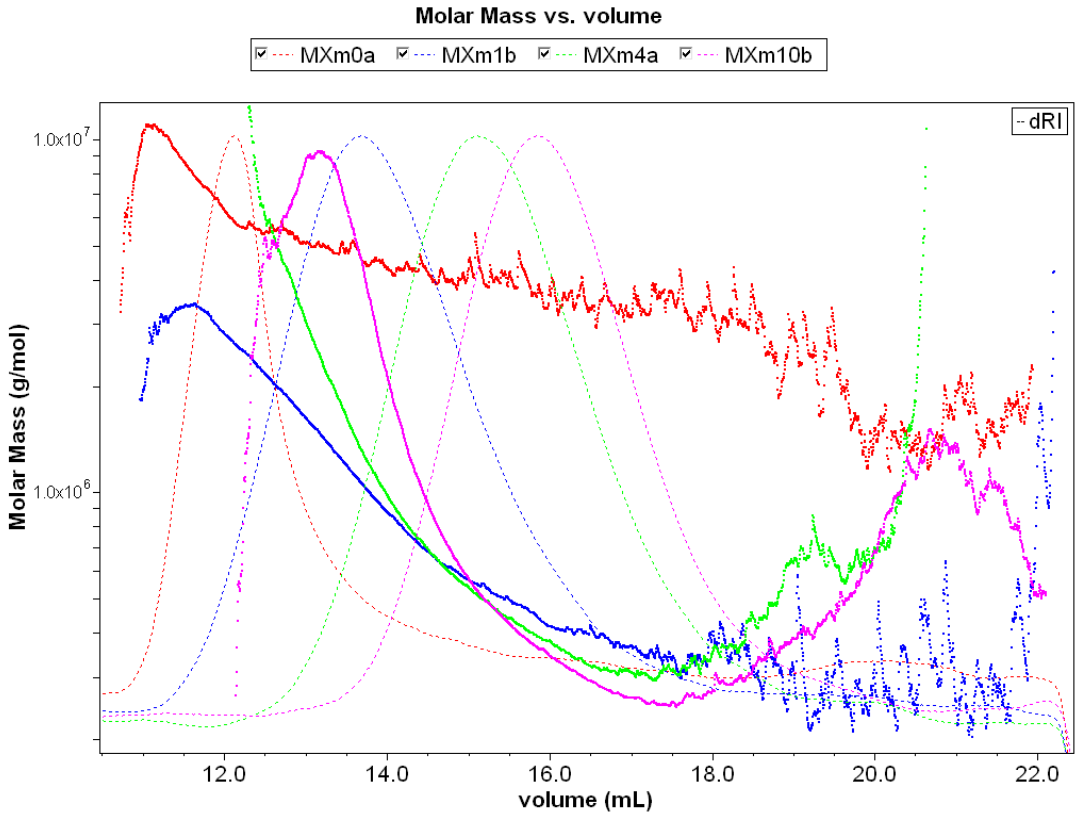

Figure 4.3: Chromatograms and molecular weight distributions for a selection of results from mechanically degraded MX samples. Dashed lines with thinner line widths correspond to the differential refractive index signals, scaled relatively against their respective magnitudes. Data plotted as squares correspond to molecular weights. The SEC columns used were TSK G6000 + G5000 PWXL, and the buffer used was 150 mM $NaNO_3$/10 mM EDTA.

Table 4.6: Weight-average molecular weights for mechanically degraded MX samples obtained by SEC-MALLS. Columns: TSK G6000 + G5000 PWXL.

Sample	**Pulverising cycles**	M_w **(kDa)**
MXm0	0	6514 ± 385
MXm1	1	1080 ± 24
MXm2	2	747 ± 12
MXm3	3	665 ± 10
MXm4	4	632 ± 6
MXm6	6	597 ± 3
MXm10	10	546 ± 4

Values for M_w are means ± uncertainties computed with ASTRA.

Similar to the results obtained from intrinsic viscosity measurements as seen in Fig. 4.2 in Section 4.2.1.1, molecular weight decreases with the number of pulverising cycles. The reduction is by far largest after the first cycle with a 6-fold lowering of M_w. With every subsequent cycle it becomes more difficult to degrade the xanthan polymer. The included trendline suggests that M_w will level off around 400-500 kDa with continued use of this degradation method. This is somewhat disappointing considering that attempts of degradation by using sonication instead have resulted in molecular weights even down to 74 kDa[18]. As mentioned in Section 4.2.1.1, however, the degradation during sonication is largely dependent on polymer concentration[52]. This should therefore be taken into consideration.

Processing of light scattering data in ASTRA was challenging for the undegraded MX sample (0 cycles) as extrapolations during regression analyses were heavily influenced by which detectors were enabled or not. For all samples in Table 4.6, detector 4 measuring a scattering angle of 29.6° was the lowest to be included when performing regression with the second order Berry fit method. Detector 16 with 140.0° was the highest scattering angle to be included, but this was only appropriate for the most degraded samples (pulverised for 6 and 10 cycles). For the other samples, the amount of detectors at higher angles were enabled/disabled after careful consideration.

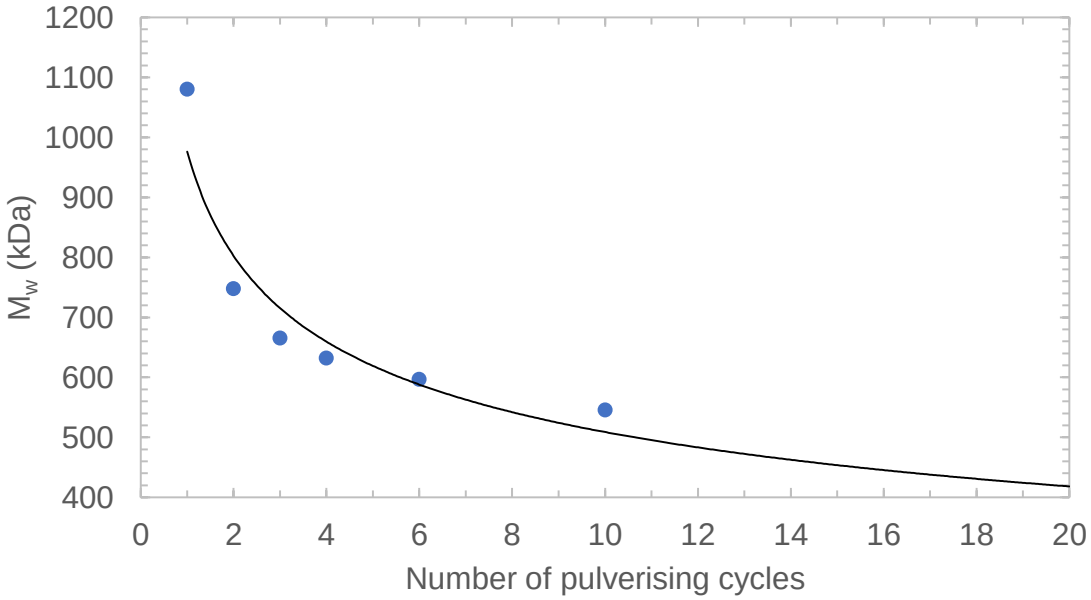

Figure 4.4: Decrease in weight-average molecular weight of MX degraded by a wet pulverising system at a chamber pressure of 210 MPa. The result for the undegraded sample MXm0 has not been included. A power trendline ($R^2 = 0.906$) was used as a guide to the eye and for approximately predicting the outcome of continued degradation with this method. SEC columns: TSK G6000 + G5000 PWXL.

4.2.2.2 Mechanically Degraded XCD

All seven samples originating from the mechanically degraded XCD series were analysed with SEC-MALLS, but only with one single injection per sample. The buffer was the same as for MX ($NaNO_3$/EDTA), but a TSK G6000PW column was used instead of TSK G6000 + G5000 PWXL. The Berry model with fit degree 2 was also used for all samples.

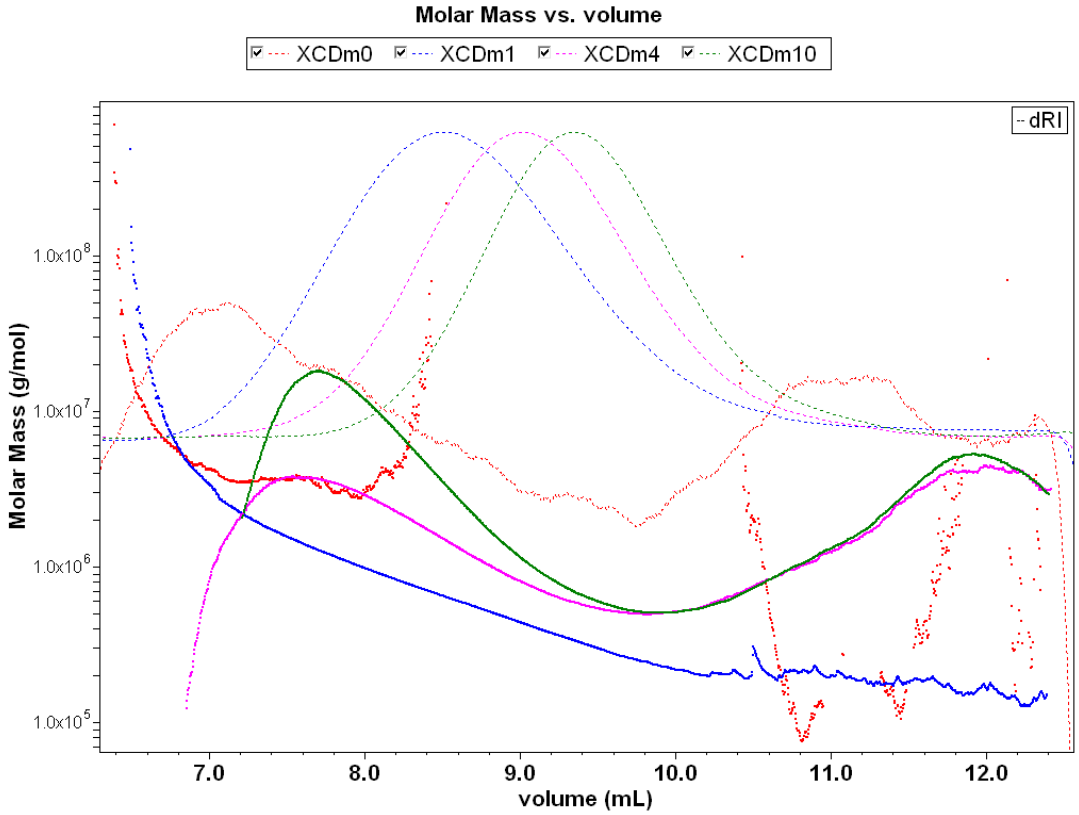

Figure 4.5: Chromatograms and molecular weight distributions for a selection of results from the series of mechanically degraded XCD. Dashed lines with thinner line widths correspond to the differential refractive index signals, scaled relatively against their respective magnitudes. Data plotted as squares correspond to molecular weights. The SEC column used was TSK G6000PW, and the buffer was 150 mM $NaNO_3$/10 mM EDTA.

A selection of chromatograms and molecular weight distributions are presented in Fig. 4.5. For results from all injections, see Fig. C.3 in Appendix C. The concentration profiles (dRI signals) are smooth and as expected for most samples, but for XCDm0 (red dashed curve) it fluctuates inconsistently. As previously mentioned in Section 4.2.1.1, this sample also posed a challenge for capillary viscometry measurements. Before SEC-MALLS analysis, XCDm0 was diluted to a concentration of $c = 31\,\mu g/mL$ in order to be successfully filtrated. This resulted in a low dRI signal intensity and may therefore explain the irregular chromatogram. Nevertheless, the largest dRI peak for XCDm0 appears further to the left than any of the other chromatograms, and the molar mass for its associated peak is of higher magnitude than the case is for the other samples. $M_w = 4923$ kDa calculated for XCDm0 seems therefore like a reasonable value, but the data is of insufficient quality to state this for certain.

Table 4.7: Weight-average molecular weights for mechanically degraded XCD samples obtained by SEC-MALLS. Column: TSK G6000PW.

Sample	Pulverising cycles	M_w (kDa)
XCDm0	0	4923 ± 350
XCDm1	1	721 ± 9
XCDm2	2	542 ± 4
XCDm3	3	1167 ± 5
XCDm4	4	1113 ± 6
XCDm6	6	1242 ± 5
XCDm10	10	1414 ± 4

Values for M_w are means ± uncertainties computed with ASTRA.

The same cannot be said for the other samples. As seen in Table 4.7, M_w decreases from 4923 kDa for XCDm0 to 542 for XCDm2, but then starts to increase up till 1414 kDa for XCDm10. The same data has been plotted in Fig. 4.6. This might be a result of an even more extensive agglomeration than what was observed for MX, or possibly due to the column TSK G6000PW being used. What is surprising is that the dRI peaks are still shifted towards higher elution volumes for every successive sample. Moreover, the value for R_w decreases with pulverising cycles according to Table C.4 in Appendix C. These results remain to be explained, and the experiment should probably be repeated, possibly with a different solvent and/or column.

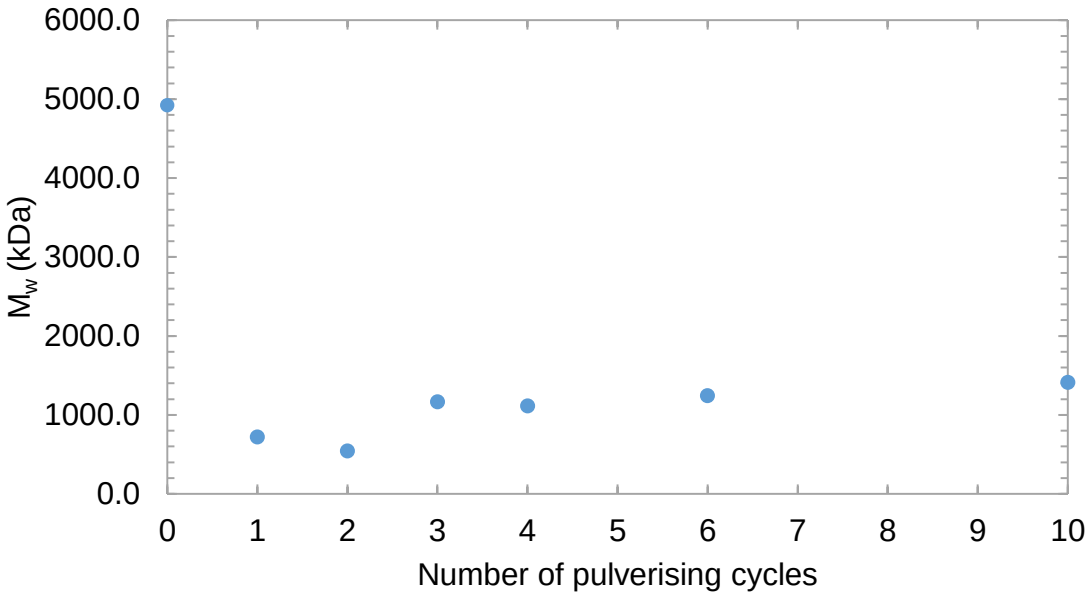

Figure 4.6: Change in weight-average molecular weight of XCD degraded by a wet pulverising system at a chamber pressure of 210 MPa. SEC column: TSK G6000PW.

4.2.2.3 The Mechanism of High Shear Degradation

A previous study by Lagoueyte & Paquin (1998)[54] confirms that xanthan degradation by microfluidisation causes a decrease in dynamic viscosity and pseudoplastic behaviour. However, there is no fully accepted explanation of how this degradation occurs. In the same article it was postulated that the high shear stress causes a transition from the xanthan molecule's double-stranded, ordered conformation towards a single-stranded, disordered conformation. The degree of change in conformation was therefore suspected to increase with higher pressure and number of passes.

The purpose of this project was to study how xanthan in its *ordered* conformation would be degraded by high pressure mechanical shear. Thus, any ordered-disordered transitions were unwanted during pulverisation with the Star Burst Mini. It was believed that the conformation would not change as long as the temperature was kept lower than the point of transition, which is approx. 80 °C in pure water[20]. The transition temperature was probably higher for the experiments in this project as the greater ionic strength of the 150 mM $NaNO_3$/10 mM EDTA solvent was expected to contribute in stabilising the ordered conformation. Initial temperature testing with xanthan filtrate showed that the temperature increased from approx. 25 °C to 50 °C after one pulverising cycle. It was therefore assumed that the conformation transition would be avoided as long as the samples were allowed to cool down sufficiently in an ice bath before continuing with the next pulverising cycle. Although this practice was carefully applied when performing the degradation of all the samples, one can still not be certain that the xanthan was always in its ordered conformation. It could therefore be interesting to try the same experiments under conditions where xanthan is expected to be in its *disordered* conformation, and then compare the results with those obtained in this project. One way of achieving this is to acidify the xanthan and then dissolve it in dimethyl sulfoxide (DMSO) prior to degradation; using a procedure previously published by Fantou et al. (2017)[8].

4.2.3 Determination of Molecular Shape

As explained in Section 2.4.5 in Chapter 2, the Mark-Houwink-Sakurada equation (Eq. 2.16) gives the relation between the intrinsic viscosity, molecular weight and the molecular shape of a polymer. By combining the results from Tables 4.2 and 4.6, the MHS plot for MX in Fig. 4.7a was created. Note that data from MXm0 were excluded due to its high M_w and $[\eta]_{avg}$ compared to the rest of the samples. An MHS plot was not made for XCD due to the results for M_w from SEC-MALLS analyses not being consistent with the values for $[\eta]_{avg}$ obtained from capillary viscometry.

The power trendline included in the diagram is analogous to the MHS equation. The exponent a in the equation describing the trendline is approx. 1.7, and thus close to the value of 1.8 for an ideal rigid rod[3]. This suggests that MX behaves as a semi-rigid rod for this range of molecular weights. However, it must be stressed that the results were obtained under non-ideal conditions, as $[\eta]_{avg}$ were obtained at a shear rate of 2500 s^{-1} and not 0. More data are also needed for the interval between 800 and 1000 kDa.

In Fig. 4.7b the same results as in Fig. 4.7a are plotted together with data obtained from Sato & Fujita (1984)[18]. Unlike in this project, they were using values for $[\eta]_{\dot{\gamma}=0}$. Their results give a power regression curve with exponent $a = 1.2$ for samples with M_w ranging from 362-1420 kDa. This is a lower value than the one obtained for MX in

this project, suggesting that xanthan is rather somewhat more flexible for this range of molecular weights than the results for MX indicate.

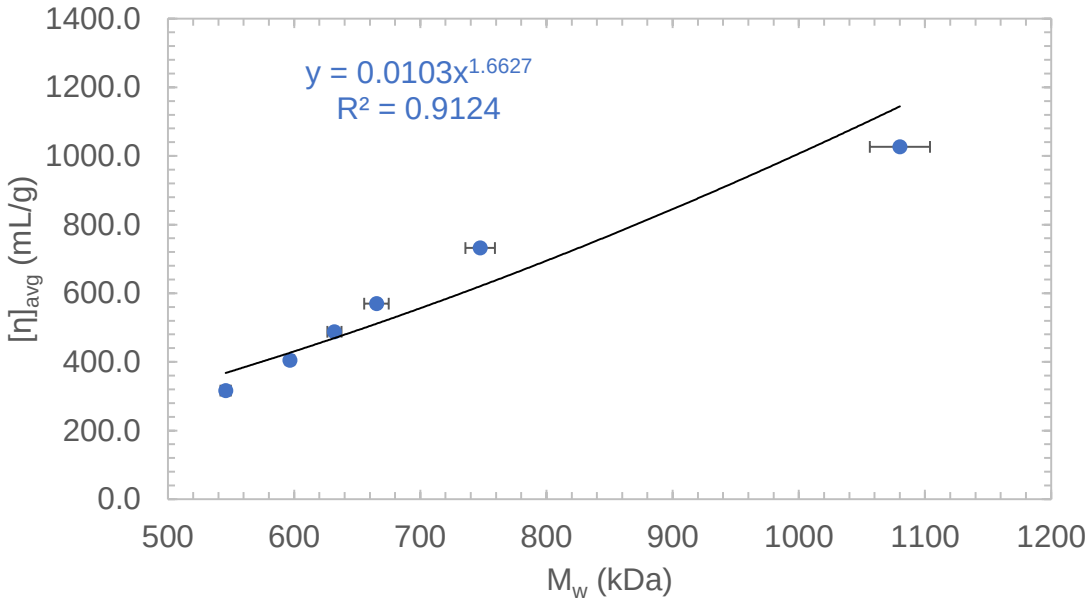

(a) Mark-Houwink-Sakurada (MHS) plot of MX.

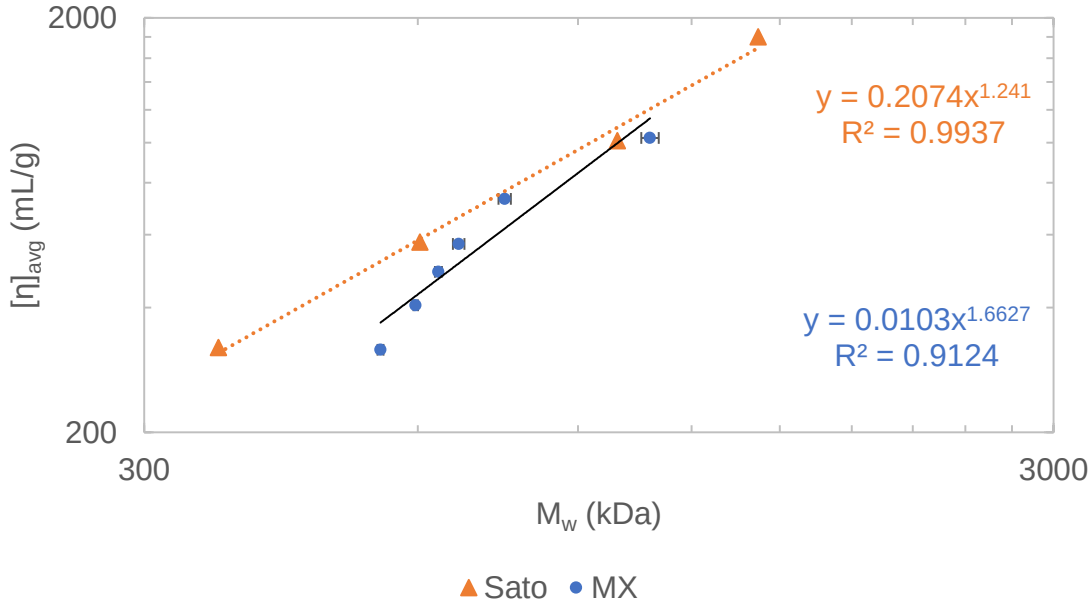

(b) Double-logarithmic MHS plot of MX compared with results from Sato & Fujita.

Figure 4.7: Mark-Houwink-Sakurada (MHS) plots of MX and selected results from Sato & Fujita (1984)[18]. The plot for MX was created by combining the results from capillary viscometry and SEC-MALLS measurements. MXm0 has been excluded. The power trendlines are analogous to the MHS equation (see Eq. 2.16 in Section 2.4.5). Intrinsic viscosity data were obtained at shear rate $\dot{\gamma}$=2500 s^{-1} for MX and $\dot{\gamma}$=0 s^{-1} for the results from Sato & Fujita.

4.3 Rheology of MX and XCD

The dependence of dynamic viscosity on shear rate for undegraded MX and XCD in the ordered conformation was studied during the master's project by using a Kinexus ultra+ rotational rheometer. Upon preparation of samples for capillary viscometry and SEC-MALLS experiments (Sections 4.2.1.1 and 4.2.2.2) it was found that undegraded XCD was difficult to dissolve in the conventional $NaNO_3$ (150 mM)/EDTA (10 mM) buffer. Thus, it was decided to use $NaHCO_3$ (25 mM)/NaOH (19.1 mM) (pH 10.8) as a solvent during rheometry as it had previously been shown to be effective for obtaining a homogeneous mixture when dissolving XCD (B.E. Christensen, personal communication). The same solvent was used for MX in order to have similar conditions for both xanthans. Several concentrations of MX and XCD were prepared, ranging from 4 mg/mL down to 62.5 µg/mL. For concentrations of 1.0 mg/mL and below, data were acquired for shear rates between 10^{-2} and 10^{3} s^{-1}. The lower limit was adjusted to 10^{-3} s^{-1} for samples of higher concentrations. Four parallel measurements were performed for each sample.

4.3.1 Flow Curves

The dependence of shear viscosity on shear rate for MX and XCD at different concentrations is shown in Fig. 4.8. The plotted data are avg. values based on three of the four parallel measurements. The first parallel was neglected for all samples due to the low shear rate viscosities, i.e. data for the first decade of shear rates, being discrepant with the results of the other three parallels. This is believed to be a consequence of the xanthan solution not being properly distributed in the interface between the cone and plate when the cone was first lowered to be in contact with the sample. It only seemed to affect the first measurements at low shear rates, however, as the sample would spread out on the plate as the rotational speed increased. The cone was kept in contact with the sample when performing the following three parallels, and was only raised when changing samples.

The viscosity-shear rate curves display the shear thinning behaviour which is common for solutions containing rod-like polymers[3]. For lower shear rates the viscosity appears to be rather constant and thus within the Newtonian range. However, above a critical shear rate $\dot{\gamma}_c$ the viscosity becomes shear rate dependent and tends to decrease substantially. The value of $\dot{\gamma}_c$ seems further to be concentration-dependent, as the cut-off point occurs at lower shear rates as concentration increases. Similar results were obtained by Milas, Rinaudo & Tinland (1985)[55]. Their results further illustrate how viscosity always is dependent on molecular weight, and that $\dot{\gamma}_c$ decreases with increasing molecular weight.

The curves in Fig. 4.8 display an unexpected increase in viscosity when approaching shear rates below 0.01 s^{-1} (for 1.0 mg/mL this is seen already below 0.1 s^{-1}). Due to the logarithmic vertical axis, it is not necessarily evident that this applies to all of the samples, but it has been confirmed by closer examination. These observations are not in accordance with known theory; suggesting that the results for the first decade of measurements are either inaccurate or caused by artefacts. The vertical, dashed lines have therefore been included to separate unreliable data from the more credible. It would have been interesting to try the same experiments in reverse, i.e. going from high to low shear rates, to study if there would have been any significant differences.

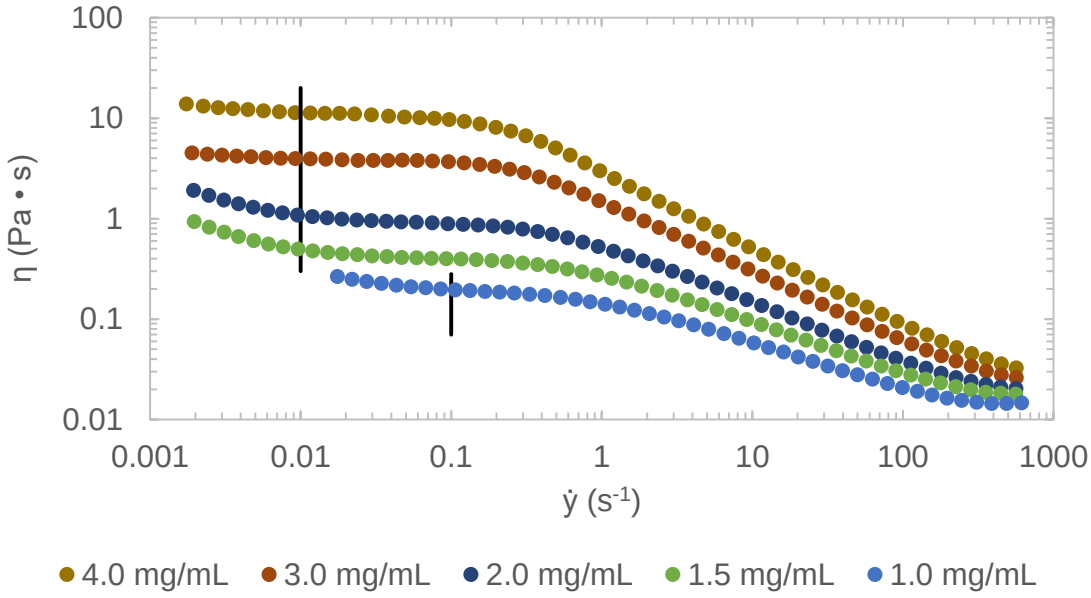

(a) Results for MX. $M_w = (6.5 \pm 0.4) \times 10^6$ Da.

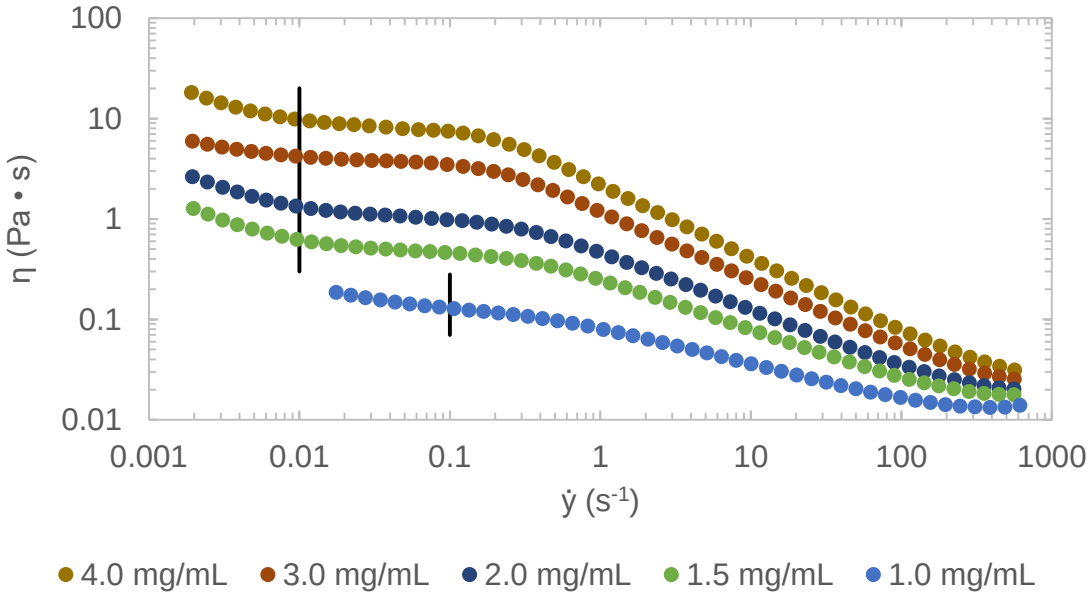

(b) Results for XCD. $M_w = (4.9 \pm 0.4) \times 10^6$ Da.

Figure 4.8: Double-logarithmic plots displaying viscosity-shear rate curves for different concentrations of **(a)** MX and **(b)** XCD in $NaHCO_3$ (25 mM)/NaOH (19.1 mM). $T = 25\,°C$. The vertical, black lines have been included to separate the more unreliable measurements to the left from the rest of the data.

Measurements for concentrations lower than 1.0 mg/mL were also performed and can be found in Appendix D. These have been left out from Fig. 4.8 as all of them were considered implausible. Too dilute solutions of viscosities similar to that of water could not be measured properly with the Kinexus ultra+ rotational rheometer. This was confirmed by doing the same experiment with the pure solvent: $NaHCO_3$ (25 mM)/NaOH (19.1 mM) in MQ water. The results suggested that the solvent had about 10 times larger viscosity than water ($\eta_{H_2O,25\,°C}$=0.89 mPa · s), which was rather doubtful.

4.3.2 Comparison of MX and XCD

Viscosity-shear rate curves for both MX and XCD (3.0 and 1.0 mg/mL) are plotted together in Fig. 4.9 to compare the two xanthans. If neglecting the measurements below $\dot{\gamma} = 0.01\,\mathrm{s}^{-1}$, the curves corresponding to each of the concentrations seem similar in shape, with XCD displaying slightly lower viscosity than MX throughout most of the shear rate range.

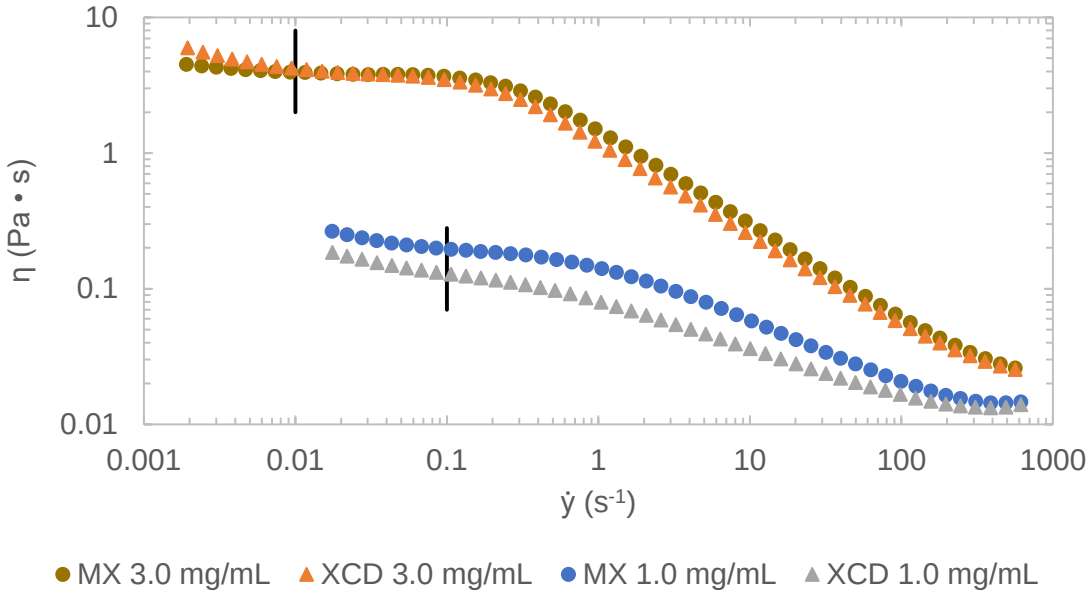

Figure 4.9: Double-logarithmic plot comparing viscosity-shear rate curves for selected concentrations of MX and XCD in $NaHCO_3$ (25 mM)/NaOH (19.1 mM). $T = 25\,°C$. The vertical, black lines have been included to separate the more unreliable measurements to the left from the rest of the data.

The differences in viscosity between MX and XCD solutions seem larger for the more dilute concentration of 1.0 mg/mL, although the logarithmic vertical axis can potentially be deceptive in this aspect. However, for shear rates above $0.1\,\mathrm{s}^{-1}$, calculations show that the viscosity of 1.0 mg/mL MX is on average 1.6 times higher than for 1.0 mg/mL XCD. For 3.0 mg/mL this ratio is reduced to 1.1, suggesting that molecular weight has increasing influence on shear viscosity the more dilute a solution is. Even so, further studies are required before stating anything conclusive.

4.4 Chemical vs. Enzymatic Degradation of Xanthan

In order to analyse the structure of xanthan by NMR, it has to be depolymerised to get oligomeric molecules that provide spectra of sufficient resolutions. It has previously been indicated that a depolymerisation protocol using H_2O_2 in basic conditions causes removal of acetyl groups from the xanthan side chains[24]. Thus, in this work it was decided to compare the traditional chemical method with one using cellulases instead. For describing the course of degradation, the number average degree of polymerisation (DP_n) was calculated based on spectrophotometric absorbance values for xanthan samples that were degraded either chemically or enzymatically for different amounts of time. Some of

the degraded samples were further selected for analysis by ^{1}H-NMR. All results presented in the following sections were obtained during the master's project.

4.4.1 Estimation of DP_n by Spectrophotometry

The DP_n, i.e. the average number of repeating units (RU), of various xanthan samples after either chemical degradation with H_2O_2/NaOH or enzymatic degradation were estimated using spectrophotometry in combination with the bicinchoninic acid (BCA) assay. A standard curve for absorbance at 560 nm as a function of the concentration of reducing ends was generated using D-glucose standards of known concentrations (see Appendix E). Reducing end concentrations in the xanthan samples were then determined from the function of the standard curve. Values for M_n could then be calculated for each sample according to Eq. 2.25 in Section 2.6.2. As the substitution degrees of of acetyl and pyruvyl were unknown at the time, the avg. molecular weight of the xanthan repeating unit was assumed to be $M_{RU} = 970$ Da for all samples. This number was acquired from Section 4.2.17 in B.E. Christensen (2016)[3] and corresponds to the molar mass of a fully pyruvated and partially acetylated xanthan RU. The DP_n of each sample was thus calculated according to Eq. 2.26, while the degree of chain scission α was obtained by Eq. 2.27.

4.4.1.1 Chemical Degradation

MX and XCD were degraded by treating the samples with H_2O_2/NaOH (4.8 mM/54.3 mM) at 80 °C (water bath) for 1 hour. One half of each of the chemically degraded xanthans were further dialysed against MQ water. All samples were then analysed by the BCA assay and spectrophotometry. The results are presented in Table 4.8.

Table 4.8: DP_n values (obtained by the BCA assay) for undegraded and chemically degraded MX and XCD. Values were acquired using standard curve 2 (Fig. E.1b in Appendix E) unless specified otherwise.

Sample	Degraded	Dialysed	DP_n	α
MX	No	No	155*	0.006
	Yes	No	1†	0.784
	Yes	Yes	32	0.031
XCD	No	No	17‡	0.059
	Yes	No	1†	0.819
	Yes	Yes	19	0.052

* $DP_n = 177$ in a previous experiment (Table E.1).
† Obtained using standard curve 1 (Fig. E.1a).
‡ $DP_n = 50$ in a previous experiment (Table E.1).
See Appendix E for details about other experiments.

A conspicuous observation is the difference between degraded samples before and after dialysis; i.e. the increase in DP_n from 1 to 32 for MX and from 1 to 19 for XCD. Without

this step one could therefore have erroneously concluded that the xanthans had almost been broken down to monosaccharides. However, after dialysis (followed by freeze drying) it becomes clear that there still is at least some oligomeric material left of the samples. It is believed that the large number of reducing ends is a consequence of the chemical reactants attacking the side chains[6, 24]. Further discussion on this topic can be found in Section 4.4.2.3.

Considering the obtained DP_n values it is evident that MX has been broken down, since the degree of polymerisation has been reduced considerably when comparing the undegraded and the degraded samples. Even so, an initial DP_n of 155 would indicate that $M_n \approx 150$ kDa. This is more than one order of magnitude less than the corresponding SEC-MALLS results for the undegraded sample MXm0 would indicate ($M_n \approx$ 4000-7000 kDa, see Table C.1 in Appendix C). The result for the undegraded XCD sample in Table 4.8 indicates that its DP_n is similar to the degraded one, which is rather impossible. One explanation could be that an experimental error has caused an underestimation of the real mass concentration, thus yielding a low value for the degree of polymerisation. From a previous BCA experiment the DP_n was estimated to be equal to 50 (see Appendix E), which seems a little more reasonable. Even so, this other result would indicate $M_n \approx$ 50 kDa, which is still almost two orders of magnitude less than the SEC-MALLS result suggested for the undegraded sample XCDm0 ($M_n \approx 4000$ kDa, see Table C.3 in Appendix C). The BCA assay seems to be too sensitive for estimating DP_n of polymers with very high molecular weights, and this should therefore be kept in mind when reading further.

4.4.1.2 Enzymatic Depolymerisation

Calculated values for DP_n and α for xanthan samples depolymerised enzymatically can be found in Table 4.9. The *Time* column refers to the duration each sample has been stored in a 60 °C water bath. Results have also been included for undegraded samples that were not added any cellulases. MX and XCD were depolymerised using BGI (1:100), EG (1:1000) and BGI (1:1000); where the numbers in parentheses denote dilutions from stock concentration before adding enzymes to the xanthan solutions. Only BGI (1:100) was used for xan0614-3. Dialysis was not carried out for any of the samples.

Fig. 4.10a shows a plot of α vs. time for MX samples throughout degradation. It is observed that the rate is fast in the beginning before gradually declining and seemingly reaching a plateau after 24 hours. BGI and EG with the same dilution (1:1000) behave similarly. BGI (1:100) causes faster degradation, reaching DP_n values that are lower by about 20 compared with the more dilute enzyme solutions. By using BGI (1:100) the degree of polymerisation was reduced (from 155 to 79) by only adding the enzyme without incubating the sample at 60 °C. This result was a bit surprising since xanthan was thought to be susceptible to enzymatic degradation only when in its disordered conformation, which was believed to require an elevated temperature in addition to the absence of salt. However, *all* samples were additionally exposed to 75 °C for 30 min during the BCA assay. Some additional degradation could therefore have happened in this procedure, given that the enzymes were not denatured during freeze-drying. For samples where the enzymes were diluted 1:1000, degrees of polymerisation were actually found to be somewhat *higher* for non-incubated samples (DP_n of 181 for EG and 189 for BGI) compared with the sample with no added enzyme ($DP_n = 155$). This is opposite to the case with BGI (1:100). As mentioned previously in Section 4.4.1.1, however, the results for undegraded samples are

Table 4.9: DP_n values (obtained by the BCA assay) for undegraded and enzymatically depolymerised MX, XCD and xan0614-3.

		MX†		XCD†		xan0614-3‡	
Enzyme	**Time (h)**	**DP_n**	α	**DP_n**	α	**DP_n**	α
No enzyme*	0	155	0.006	17	0.059	89	0.011
BGI (1:100)	0	79	0.013	4	0.271	14	0.071
	1	62	0.016	2	0.577	4	0.285
	3	46	0.022	2	0.512	2	0.446
	24	26	0.039	2	0.490	2	0.491
	48**	25	0.039	1	0.716	2	0.451
EG (1:1000)	0	181	0.006	14	0.071		
	1	76	0.013	12	0.086		
	3	63	0.016	9	0.110		
	24	42	0.024	5	0.184		
	48	43	0.023	3	0.296		
BGI (1:1000)	0	189	0.005	12	0.087		
	1	84	0.012	6	0.176		
	3	68	0.015	4	0.232		
	24	34	0.029	2	0.565		
	48	47	0.021	2	0.637		

† Results obtained with standard curve 2 (see Fig. E.1b in Appendix E).
‡ Results obtained with standard curve 3 (see Fig. E.2).
* Same undegraded MX and XCD samples as in Table 4.8.
** The final sample was taken after 44 hours for xan0614-3.

rather dubious as they do not correspond with M_n for undegraded MXm0 and XCDm0 found with SEC-MALLS (see Tables C.1 and C.3 in Appendix C).

A plot visualising α vs. time for XCD samples is given in Fig. 4.10b. The results imply that XCD has been broken down to short oligomers very fast, though $DP_n = 17$ of the sample with no added enzyme is also very small to begin with (see Section 4.4.1.1 for a previous discussion of this result). Impurities in the XCD sample were suspected to be the reason for estimating such low DP_n values. It was therefore decided to do the same procedure with xan0614-3.

DP_n for xan0614-3 samples are higher than for corresponding values for XCD degraded with BGI (1:100). This is rather peculiar considering that it initially should be more degraded; xan0614-3 is actually XCD that has been sonicated for 30 min and purified thereafter[24]. This might indicate that there in fact is a background coming from impurities in XCD which has been subdued after purification. Then again, results for xan0614-3 were obtained with a different standard curve, which is considered to be more certain than the one used for MX and XCD. The reason for this is that a completely new standard curve was generated for xan0614-3, while the one used for MX and XCD had

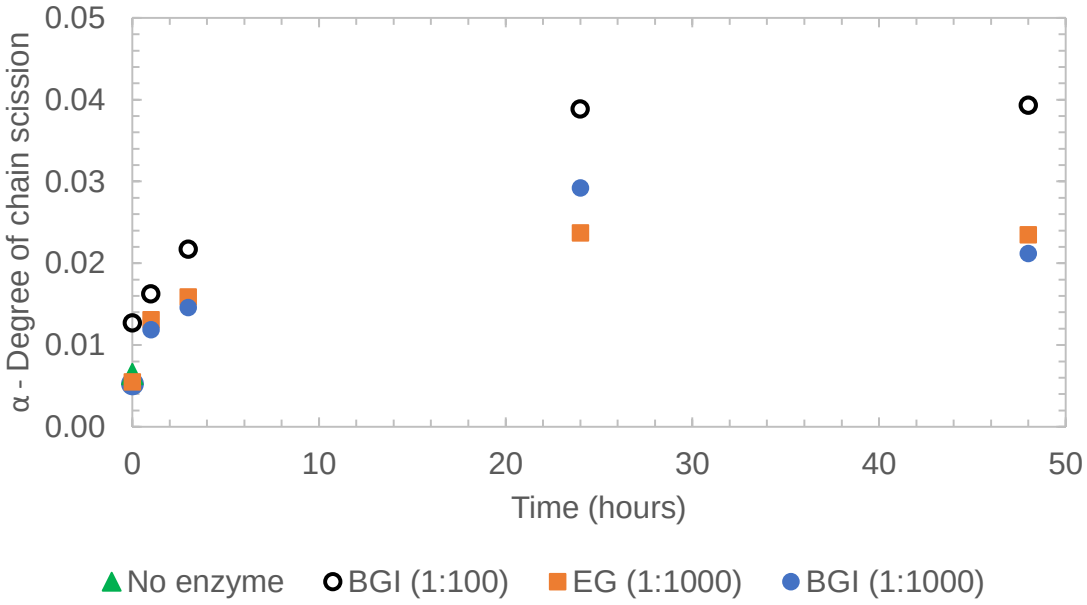

(a) Results for MX samples

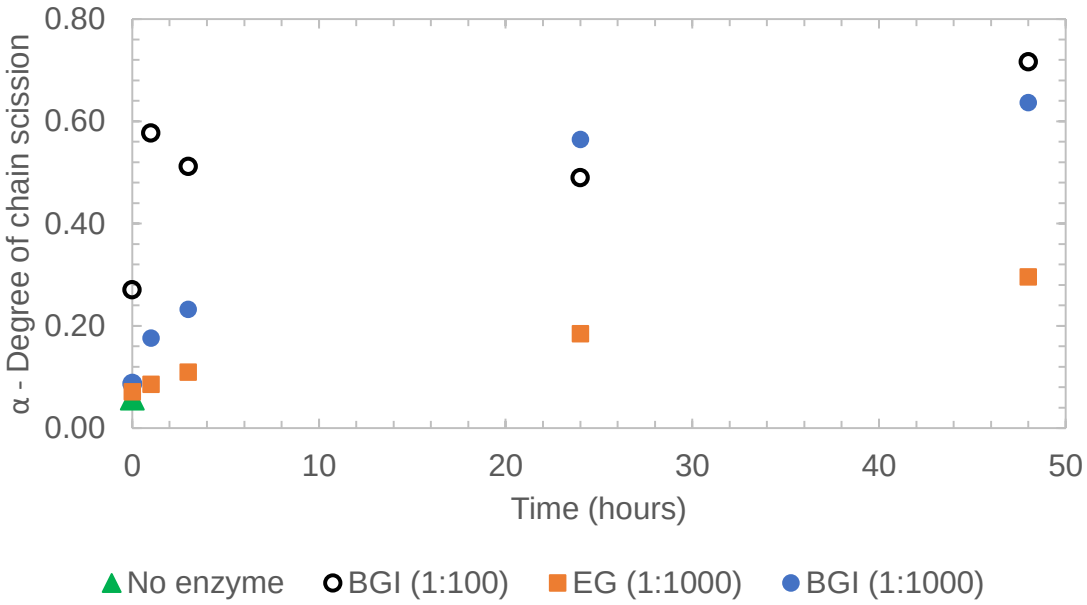

(b) Results for XCD samples

Figure 4.10: Degree of chain scission plotted vs. time of incubation at 60 °C during enzymatic depolymerisation of MX and XCD.

to be created by modifying result obtained from a previous BCA experiment. This has been explained further in Appendix E). A plot visualising α vs. time for xan0614-3 is presented in Fig. 4.11.

It appears that xan0614-3 still has been quickly depolymerised when using BGI (1:100), with DP_n decreasing from 89 to 14 even without incubation at 60 °C. The explanation could be the same as mentioned previously for MX; i.e. a substantial part of the degradation occurs during the 30 min long 75 °C water bath of the BCA assay procedure. Yet, this does not seem to suffice in justifying the extreme decrease in DP_n for both xan0614-3 and XCD. It is therefore suspected that the cellulases have been able to digest the

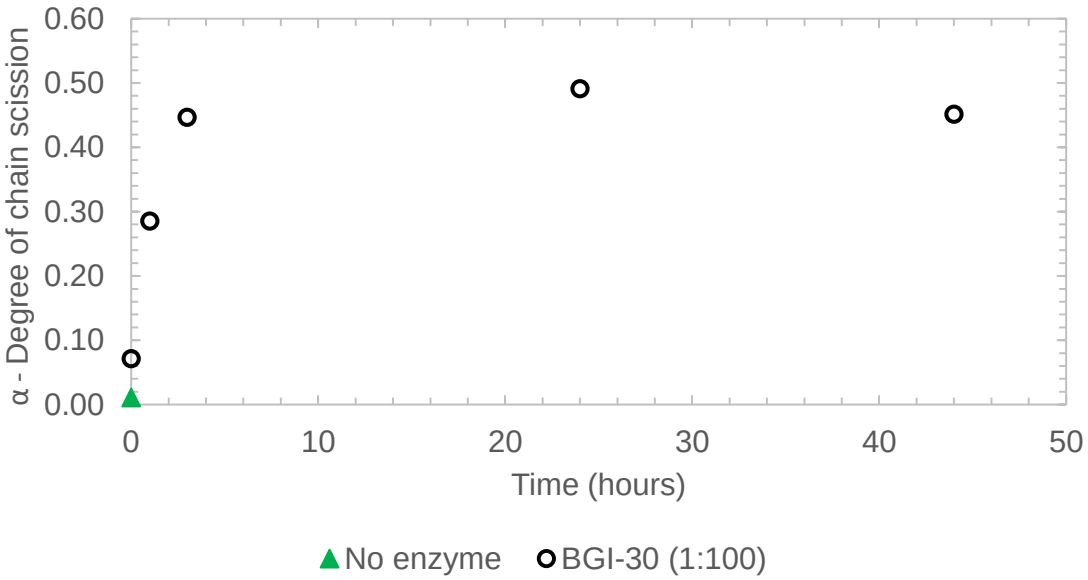

Figure 4.11: Degree of chain scission α plotted vs. time of incubation at 60 °C during enzymatic depolymerisation of xan0614-3.

xanthans to some degree without needing incubation at 60 °C. One explanation could be that enzymatic degradation is possible when xanthan is in its ordered conformation, even though Kool et al. (2013)[27] have concluded that the disordered conformation is necessary. Another explanation, which is deemed more likely, is that the samples are not *completely* ordered. It has been shown that e.g. the degree of substitutions of pyruvyl and acetyl can influence the xanthan conformation[56, 57]. Consequently, there could be some sites along the polymer backbone that are accessible to the cellulases even when the temperature is not elevated. The results obtained here, however, are not sufficient to state anything conclusive.

Data for the first three hours of enzymatic degradation of MX have been plotted again in Fig. 4.12a. Linear trendlines for each data set have also been included. All three treatments seem to follow a first order depolymerisation reaction with a similar *pseudo* first order rate constant k; which have been calculated for each respective cellulase treatment (see Table 4.10) according to Eq. 2.28 in Section 2.6.2. Corresponding calculations were not done for XCD and xan0614-3 due to the degrees of chain scission being very large ($\alpha \gg 0.02$).

As the rate constants in Fig. 4.12a are similar, it is implied that neither the enzyme type nor the concentration influence the early stages of depolymerisation significantly. However, the result here for MX degraded with BGI (1:100) does not take into account the large decrease in DP_n that occurred apart from incubation at 60 °C; which in fact did indicate that the 10-fold higher concentration causes faster degradation (see Table 4.9 and the previous discussion). The rate constant for BGI (1:100) is therefore suspected of being too low. An attempt to correct this was done by substituting α at 0 hours with the result for the undegraded MX sample with no added enzyme, yielding the modified "treatment" BGI (1:100)* (see Fig. 4.12b). Regression analysis of this data set resulted in a larger value for k (included in Table 4.10).

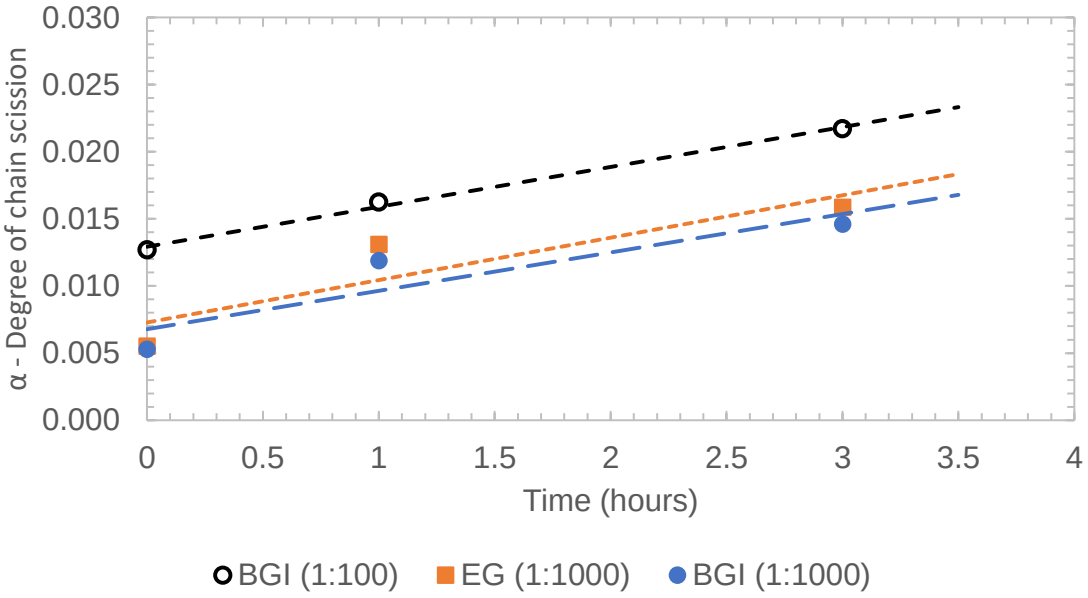

(a) Linear regressions for samples with enzymes. BGI (1:100): $y = 0.0030x + 0.0129$, $R^2 = 0.995$; EG (1:1000): $y = 0.0032x + 0.0073$, $R^2 = 0.809$; BGI (1:1000): $y = 0.0029x + 0.0068$, $R^2 = 0.829$.

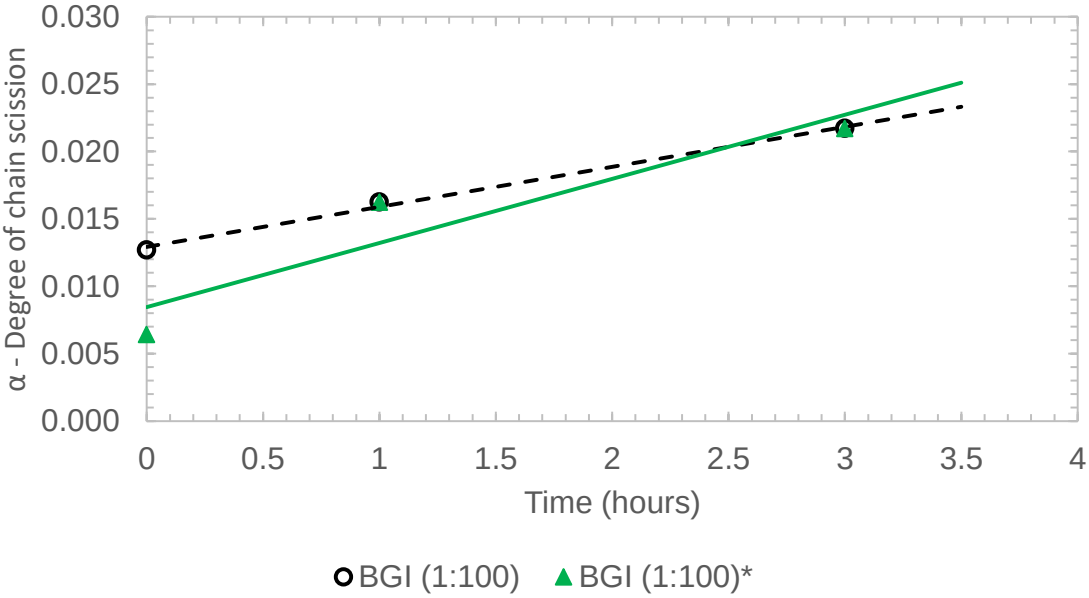

(b) Taking into account the decrease in DP_n that occurs apart from the degradation during incubation at 60 °C. BGI (1:100)*: $y = 0.0048x + 0.0085$, $R^2 = 0.881$.

Figure 4.12: Degree of chain scission plotted vs. the first three hours of incubation at 60 °C during enzymatic depolymerisation of MX.

Table 4.10: The *pseudo* first order rate constant during the earliest stage of enzymatic degradation of xanthan MX.

Treatment	$\boldsymbol{k}$ (h^{-1})
BGI (1:100)	2.97×10^{-3}
BGI (1:100)*	$4.76 \times 10^{-3*}$
EG (1:1000)	3.16×10^{-3}
BGI (1:1000)	2.86×10^{-3}

* Takes into account the decrease in DP_n that occurs apart from the degradation during incubation at 60 °C.

4.4.2 Structural Analysis by ^{1}H-NMR

A selection of xanthan samples, degraded either enzymatically with BGI or chemically with H_2O_2/NaOH, were studied using ^{1}H-NMR at 400 MHz and 80 °C. All spectra can be found in Appendix F together with details about sample preparations. Even though TSP was not added for defining the exact position at 0 ppm, centring of all spectra at 1608.52 Hz resulted in peak locations that were comparable to those found in the literature[7, 8].

4.4.2.1 Peak Annotations

An example of a typical ^{1}H-NMR spectrum of degraded xanthan can be found in Fig. 4.13. Annotation of peaks were done by comparing with results from Roy et al. (2014)[7] and Rinaudo et al. (1985)[49]. Peaks at 1.45 and 2.14 ppm have been attributed to the methyl groups of bound pyruvyl and acetyl, respectively. A significantly smaller peak corresponding to free acetate is visible at 1.89 ppm. The more deshielded signal at 5.21 ppm originates from the equatorial anomeric proton of the inner mannopyranosic unit (H-1 α-D-man).

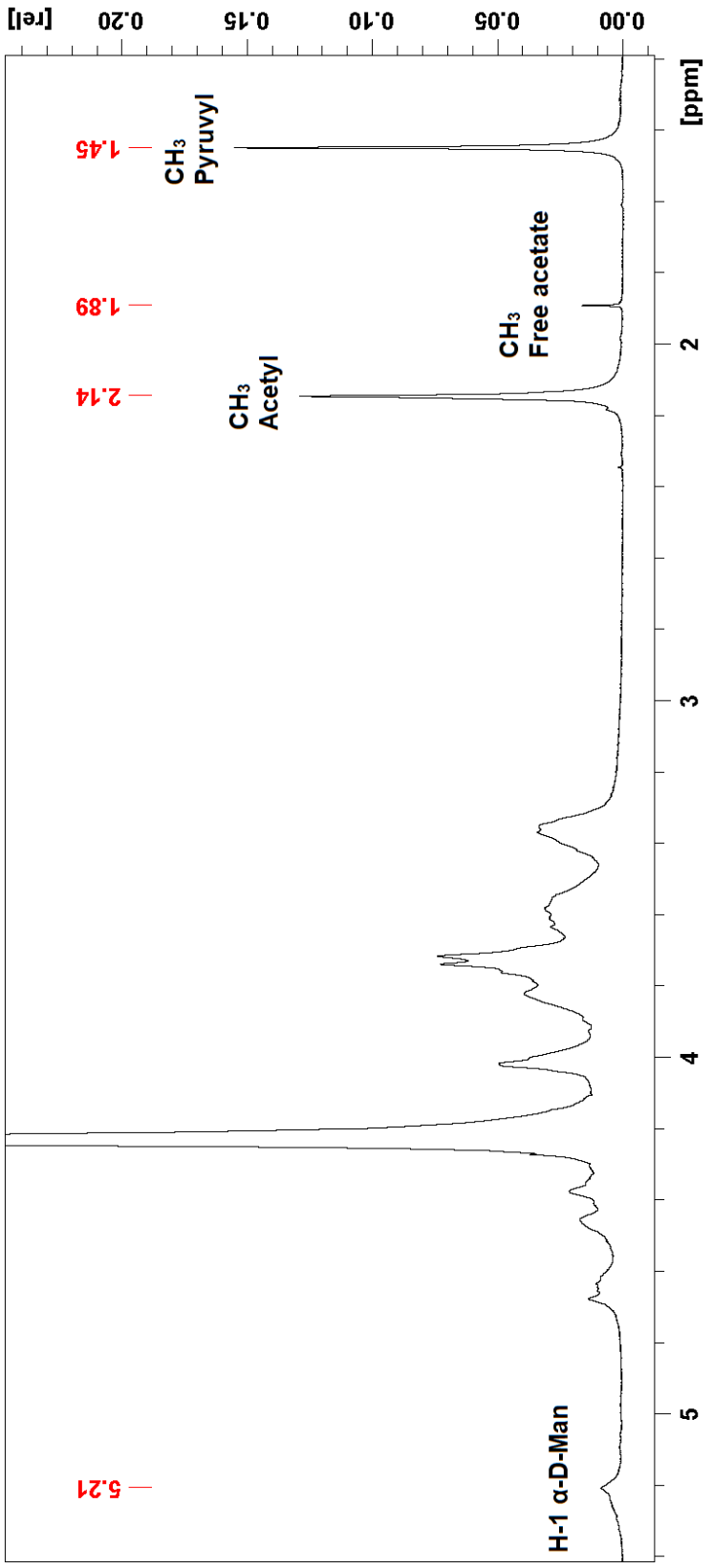

Figure 4.13: ^{1}H-NMR spectrum for MX degraded with BGI (1:100) for 24 h of incubation at 60 °C with labelled peaks of interest. Obtained with a Bruker Avance III HD 400 MHz spectrometer using a 5 mm SmartProbe. $T = 80$ °C during measurements.

For extremely degraded samples the spectra are more resolved, with new peaks becoming distinguishable. Fig. 4.14a shows the full spectrum for xan0614-3 ($DP_n = 2$ from BCA assay). Instead of a broad peak around 5.21 ppm representing H-1 α-D-man as in Fig. 4.13, there are four peaks in the range 5.21-5.33 ppm. This area has been enlarged in Fig. 4.14b. The clean doublet around 5.22 ppm ($^3J = 3.76$ Hz) is believed to stem from the anomeric proton of α-D-glucopyranose (H-1 α-Glc) on the reducing end, according to Cheetham & Mashimba (1992)[58]. Such a signal would indeed require very low DP_n to become visible. The apparent doublet around 5.31 ppm ($^3J = 10.68$ Hz) is regarded as the resonance from H-1 α-D-man, which has increased in quality and shifted down-field compared with the less degraded sample in Fig. 4.13. Similar results were obtained for XCD ($DP_n = 2$).

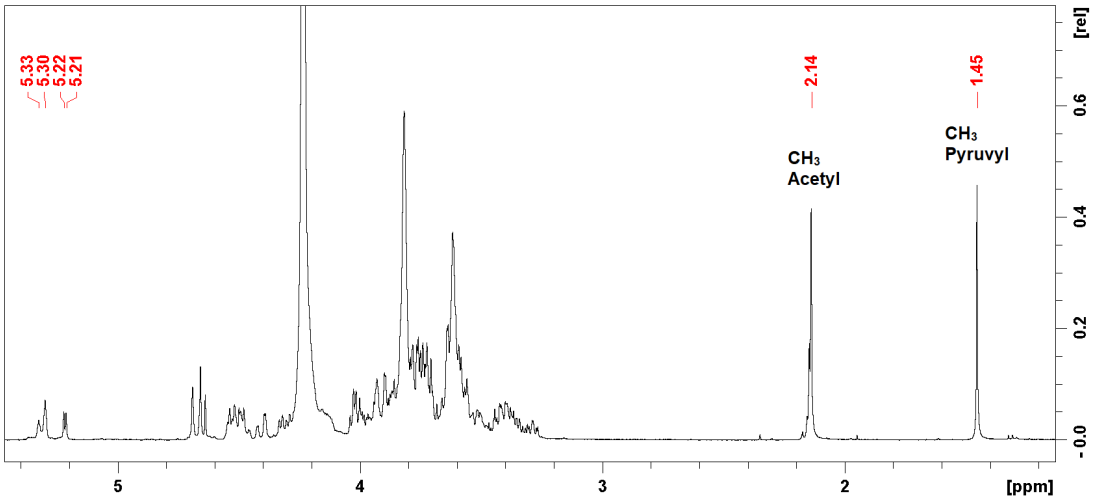

(a) Full spectrum overview with labelled acetyl and pyruvyl signals.

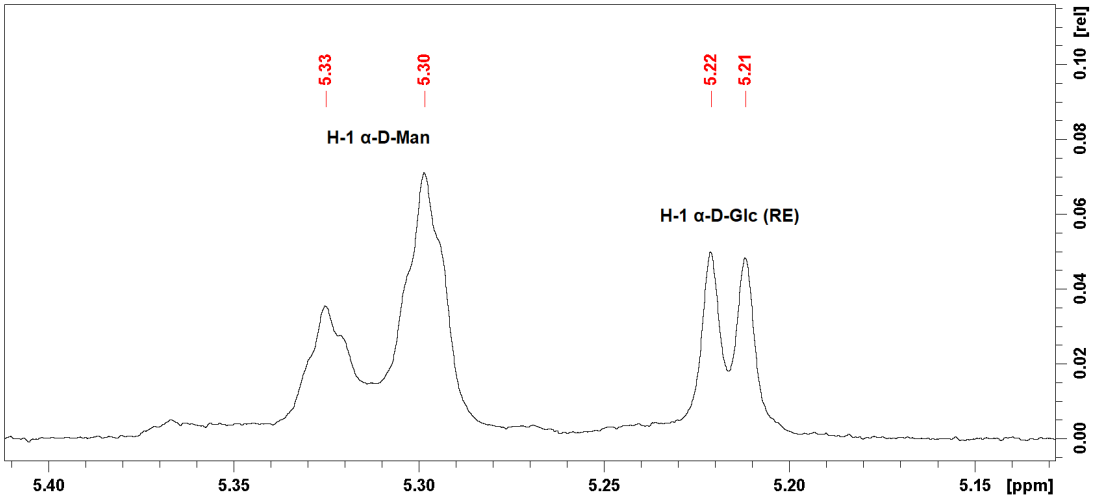

(b) Enlarged area showing anomeric proton signals from α-D-man and reducing end α-D-Glc.

Figure 4.14: ^{1}H-NMR spectrum for xan0614-3 degraded with BGI (1:100) for 24 h of incubation at 60 °C with labelled peaks of interest. Obtained with a Bruker Avance III HD 400 MHz spectrometer using a 5 mm SmartProbe. $T = 80$ °C during measurements.

4.4.2.2 Degree of Substitution of Acetyl and Pyruvyl

By integrating resonance signals from the methyl group of acetyl, pyruvyl and free acetate, quantitative yields can be calculated by reference to the integral of H-1 α-D-man. Thus, the degree of substitution of acetyl and pyruvyl, DS_{Ac} and DS_{Pyr}, can be estimated (see Eq. 2.32 in Section 2.7.2). As no acetate was added to the samples intentionally, one can further assume that all free acetate was originally substituted onto the inner mannopyranose. The amount of free acetate relative to H-1 α-D-man can therefore be regarded as the loss in DS_{Ac} throughout degradation, although this requires that the sample has not been dialysed afterwards. The sum of DS_{Ac} and the relative amount of free acetate should therefore yield DS_{Ac} of the undegraded xanthan. Results for all samples studied with ^{1}H-NMR can be found in Table 4.11.

Table 4.11: Degree of substitution of acetyl and pyruvyl, DS_{Ac} and DS_{Pyr}, and relative amount of free acetate for xanthan samples after different treatments. Calculated based on integrals of the respective ^{1}H-NMR peaks.

Sample	Treatment	Dialysed	DP_n	DS_{Ac}	Free acetate	DS_{Pyr}
MX	BGI 1:100, 24 h	No	26	1.36	0.05	1.04
	H2O2/NaOH, 1h	No	1*	0.33	1.22	1.28
	H2O2/NaOH, 1h	Yes	32	0.48	0.05†	1.53
XCD	BGI 1:1000, 0 h	No	12	1.14	0.01	1.01
	BGI 1:1000, 24 h	No	2	0.94‡	0.03‡	0.63‡
	H2O2/NaOH, 1h	No	1*	0.19	0.78	0.55
	H2O2/NaOH, 1h	Yes	19	0.34	0.02†	0.65
xan0614-3	BGI 1:100, 0 h	No	14	0.78	0.00	0.54
	BGI 1:100, 24 h	No	2	0.91‡	0.01‡	0.62‡

* Low value possibly due to reducing ends of side chains that have been cleaved off during chemical treatment.
† Low value due to removal of free acetate through dialysis.
‡ Assuming only signals within chemical shift range 5.26-5.40 ppm correspond to H-1 α-man, thus omitting those believed to be from reducing end H-1 α-Glc.

As seen in the table, results vary depending on xanthan sample and treatment. When comparing the two degradation methods, it seems that treatment with H_2O_2/NaOH leads to a high degree of deacetylation. The same is not observed during enzymatic depolymerisation. A more thorough discussion can be found in Section 4.4.2.3.

For MX, the integrals of both the acetyl and pyruvyl peaks were often large compared with the one for H-1 α-D-man. This have resulted in relative amounts well above 1.00 in some cases. As acetylation on both mannoses in the xanthan side chain have been proven possible[14], values for DS_{Ac} above 1.00 are plausible. However, pyruvation has only been found to occur on the terminal mannose, hence DS_{Pyr} is expected to be below 1.00. Neither should it be possible for the sum of DS_{Ac} and DS_{Pyr} to exceed 2.00. A shared difficulty for the MX samples was the lack of complete baseline separation. Since the

limits of integration were chosen by hand, the accuracy of these calculations are therefore somewhat disputable. In contrast, the ^{1}H-NMR spectra of XCD and xan0614-3 samples were mostly of higher quality, resulting in more reasonable results. This suggests that the depolymerised MX samples still have too large DP_n for obtaining accurate estimations.

If not considering deacetylation caused by degradation with H_2O_2/NaOH, almost all samples originating from XCD and xan0614-3 have similar DS_{Ac} and DS_{Pyr}. As a reminder, xan0614-3 is XCD which has been purified and sonicated for 30 min[24]. The most notable deviation is the high amount of pyruvate estimated for XCD (BGI 1:1000, 0h) with $DS_{Pyr} = 1.01$. As the spectrum for this particular sample was of poor quality compared with the others (see Fig. F.4 in Appendix F), the uncertainties of the integrals are believed to be larger.
The results, when neglecting XCD (BGI 1:1000, 0h), indicate that none of the degradation methods caused a significant decrease in signal from pyruvyl. Assuming that the initial degree of acetyl substitution is just the sum of DS_{Ac} and the relative amount of free acetate (non-dialysed samples only), it is possible to estimate both DS_{Ac} and DS_{Pyr} of the undegraded xanthans (see Table 4.12).

Table 4.12: Estimated degree of substitution of acetate and pyruvyl, DS_{Ac} and DS_{Pyr}, for undegraded xanthan samples.

Sample	**DS_{Ac}**	**DS_{Pyr}**
MX*	1.48 ± 0.07	1.28 ± 0.14
XCD	0.970 ± 0.003	0.61 ± 0.03
xan0614-3	0.85 ± 0.06	0.58 ± 0.04

Values are means ± SE based on data from Table 4.11.
* Estimated mean values for MX appears to overestimate the true DS more than SE indicates.

As previously explained, both DS_{Ac} and DS_{Pyr} for MX are probably overestimated since their sum of is significantly larger than 2.00. One can only suggest that most of the repeating units in MX are fully substituted, with some amount being double acetylated as indicated by DS_{Ac} being larger than DS_{Pyr}. However, optimisation of degradation protocols to obtain better resolved NMR spectra is necessary to conclude on the degree of substitutions for MX.

For XCD and xan0614-3 the results appear more reasonable. As opposed to MX, DS_{Pyr} is considerably lower, suggesting that merely 60% of the repeating units in XCD and xan0614-3 are pyruvated. As their estimates are also quite similar, this would indicate that the sonication procedure performed by Ina Beate Jenssen[24] did not cause removal of any of these substituents. Even so, the degree of substitutions obtained here for xan0614-3 are quite different from previous results (sample xan30 in Table 3.1.7, Section 3.1.6 in I.B. Jenssen 2014[24]). The sample xan30 was reported to have $DS_{Ac} = 23.8\%$ and $DS_{Pyr} = 18.6\%$. Contrary to the method applied here, these values were determined using the integral of a TSP peak as an external reference. It was stated in Section 4.3 of I.B. Jenssen (2014)[24] that an external reference could give inaccurate results for the degree

of substitutions as there are uncertainties in both the TSP and xanthan concentrations. Utilising an internal reference such as the H-1 α-D-man peak is therefore recommended as calculations become simpler with fewer variables and less uncertainty. Nonetheless, this still requires that samples are sufficiently depolymerised for obtaining ^{1}H-NMR spectra of sufficient resolution.

4.4.2.3 Comparison of Degradation Methods

The results obtained here indicated that degradation with H_2O_2/NaOH causes a high degree of deacetylation compared with enzymatic depolymerisation (Table 4.11). It was possible to remove the free acetate through dialysis using bags with cutoff 12-14 kDa. In Fig. 4.15 the ^{1}H-NMR spectrum of a dialysed sample (blue) has been superimposed with one that was not dialysed (red). The samples were otherwise subjected to the same treatment. It is clear that the large peak occurring around 1.9 ppm becomes severely diminished, while the relative magnitudes of all other peaks stay about the same. One reason for why deacetylation occurs with the H_2O_2/NaOH method is that the high pH ($\approx$ 11.7, calculated value) causes hydrolysis of acetyl[59]. It could therefore be interesting to study if there would be similar results when degrading MX and XCD with only H_2O_2 at a lower pH.

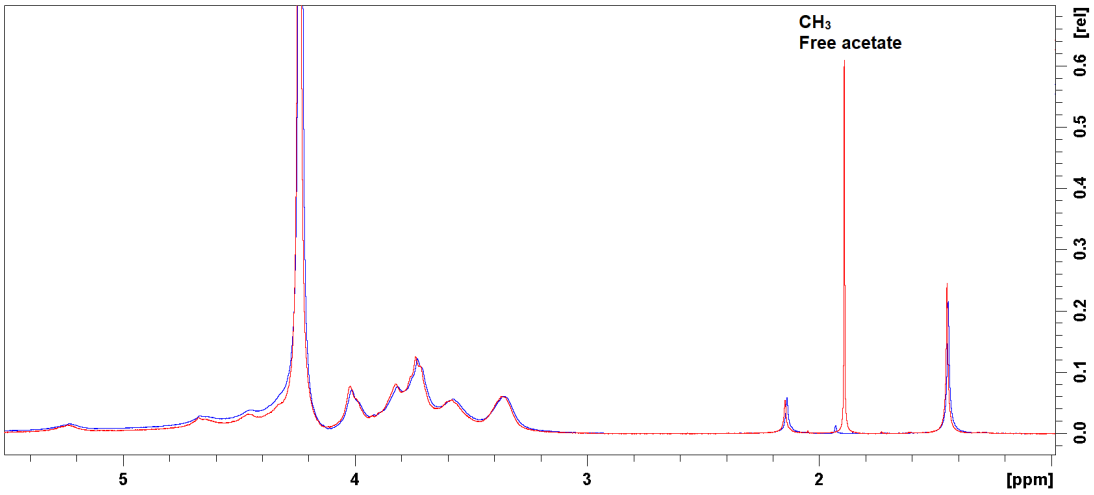

Figure 4.15: Superimposed ^{1}H-NMR spectra of MX degraded with H_2O_2 for 1 h at 80 °C. Blue: dialysed before freeze drying. Red: Not dialysed. Red has been scaled up with factor 1.4142 with respect to blue. Obtained with a Bruker Avance III HD 400 MHz spectrometer using a 5 mm SmartProbe. $T = 80$ °C during measurements.

Experiments of depolymerising xanthan using H_2O_2/Fe^{2+} showed that the side chain composition can be completely altered[6]. According to Christensen, Myhr and Smidsrød (1996), the explanation was proposed to be "preferential attack on the inner α-D-mannose, with concomitant removal of the entire side chain." There is reason to believe that the same could have happened during degradation with H_2O_2/NaOH, as proposed by Jenssen (2014)[24]. Dialysis would have removed any side chains that were cleaved off. This includes the acetyl and pyruvyl groups still bound to the side chains, but also H-1 α-D-man which was used as an internal reference for calculating the degrees of substitution. Hence, the results in Table 4.11 cannot be used to substantiate nor disprove this hypothesis.

Enzymatic degradation with BGI did not result in a significant ^{1}H-NMR signal of free acetate for any of the xanthan samples. DS_{Pyr} is however similar to those obtained for degradation with H_2O_2/NaOH, when looking at MX and XCD separately. Comparing XCD and xan0614-3, it also appears that differences in enzyme concentration do not influence these values either. This indicates that depolymerisation with cellulases is successful at breaking down the xanthan backbone without affecting the acetate and pyruvate substituents.

Chapter 5

Conclusions

The purpose of this master's thesis has been to study and characterise a range of different xanthan samples with the aim of investigating properties that are relevant for enhanced oil recovery applications. Two main samples were studied. The first, named MX, was precipitated from a fermentation broth procured from IRIS AS. The second, called XCD, was a commercial product by the name KELZAN XCD Xanthan Gum obtained from CP Kelco. This chapter has been split into two sections; the first presenting a summary of the conclusions of the results obtained during the specialisation project in 2017[9] and the second giving the conclusions of the master's project of 2018.

5.1 Specialisation Project

Thermogravimetric analysis of undegraded xanthan MX showed an average mass reduction of $(10.43 \pm 0.05)\%$ of the original mass. It was assumed that the decrease was only due to evaporation of water, thus this value is supposed to represent the moisture content of MX when exposed to normal air atmosphere at room temperature.

A Star Burst Mini microfluidiser was used to degrade xanthan samples by high pressure mechanical shear. This resulted in series of MX and XCD samples that were pulverised for different numbers of cycles. For the MX series, SEC-MALLS and capillary viscometry experiments showed that weight average molecular weight and intrinsic viscosity decreased for every consecutive cycle. Trend analysis indicated that continued degradation at a jet pressure of 210 MPa and 1 mg/mL concentration would be unable to produce samples of M_{w} lower than around 400-500 kDa and $[\eta]_{\dot{\gamma}=2500\,\mathrm{s}^{-1}}$ below 200 mL/g. Viscometry of the XCD series of samples implied a similar limiting behaviour of intrinsic viscosity with continued mechanical degradation. SEC-MALLS results for XCD samples, however, indicated M_{w} to be increasing following the third pulverising cycle. These results remain to be explained, and the experiment should probably be repeated with a different solvent and/or SEC column (TSK G6000PW was used for XCD).

The mechanics behind high pressure mechanical shear degradation of xanthan were not readily explained, but all results indicate that it becomes increasingly more difficult to degrade the xanthan polymers for each pulverising cycle. It was further assumed that the xanthan polymers would retain their ordered, double-stranded conformation throughout depolymerisation, although this could not be confirmed.

A Mark-Houwink-Sakurada plot was obtained for the degraded MX samples using

data from both capillary viscometry and SEC-MALLS measurements. The exponent of the fitted power trendline was found to be $a \approx 1.7$, indicating that xanthan MX with molecular masses in the range 500-1100 kDa behave as semi-rigid rods in solution when using an aqueous solvent containing 150 mM $NaNO_3$ and 10 mM EDTA.

5.2 Master's Project

Experiments with a Kinexus ultra+ rotational rheometer resulted in viscosity-shear rate curves for undegraded MX and XCD samples at different concentrations, which displayed the expected shear-thinning behaviour of xanthan solutions. Comparison of flow curves showed that MX solutions are more viscous than XCD solutions of the same concentration. This was as expected since the previous SEC-MALLS experiments indicated that the former sample has higher molecular weight.

MX and XCD were also depolymerised either chemically with H_2O_2/NaOH or enzymatically using the cellulases BGI-30 and Ecostone Goo. The BCA assay was used in combination with spectrophotometry to quantify the concentration of reducing ends of the resulting series of samples. This made it possible to calculate and visualise how the average chain length, i.e. the avg. degree of polymerisation (DP_n), of each xanthan changed for different treatments. For chemical degradation it was necessary to dialyse the samples afterwards as the chemical reactants seemed also to attack the side chains; thus yielding a very high concentration of reducing ends. This was not observed for enzymatically degraded xanthans, thus indicating that only the backbone experienced chain scission. The cellulases were, however, quite effective at digesting the biopolymers. Especially BGI-30 (diluted 1:100 from stock concentration) apparently reduced the chain length of XCD to 2 repeating units after just 1 hour of incubation at 60 °C (not including the 30 min at 75 °C during the BCA assay). It is therefore suspected that the cellulases were able to depolymerise the xanthans to some degree without needing to heat up the samples, but this still needs to be confirmed.

Some of the MX and XCD samples that had been degraded either chemically or enzymatically were selected for structural analysis by ^{1}H-NMR. The intention was to determine the amount of acetyl, free acetate and pyruvyl relative to the internal reference signal arising from the anomeric proton of the inner mannopyranosic unit (H-1 α-D-man). This required the samples to be sufficiently depolymerised for achieving spectra of suitable resolutions. It was found that MX samples with $DP_n = 26$ and 32 were possibly still too large for accurately determining the degree of substitutions (DS) of acetyl and pyruvyl, but the results yet indicate that undegraded MX is close to fully pyruvated and acetylated ($DS_{Ac,MX} = 1.48$ and $DS_{Pyr,MX} = 1.28$). On the other hand, XCD samples from $DP_n = 19$ and down to 2 appeared to be sufficiently depolymerised. The results estimated for undegraded XCD were $DS_{Ac,XCD} = 0.97$ and $DS_{Pyr,XCD} = 0.61$, revealing a significantly lower pyruvyl content compared with MX. The ^{1}H-NMR results showed further that degradation with H_2O_2/NaOH causes a high degree of deacetylation, while the amount of free acetate in samples depolymerised by cellulases were negligible. It can therefore be concluded that the method using enzymes is favourable to the chemical approach for breaking down xanthan if it is desired to keep the side chain composition unchanged.

Chapter 6

Recommendations

Suggestions for improving the characterisation of the xanthans are presented here together with ideas for other experiments that can provide supplementary results.

Although mechanical degradation with the Star Burst Mini was an effective method for breaking down the samples, SEC-MALLS results for MX indicated that the weight average molecular weight would reach a plateau around 400-500 kDa even with a jet pressure of 210 MPa. A few changes can be implemented for potentially achieving lower molar masses. One is to ensure that jet pressure is operated at maximum, i.e. 245 MPa. Another is to experiment with lower concentrations, as this has previously been shown to result in lower limiting molecular weight by sonication of polystyrene[52]. A third option is to break down xanthan under conditions favouring its disordered conformation. This can be achieved by acidification followed by dissolution in dimethyl sulfoxide (DMSO)[8]. However, the latter alternative can potentially cause structural changes that are different from mechanical degradation of xanthan in its ordered conformation.

Studies of the order-disorder transition was originally planned for the master's project, but the experiments were discontinued. The change in specific rotation with temperature can be measured by optical rotatory dispersion, which in turn can be used to quantify the transition temperature. This would have been useful information to include for a more complete description of the undegraded and depolymerised MX and XCD samples.

Capillary viscometry was only used to determine intrinsic viscosities for a shear rate of $2500\,\mathrm{s}^{-1}$. Due to xanthan's pseudoplastic behaviour, it would have been interesting to estimate intrinsic viscosities at other shear rates and to extrapolate a value for $[\eta]$ at $\dot{\gamma} = 0$. This was attempted with the data acquired by the rotational rheometer. The concentrations (1 to 4 mg/mL) appeared to be too large for successful regression analyses using the models presented in Section 2.4.4, perhaps with exception of the Solomon-Ciuta model. Other experimental methods should therefore be tried instead. A suggestion is the electrocapillarity method, which has been shown to be effective for determination of viscosity for xanthan solutions at low concentrations and very low shear rates[60].

As the acquired ^{1}H-NMR spectra for the degraded MX samples were not of sufficient resolution for accurate determination of the degree of substitutions of acetate and pyruvate, it is proposed that the cellulase concentration should be higher than the 1:100 dilution of enzyme stock concentration. This could potentially yield samples of lower molecular weight that are more apt for structural analysis. Alternatively, the samples could be incubated for longer than 24 hours. However, results from the BCA assay analyses indicated that DP_n would not change significantly when increasing the incubation

time from 24 to 48 hours.

The mode of action for the cellulases used in this study (BGI-30 and Ecostone Goo) is not known, i.e. if they digest the xanthans only from the ends (*exo* mode) or at random locations along the polymer backbone (*endo* mode). This can be decided by determining the number average molecular weight M_{n} before and after dialysis[3]. If the decrease in M_{n} changes from being hyperbolic to nearly constant, they are *exo*-enzymes. If there is no notable change, the cellulases are *endo*.

The next stage on the path to discover the true potential of xanthan for enhanced oil recovery would be to chemically modify MX and XCD using a similar method to the protocol developed by Roy et al. (2014)[7]. By repeating some of the performed and suggested experiments in this thesis for hydrophobised samples, it should be possible to study the influence of chemical modification on the rheological properties of these xanthans.

Bibliography

[1] James Sheng. *Modern Chemical Enhanced Oil Recovery: Theory and Practice*. Elsevier Inc., 2010. ISBN 978-1-85617-745-0. URL https://www.sciencedirect.com/science/book/9781856177450.

[2] Mari Stokka. Improved oil recovery by low shear handling of injection polymers. URL http://www.typhonix.com/home/low-shear-oil-production/improved-oil-recovery-by-low-shear-handling-of-injection-polymers.

[3] Bjørn E. Christensen. *Compendium TBT4135 Biopolymers*. NOBIPOL Department of Biotechnology, NTNU, 2016.

[4] Feng Yu, Ruimin Fu, Yun Xie, and Wuling Chen. Isolation and characterization of polyacrylamide-degrading bacteria from dewatered sludge. *International Journal of Environmental Research and Public Health*, 12(4):4214–4230, apr 2015. doi: 10.3390/ijerph120404214. URL https://doi.org/10.3390/ijerph120404214.

[5] Mutai Bao, Qingguo Chen, Yiming Li, and Guancheng Jiang. Biodegradation of partially hydrolyzed polyacrylamide by bacteria isolated from production water after polymer flooding in an oil field. *Journal of Hazardous Materials*, 184(1-3):105–110, dec 2010. doi: 10.1016/j.jhazmat.2010.08.011. URL https://doi.org/10.1016/j.jhazmat.2010.08.011.

[6] Bjørn E. Christensen and Olav Smidsrød. Dependence of the content of unsubstituted (cellulosic) regions in prehydrolysed xanthans on the rate of hydrolysis by trichoderma reesei endoglucanase. *International Journal of Biological Macromolecules*, 18(1-2):93–99, feb 1996. doi: 10.1016/0141-8130(95)01063-7. URL https://doi.org/10.1016/0141-8130(95)01063-7.

[7] Audrey Roy, Sébastien Comesse, Michel Grisel, Nicolas Hucher, Zied Souguir, and Frédéric Renou. Hydrophobically modified xanthan: An amphiphilic but not associative polymer. *Biomacromolecules*, 15(4):1160–1170, mar 2014. doi: 10.1021/bm4017034. URL https://doi.org/10.1021/bm4017034.

[8] Céline Fantou, Audrey N. Roy, Emmanuelle Dé, Sébastien Comesse, Michel Grisel, and Frédéric Renou. Chemical modification of xanthan in the ordered and disordered states: An open route for tuning the physico-chemical properties. *Carbohydrate Polymers*, 178:115–122, dec 2017. doi: 10.1016/j.carbpol.2017.09.039. URL https://doi.org/10.1016/j.carbpol.2017.09.039.

[9] Christian Holmvik. Preparation, depolymerization and characterization of xanthan for EOR applications. Unpublished project thesis, NTNU, December 2017.

[10] Lisa Crossman and J.Maxwell Dow. Biofilm formation and dispersal in xanthomonas campestris. *Microbes and Infection*, 6(6):623–629, may 2004. doi: 10.1016/j.micinf.2004.01.013. URL https://doi.org/10.1016/j.micinf.2004.01.013.

[11] Luciano A. Rigano, Florencia Siciliano, Ramón Enrique, Lorena Sendín, Paula Filippone, Pablo S. Torres, Julia Qüesta, J. Maxwell Dow, Atilio P. Castagnaro, Adrián A. Vojnov, and María Rosa Marano. Biofilm formation, epiphytic fitness, and canker development inXanthomonas axonopodispv.citri. *Molecular Plant-Microbe Interactions*, 20(10):1222–1230, oct 2007. doi: 10.1094/mpmi-20-10-1222. URL https://doi.org/10.1094/mpmi-20-10-1222.

[12] Barbara Katzbauer. Properties and applications of xanthan gum. *Polymer Degradation and Stability*, 59(1-3):81–84, jan 1998. doi: 10.1016/s0141-3910(97)00180-8. URL https://doi.org/10.1016/s0141-3910(97)00180-8.

[13] George Holzwarth. Molecular weight of xanthan polysaccharide. *Carbohydrate Research*, 66(1):173–186, oct 1978. doi: 10.1016/s0008-6215(00)83250-4. URL https://doi.org/10.1016/s0008-6215(00)83250-4.

[14] Marijn M. Kool, Harry Gruppen, Graham Sworn, and Henk A. Schols. Comparison of xanthans by the relative abundance of its six constituent repeating units. *Carbohydrate Polymers*, 98(1):914–921, oct 2013. doi: 10.1016/j.carbpol.2013.07.003. URL https://doi.org/10.1016/j.carbpol.2013.07.003.

[15] National Center for Biotechnology Information. Pyruvate, 2018. URL https://pubchem.ncbi.nlm.nih.gov/compound/pyruvate.

[16] National Center for Biotechnology Information. Acetate, 2018. URL https://pubchem.ncbi.nlm.nih.gov/compound/acetate.

[17] Vânia Blasques Bueno and Denise Freitas Siqueira Petri. Xanthan hydrogel films: Molecular conformation, charge density and protein carriers. *Carbohydrate Polymers*, 101:897–904, jan 2014. doi: 10.1016/j.carbpol.2013.10.039. URL https://doi.org/10.1016/j.carbpol.2013.10.039.

[18] Takahiro Sato, Takashi Norisuye, and Hiroshi Fujita. Double-stranded helix of xanthan: dimensional and hydrodynamic properties in 0.1 m aqueous sodium chloride. *Macromolecules*, 17(12):2696–2700, dec 1984. doi: 10.1021/ma00142a043. URL https://doi.org/10.1021/ma00142a043.

[19] Bjørn E. Christensen, Kenneth D. Knudsen, Olav Smidsrød, Shinichi Kitamura, and Kenichi Takeo. Temperature-induced conformational transition in xanthans with partially hydrolyzed side chains. *Biopolymers*, 33(1):151–161, jan 1993. doi: 10.1002/bip.360330115. URL https://doi.org/10.1002/bip.360330115.

[20] Yasuhiro Matsuda, Yusuke Biyajima, and Takahiro Sato. Thermal denaturation, renaturation, and aggregation of a double-helical polysaccharide xanthan in aqueous solution. *Polymer Journal*, 41(7):526–532, 2009. doi: 10.1295/polymj.pj2008300. URL https://doi.org/10.1295/polymj.pj2008300.

[21] Kaken Pharmaceutical Co. Ltd., Taito Co. Ltd., T. Kojima, K. Tabata, T. Yanaki, and M. Mitani. Method for a specific depolymerization of a polysaccharide having a rod-like helical conformation, 1983. URL http://www.google.si/patents/US4505757. U.S. Patent 4,505,757. Date of access: 15.12.17.

[22] Shiho Suzuki, Mariko Ono, Toshiya Toda, and Shinichi Kitamura. Preparation and intestinal immunostimulating activity of low molecular weight alginate from saccharina (laminaria) species in japan. *Journal of Applied Glycoscience*, 63(1):1–5, 2016. doi: 10.5458/jag.jag.jag-2015_017. URL https://doi.org/10.5458/jag.jag.jag-2015_017.

[23] Sugino Machine Ltd. Star Burst Mini. URL http://www.sugino.com/site/wet-pulverizing-and-dispersing-equipment-e/sbs-type-mini-e.html. Date of access: 15.12.17.

[24] Ina Beate Jenssen. Preparation and characterisation of hydrophobically modified xanthan. Master's thesis, NTNU, june 2014. URL http://hdl.handle.net/11250/246126.

[25] R. E. Harrington and B. H. Zimm. Degradation of polymers by controlled hydrodynamic shear1. *The Journal of Physical Chemistry*, 69(1):161–175, jan 1965. doi: 10.1021/j100885a025. URL https://doi.org/10.1021/j100885a025.

[26] Kenneth L. Bridges and Kerry L. Kalinski. Reduction of the viscosity of solutions viscosified with Xanthan gum polymers, october 1991. URL https://patents.google.com/patent/US5055209. US Patent US5055209A.

[27] Marijn M. Kool, Henk A. Schols, Roy J.B.M. Delahaije, Graham Sworn, Peter A. Wierenga, and Harry Gruppen. The influence of the primary and secondary xanthan structure on the enzymatic hydrolysis of the xanthan backbone. *Carbohydrate Polymers*, 97(2):368–375, sep 2013. doi: 10.1016/j.carbpol.2013.05.045. URL https://doi.org/10.1016/j.carbpol.2013.05.045.

[28] M. Rinaudo and M. Milas. Enzymic hydrolysis of the bacterial polysaccharide xanthan by cellulase. *International Journal of Biological Macromolecules*, 2(1):45–48, feb 1980. doi: 10.1016/0141-8130(80)90009-4. URL https://doi.org/10.1016/0141-8130(80)90009-4.

[29] Bjørn E. Christensen and Olav Smidsrød. Dependence of the content of unsubstituted (cellulosic) regions in prehydrolysed xanthans on the rate of hydrolysis by trichoderma reesei endoglucanase. *International Journal of Biological Macromolecules*, 18(1-2):93–99, feb 1996. doi: 10.1016/0141-8130(95)01063-7. URL https://doi.org/10.1016/0141-8130(95)01063-7.

[30] Inc. PhotoMetrics. Thermogravimetric Analysis (TGA). URL http://photometrics.net/thermogravimetric-analysis-tga/. Date of access: 15.12.17.

[31] Chompak Pirayavaraporn, Thomas Rades, and Ian G. Tucker. Determination of moisture content in relation to thermal behaviour and plasticization of eudragit RLPO. *International Journal of Pharmaceutics*, 422(1-2):68–74, jan 2012. doi: 10.1016/j.ijpharm.2011.10.028. URL https://doi.org/10.1016/j.ijpharm.2011.10.028.

[32] Matthew J. Boyd, Frank C. Hampson, Ian G. Jolliffe, Peter W. Dettmar, John R. Mitchell, and Colin D. Melia. Strand-like phase separation in mixtures of xanthan gum with anionic polyelectrolytes. *Food Hydrocolloids*, 23(8):2458–2467, dec 2009. doi: 10.1016/j.foodhyd.2009.07.008. URL https://doi.org/10.1016/j.foodhyd.2009.07.008.

[33] Jürgen Wilke, Holger Kryk, and Jutta Hartmann. Theory and Praxis of Capillary Viscometry - An Introduction. URL http://www.dongjins.com/service/file/VISCO_PRIMER_ENGLISH.PDF. SCHOTT-GERÄTE GmbH. Based on Equation (4.19), page 11. Date of access: 18.12.17.

[34] Maurice L. Huggins. The viscosity of dilute solutions of long-chain molecules. IV. dependence on concentration. *Journal of the American Chemical Society*, 64(11):2716–2718, nov 1942. doi: 10.1021/ja01263a056. URL https://doi.org/10.1021/ja01263a056.

[35] Ramón Pamies, José Ginés Hernández Cifre, María del Carmen López Martínez, and José García de la Torre. Determination of intrinsic viscosities of macromolecules and nanoparticles. comparison of single-point and dilution procedures. *Colloid and Polymer Science*, 286(11):1223–1231, jul 2008. doi: 10.1007/s00396-008-1902-2. URL https://doi.org/10.1007/s00396-008-1902-2.

[36] Tsukasa Sakai. Huggins constant k′ for flexible chain polymers. *Journal of Polymer Science Part A-2: Polymer Physics*, 6(8):1535–1549, aug 1968. doi: 10.1002/pol.1968.160060810. URL https://doi.org/10.1002/pol.1968.160060810.

[37] Darwin J. Mead and Raymond M. Fuoss. Viscosities of solutions of polyvinyl chloride. *Journal of the American Chemical Society*, 64(2):277–282, feb 1942. doi: 10.1021/ja01254a020. URL https://doi.org/10.1021/ja01254a020.

[38] Tadashi Inoue, Naoto Oba, and Osamu Urakawa. Reliability of intrinsic viscosity estimated by single point procedure at high concentrations. *Nihon Reoroji Gakkaishi*, 42(4):261–264, 2014. doi: 10.1678/rheology.42.261. URL https://doi.org/10.1678/rheology.42.261.

[39] O. F. Solomon and I. Z. Ciută. Détermination de la viscosité intrinsèque de solutions de polymères par une simple détermination de la viscosité. *Journal of Applied Polymer Science*, 6(24):683–686, nov 1962. doi: 10.1002/app.1962.070062414. URL http://onlinelibrary.wiley.com/doi/10.1002/app.1962.070062414/abstract.

[40] Bruno H. Zimm. The scattering of light and the radial distribution function of high polymer solutions. *The Journal of Chemical Physics*, 16(12):1093–1099, dec 1948. doi: 10.1063/1.1746738. URL https://doi.org/10.1063/1.1746738.

[41] Wyatt Technology Corporation. ASTRA V User's Guide, 2008. URL https://www.biozentrum.unibas.ch/fileadmin/redaktion/Forschung/Research_Groups/BF/instruments/Astra_Manual.pdf. Date of access: 19.12.17.

[42] Fanglian He. BCA (bicinchoninic acid) protein assay. *BIO-PROTOCOL*, 1(5), 2011. doi: 10.21769/bioprotoc.44. URL https://doi.org/10.21769/bioprotoc.44.

[43] Clemens Niederberger. Carbohydrates, 2015. URL http://ctan.math.washington.edu/tex-archive/macros/latex/contrib/carbohydrates/carbohydrates_en.pdf.

[44] P.K. Smith, R.I. Krohn, G.T. Hermanson, A.K. Mallia, F.H. Gartner, M.D. Provenzano, E.K. Fujimoto, N.M. Goeke, B.J. Olson, and D.C. Klenk. Measurement of protein using bicinchoninic acid. *Analytical Biochemistry*, 150(1):76–85, oct 1985. doi: 10.1016/0003-2697(85)90442-7. URL https://doi.org/10.1016/0003-2697(85)90442-7.

[45] Y.-H. Percival Zhang and Lee R. Lynd. Determination of the number-average degree of polymerization of cellodextrins and cellulose with application to enzymatic hydrolysis. *Biomacromolecules*, 6(3):1510–1515, May 2005. doi: 10.1021/bm049235j. URL https://doi.org/10.1021/bm049235j.

[46] Chemistry LibreTexts. Spectrophotometry, 2015. URL https://chem.libretexts.org/Core/Physical_and_Theoretical_Chemistry/Kinetics/Reaction_Rates/Experimental_Determination_of_Kinetcs/Spectrophotometry.

[47] William Reusch. Nuclear Magnetic Resonance Spectroscopy, 2013. URL https://www2.chemistry.msu.edu/faculty/reusch/virttxtjml/spectrpy/nmr/nmr1.htm.

[48] Dr. Ian Hunt. Spectrophotometry, 2015. URL http://www.chem.ucalgary.ca/courses/350/Carey5th/Ch13/ch13-nmr-1.html.

[49] M. Rinaudo, M. Milas, F. Lambert, and M. Vincendon. Proton and carbon-13 NMR investigation of xanthan gum. *Macromolecules*, 16(5):816–819, sep 1983. doi: 10.1021/ma00239a018. URL https://doi.org/10.1021/ma00239a018.

[50] Stephen So. Why is the sample variance a biased estimator? Technical report, Griffith School of Engineering, Griffith University, 09 2008.

[51] Douglas G Altman and J Martin Bland. Standard deviations and standard errors. *BMJ*, 331(7521):903, oct 2005. doi: 10.1136/bmj.331.7521.903. URL https://doi.org/10.1136/bmj.331.7521.903.

[52] Gareth J. Price and Paul F. Smith. Ultrasonic degradation of polymer solutions. 1. polystyrene revisited. *Polymer International*, 24(3):159–164, 1991. doi: 10.1002/pi.4990240306. URL https://doi.org/10.1002/pi.4990240306.

[53] B.T. Stokke, A. Elgsaeter, E.Ø. Bjørnestad, and T. Lund. Rheology of xanthan and scleroglucan in synthetic seawater. *Carbohydrate Polymers*, 17(3):209–220, jan 1992. doi: 10.1016/0144-8617(92)90006-c. URL https://doi.org/10.1016/0144-8617(92)90006-c.

[54] N Lagoueyte and P Paquin. Effects of microfluidization on the functional properties of xanthan gum. *Food Hydrocolloids*, 12(3):365–371, july 1998. doi: 10.1016/s0268-005x(98)00004-6. URL https://doi.org/10.1016/s0268-005x(98)00004-6.

[55] M. Milas, M. Rinaudo, and B. Tinland. The viscosity dependence on concentration, molecular weight and shear rate of xanthan solutions. *Polymer Bulletin*, 14 (2):157–164, aug 1985. doi: 10.1007/bf00708475. URL https://doi.org/10.1007/bf00708475.

[56] Françoise Callet, Michel Milas, and Marguerite Rinaudo. Influence of acetyl and pyruvate contents on rheological properties of xanthan in dilute solution. *International Journal of Biological Macromolecules*, 9(5):291–293, oct 1987. doi: 10.1016/0141-8130(87)90068-7. URL https://doi.org/10.1016/0141-8130(87)90068-7.

[57] M. Dentini, V. Crescenzi, and D. Blasi. Conformational properties of xanthan derivatives in dilute aqueous solution. *International Journal of Biological Macromolecules*, 6(2):93–98, apr 1984. doi: 10.1016/0141-8130(84)90070-9. URL https://doi.org/10.1016/0141-8130(84)90070-9.

[58] Norman W.H. Cheetham and Ernest N.M. Mashimba. Proton and carbon-13 NMR studies on xanthan derivatives. *Carbohydrate Polymers*, 17(2):127–136, jan 1992. doi: 10.1016/0144-8617(92)90106-z. URL https://doi.org/10.1016/0144-8617(92)90106-z.

[59] Yateendra Shanmukha Puvvada, Saikishore Vankayalapati, and Sudheshnababu Sukhavasi. Extraction of chitin from chitosan from exoskeleton of shrimp for application in the pharmaceutical industry. *International Current Pharmaceutical Journal*, 1(9), aug 2012. doi: 10.3329/icpj.v1i9.11616. URL https://doi.org/10.3329/icpj.v1i9.11616.

[60] M.H. Allouche, V. Botton, D. Henry, S. Millet, R. Usha, and H. Ben Hadid. Experimental determination of the viscosity at very low shear rate for shear thinning fluids by electrocapillarity. *Journal of Non-Newtonian Fluid Mechanics*, 215:60–69, jan 2015. doi: 10.1016/j.jnnfm.2014.11.003. URL https://doi.org/10.1016/j.jnnfm.2014.11.003.

Appendix A

Thermogravimetric Analyses

This appendix contains supplementary data and information obtained by thermogravimetric experiments.

A.1 Change of Mass and Temperature with Time

Fig. A.1 shows how temperature and mass percentage varied for the duration of the thermogravimetric analyses of both xanthan parallels.

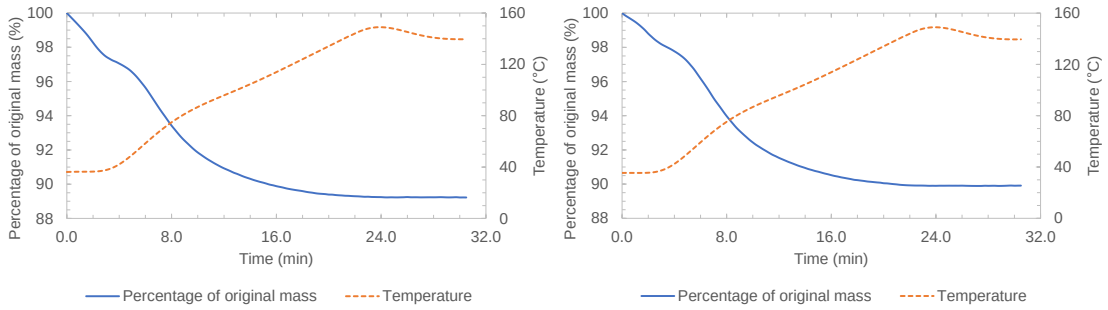

(a) MX - TGA parallel 1 **(b)** MX - TGA parallel 2

Figure A.1: Percentage of original mass and temperature plotted as functions of time during thermogravimetric analysis. Instrument: STA 449 C Jupiter (Netzsch-Gerätebau GmbH).

A.2 Raw Data from TGA

Raw data obtained by thermogravimetric analyses of MX are presented in Table A.1. The same data can be found as .txt files in the digital attachment under "Supplementary files/TGA/".

Table A.1: Raw data obtained by TGA of xanthan MX.

	Parallel 1		Parallel 2	
Time (min)	**Temp.** (°C)	**Mass (%)**	**Temp.** (°C)	**Mass (%)**
0.00	36.164 00	100.000 00	35.403 00	100.000 00
0.25	36.255 80	99.802 55	35.426 05	99.860 05
0.50	36.301 17	99.605 32	35.419 72	99.740 60
0.75	36.346 81	99.405 11	35.426 22	99.618 97
1.00	36.365 00	99.200 00	35.403 00	99.492 45
1.25	36.369 95	98.990 38	35.400 25	99.346 95
1.50	36.387 78	98.772 21	35.407 00	99.184 20
1.75	36.410 20	98.529 95	35.446 59	99.006 83
2.00	36.475 00	98.274 07	35.552 00	98.801 89
2.25	36.583 54	98.023 63	35.748 66	98.626 32
2.50	36.818 09	97.801 46	36.072 32	98.455 67
2.75	37.180 36	97.608 48	36.590 27	98.313 57
3.00	37.716 00	97.450 00	37.319 00	98.184 91
3.25	38.471 08	97.334 64	38.256 71	98.082 90
3.50	39.465 48	97.227 00	39.424 99	97.984 85
3.75	40.678 80	97.148 29	40.841 72	97.884 83
4.00	42.129 00	97.048 15	42.439 00	97.769 81
4.25	43.792 40	96.945 66	44.227 39	97.650 78
4.50	45.614 59	96.828 98	46.162 41	97.514 61
4.75	47.576 14	96.699 65	48.220 84	97.358 21
5.00	49.653 00	96.533 33	50.368 00	97.169 81
5.25	51.797 96	96.343 17	52.556 15	96.951 43
5.50	54.013 57	96.123 05	54.765 67	96.720 81
5.75	56.250 31	95.885 75	57.017 00	96.450 07
6.00	58.490 00	95.642 59	59.261 00	96.175 47
6.25	60.701 47	95.365 22	61.463 47	95.903 73
6.50	62.917 68	95.077 29	63.641 18	95.624 30
6.75	65.062 35	94.787 21	65.742 65	95.330 40
7.00	67.168 00	94.498 15	67.828 00	95.028 30
7.25	69.203 75	94.218 82	69.793 00	94.758 99
7.50	71.172 01	93.953 87	71.704 92	94.502 00
7.75	73.064 17	93.680 23	73.531 30	94.231 77
8.00	74.880 00	93.418 52	75.287 00	93.975 47
8.25	76.611 51	93.185 73	76.964 11	93.742 18
8.50	78.269 15	92.952 08	78.562 68	93.513 78

8.75	79.849 37	92.732 19	80.089 30	93.293 71
9.00	81.356 00	92.537 04	81.558 00	93.105 66
9.25	82.815 55	92.356 51	82.948 61	92.927 20
9.50	84.200 40	92.174 07	84.289 58	92.756 36
9.75	85.527 27	92.003 02	85.581 00	92.587 00
10.00	86.808 00	91.850 00	86.817 00	92.437 74
10.25	88.048 45	91.715 03	88.009 39	92.295 91
10.50	89.236 83	91.581 70	89.176 43	92.175 73
10.75	90.405 21	91.455 41	90.304 60	92.054 19
11.00	91.535 00	91.340 74	91.413 00	91.941 51
11.25	92.628 79	91.226 78	92.495 47	91.827 05
11.50	93.720 53	91.122 42	93.579 05	91.717 93
11.75	94.793 71	91.018 99	94.643 10	91.630 77
12.00	95.865 00	90.925 93	95.710 00	91.535 85
12.25	96.932 91	90.843 57	96.765 56	91.453 78
12.50	97.993 23	90.759 20	97.836 64	91.371 65
12.75	99.065 17	90.668 81	98.898 06	91.290 95
13.00	100.144 00	90.601 85	99.973 00	91.218 87
13.25	101.229 95	90.521 78	101.068 38	91.144 75
13.50	102.337 83	90.443 50	102.168 90	91.070 82
13.75	103.434 00	90.377 23	103.286 76	91.008 91
14.00	104.553 00	90.314 81	104.425 00	90.947 17
14.25	105.683 78	90.247 23	105.572 46	90.879 74
14.50	106.829 36	90.190 17	106.728 31	90.828 57
14.75	107.994 54	90.134 11	107.907 74	90.770 51
15.00	109.167 00	90.087 04	109.105 00	90.726 42
15.25	110.361 45	90.030 53	110.292 75	90.672 89
15.50	111.552 67	89.971 79	111.502 40	90.619 86
15.75	112.759 10	89.934 42	112.716 66	90.576 40
16.00	113.988 00	89.883 33	113.948 00	90.524 53
16.25	115.219 11	89.843 58	115.183 67	90.478 36
16.50	116.468 86	89.803 64	116.427 61	90.442 47
16.75	117.719 17	89.754 92	117.659 17	90.397 88
17.00	118.955 00	89.716 67	118.914 00	90.364 15
17.25	120.216 72	89.683 39	120.158 45	90.328 33
17.50	121.482 53	89.652 02	121.422 81	90.293 65
17.75	122.743 97	89.623 74	122.689 64	90.252 42
18.00	124.016 00	89.594 44	123.961 00	90.233 96
18.25	125.279 54	89.556 01	125.228 10	90.207 85
18.50	126.561 53	89.525 07	126.493 16	90.184 94
18.75	127.822 03	89.501 53	127.758 58	90.154 65
19.00	129.089 00	89.468 52	129.039 00	90.137 74
19.25	130.362 71	89.446 22	130.313 75	90.118 57
19.50	131.639 76	89.432 35	131.586 13	90.099 29
19.75	132.898 72	89.418 11	132.871 14	90.084 60
20.00	134.171 01	89.392 59	134.126 01	90.052 83
20.25	135.442 21	89.389 25	135.396 73	90.043 89

20.50	136.704 69	89.367 54	136.653 18	90.022 54
20.75	137.981 47	89.351 59	137.917 38	90.001 78
21.00	139.246 99	89.340 74	139.169 01	89.984 91
21.25	140.499 59	89.324 27	140.435 86	89.960 98
21.50	141.753 37	89.318 92	141.670 03	89.947 43
21.75	142.844 69	89.305 81	142.753 65	89.935 51
22.00	144.069 96	89.295 83	143.983 08	89.927 98
22.25	145.232 43	89.289 04	145.146 42	89.921 35
22.50	146.269 87	89.276 08	146.199 61	89.916 96
22.75	147.159 55	89.262 43	147.101 22	89.917 18
23.00	147.884 99	89.266 67	147.847 00	89.915 09
23.25	148.410 44	89.253 13	148.395 73	89.908 83
23.50	148.770 91	89.249 70	148.769 88	89.901 80
23.75	148.960 36	89.245 37	148.968 40	89.904 84
24.00	148.970 74	89.243 36	149.006 15	89.900 88
24.25	148.839 79	89.231 17	148.883 29	89.907 35
24.50	148.572 32	89.227 55	148.628 10	89.907 09
24.75	148.192 00	89.233 33	148.265 00	89.907 55
25.00	147.715 98	89.229 13	147.799 08	89.909 35
25.25	147.168 59	89.227 83	147.248 16	89.907 71
25.50	146.560 84	89.232 47	146.650 84	89.908 38
25.75	145.913 95	89.236 97	146.004 57	89.907 48
26.00	145.249 78	89.247 83	145.344 80	89.910 81
26.25	144.586 73	89.235 12	144.683 37	89.904 04
26.50	143.934 01	89.235 19	144.021 00	89.900 00
26.75	143.312 38	89.235 25	143.377 94	89.895 95
27.00	142.718 93	89.229 67	142.773 18	89.894 40
27.25	142.182 09	89.231 31	142.218 09	89.893 49
27.50	141.686 11	89.233 22	141.710 68	89.895 19
27.75	141.247 90	89.234 83	141.249 96	89.905 59
28.00	140.871 41	89.233 28	140.861 67	89.899 97
28.25	140.539 00	89.235 19	140.524 99	89.903 77
28.50	140.275 48	89.241 02	140.242 01	89.905 27
28.75	140.055 94	89.237 01	140.015 93	89.896 03
29.00	139.879 25	89.228 99	139.833 30	89.897 31
29.25	139.746 10	89.227 36	139.704 38	89.902 23
29.50	139.657 97	89.232 66	139.612 16	89.910 13
29.75	139.595 37	89.238 87	139.564 28	89.917 10
30.00	139.578 00	89.224 07	139.542 01	89.907 55
30.25	139.561 72	89.225 95	139.547 37	89.911 34
30.50	139.582 45	89.222 51	139.564 09	89.913 77

Appendix B

Capillary Viscometry

The following pages present reports of intrinsic viscosity measurements for each sample that has been studied in this project; grouped according to how the main results were presented in Sections 4.2.1.1-4.2.1.3 in Chapter 4. Each report contains data about mean flow-through-times for the solvent and each of the six sample concentrations, as well as the four linear curves plotted to fit the data according to the four regression models presented in Section 2.4.4 in Chapter 2. Calculations of intrinsic viscosities and Huggins constants are also included.

The original Excel file for performing regression analyses and calculations were provided by Senior Engineer Ann-Sissel T. Ulset from the Department of Biotechnology and Food Science, thus the author does not claim full credit for making these reports. Only some modifications have been performed for e.g. graph presentations, calculations of standard deviations, and of course the inserted raw data. All files can be found in the digital attachment under ”Supplementary files/Capillary Viscometry/”.

B.1 Mechanically Degraded MX

The following pages present reports about each sample belonging to the series of mechanically degraded MX (see Table 4.2 in Section 4.2.1).

Sample: MXm0 **Temp. (°C):** 20
Solvent: 0.15 M NaNO3/0.01 M EDTA, pH 6.0 **Analyst:** CH

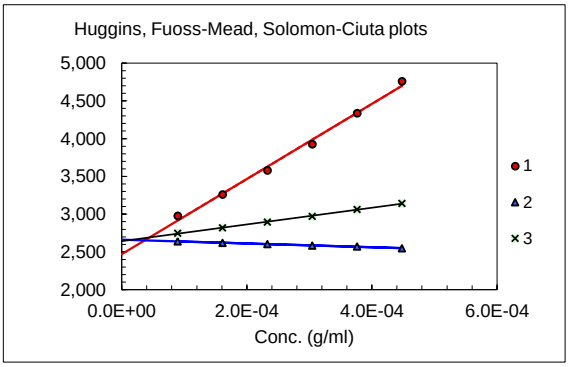

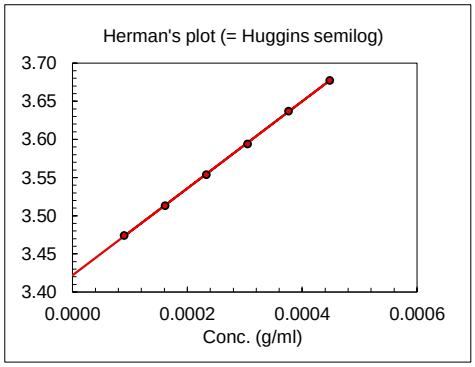

Calculations of the intrinsic viscosity

Fit type.	Fitted data		Linear 1-3 [h] (ml/g)	SD (ml/g)	k'	SD
1	h_{sp}/c vs. c	(Huggins)	**2,470.3**		0.82	
2	$(\ln h_r)/c$ vs. c	(Mead-Fuoss)	**2,661.8**		0.46	
3	$[2(h_{sp}-\ln h_r)]^{1/2}/c$	(Solomon-Ciuta)	**2,642.8**		0.49	
4	$\log h_{sp}/c$ vs. c	(Herman)	**2,641.8**			
Average			**2,604.2**	89.7	0.59	0.20
Avg. w/o Huggins			**2,648.8**	11.3	0.48	0.02

Raw data

Conc. (mg/ml)	t (sec)	t(sec)*	h_r	h_{sp}/c (ml/g)	Accepted in regression
0 (solvent)	201.00	200.24			
0.448		627.14	3.13	4,761	Yes
0.376		526.88	2.63	4,336	Yes
0.305		439.78	2.20	3,928	Yes
0.233		367.17	1.83	3,580	Yes
0.161		305.51	1.53	3,261	Yes
0.090		253.67	1.27	2,979	Yes

*) Hagenbach corrected

Dried *in vacuo* over P_2O_5:	Yes	Corrected for water content	Yes
Assumed water content	10.43 %	Filter type (porosity (µm))	5
Measured water content:	10.43%		

Sample: MXm1 **Temp. (°C):** 20
Solvent: 0.15 M NaNO3/0.01 M EDTA, pH 6.0 **Analyst:** CH

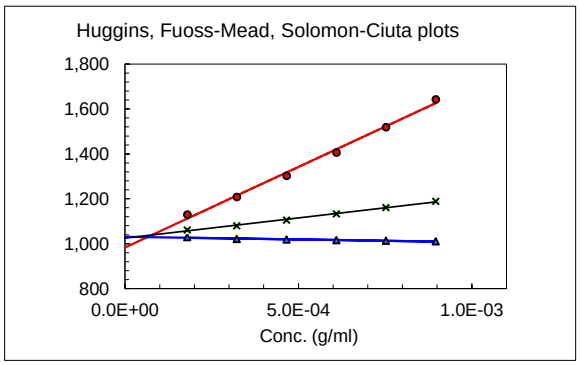

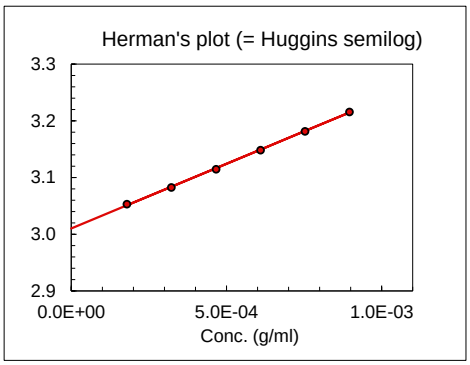

Calculations of the intrinsic viscosity

Fit type.	Fitted data		Linear 1-3 [h] (ml/g)	SD (ml/g)	k'	SD
1	h_{sp}/c vs. c	(Huggins)	**982.8**		0.74	
2	$(\ln h_r)/c$ vs. c	(Mead-Fuoss)	**1,030.8**		0.48	
3	$[2(h_{sp}-\ln h_r)]^{1/2}/c$	(Solomon-Ciuta)	**1,024.9**		0.50	
4	log h_{sp}/c vs. c	(Herman)	**1,023.6**			
Average			**1,015.5**	22.0	0.58	0.15
Avg. w/o Huggins			**1,026.4**	3.8	0.49	0.02

Raw data

Conc. (mg/ml)	t (sec)	t(sec)*	h_r	h_{sp}/c (ml/g)	Accepted in regression
0 (solvent)	200.91	200.15			
0.896		494.77	2.47	1,643	Yes
0.752		428.98	2.14	1,520	Yes
0.609		371.70	1.86	1,407	Yes
0.466		321.62	1.61	1,303	Yes
0.322		278.19	1.39	1,209	Yes
0.179		240.67	1.20	1,130	Yes

*) Hagenbach corrected

Dried *in vacuo* over P_2O_5:	Yes	Corrected for water content	Yes
Assumed water content	10.43%	Filter type (porosity (µm))	5
Measured water content:	10.43%		

Sample: MXm2 **Temp. (°C):** 20
Solvent: 0.15 M NaNO3/0.01 M EDTA, pH 6.0 **Analyst:** CH

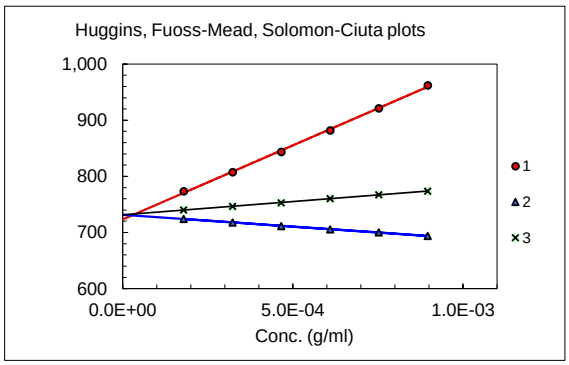

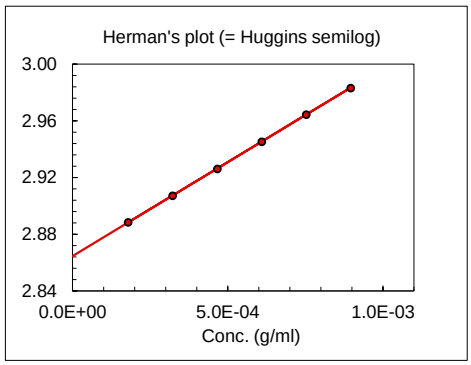

Calculations of the intrinsic viscosity

Fit type.	Fitted data		Linear 1-3 [h] (ml/g)	SD (ml/g)	k'	SD
1	h_{sp}/c vs. c	(Huggins)	**723.3**		0.50	
2	$(\ln h_r)/c$ vs. c	(Mead-Fuoss)	**731.5**		0.42	
3	$[2(h_{sp}-\ln h_r)]^{1/2}/c$	(Solomon-Ciuta)	**731.5**		0.42	
4	log h_{sp}/c vs. c	(Herman)	**732.1**			
Average			**729.6**	4.2	0.45	0.05
Avg. w/o Huggins			**731.7**	0.3	0.42	0.00

Raw data

Conc. (mg/ml)	t (sec)	t(sec)*	h_r	h_{sp}/c (ml/g)	Accepted in regression
0 (solvent)	200.91	200.15			
0.896		372.61	1.86	962	Yes
0.752		338.92	1.69	921	Yes
0.609		307.64	1.54	882	Yes
0.466		278.79	1.39	844	Yes
0.322		252.28	1.26	808	Yes
0.179		227.88	1.14	773	Yes

*) Hagenbach corrected

Dried *in vacuo* over P_2O_5:	Yes	Corrected for water content	Yes
Assumed water content	10.43%	Filter type (porosity (µm))	5
Measured water content:	10.43%		

Sample: MXm3 **Temp. (°C):** 20
Solvent: 0.15 M NaNO3/0.01 M EDTA, pH 6.0 **Analyst:** CH

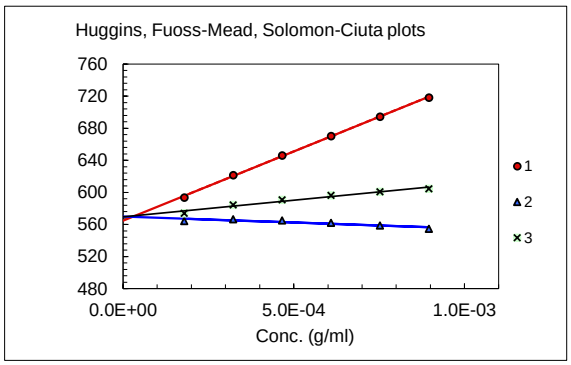

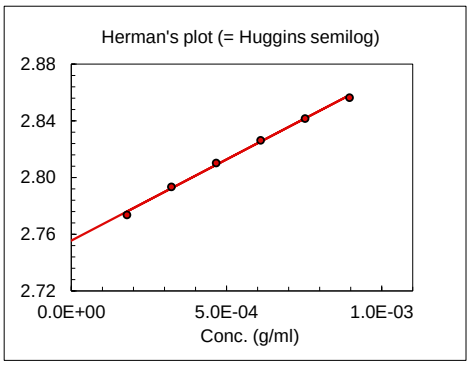

Calculations of the intrinsic viscosity

Fit type.	Fitted data		Linear 1-3 [h] (ml/g)	SD (ml/g)	k'	SD
1	h_{sp}/c vs. c	(Huggins)	**564.7**		0.54	
2	$(\ln h_r)/c$ vs. c	(Mead-Fuoss)	**569.9**		0.45	
3	$[2(h_{sp}-\ln h_r)]^{1/2}/c$	(Solomon-Ciuta)	**569.5**		0.46	
4	log h_{sp}/c vs. c	(Herman)	**569.5**			
Average			**568.4**	2.5	0.49	0.05
Avg. w/o Huggins			**569.6**	0.2	0.46	0.00

Raw data

Conc. (mg/ml)	t (sec)	t(sec)*	h_r	h_{sp}/c (ml/g)	Accepted in regression
0 (solvent)	201.49	200.73			
0.896		329.88	1.64	718	Yes
0.752		305.62	1.52	695	Yes
0.609		282.70	1.41	670	Yes
0.466		261.14	1.30	646	Yes
0.322		240.96	1.20	622	Yes
0.179		222.08	1.11	594	Yes

*) Hagenbach corrected

Dried *in vacuo* over P_2O_5:	Yes	Corrected for water content	Yes
Assumed water content	10.43%	Filter type (porosity (µm))	5
Measured water content:	10.43%		

Sample: MXm4 **Temp. (°C):** 20
Solvent: 0.15 M NaNO3/0.01 M EDTA, pH 6.0 **Analyst:** CH

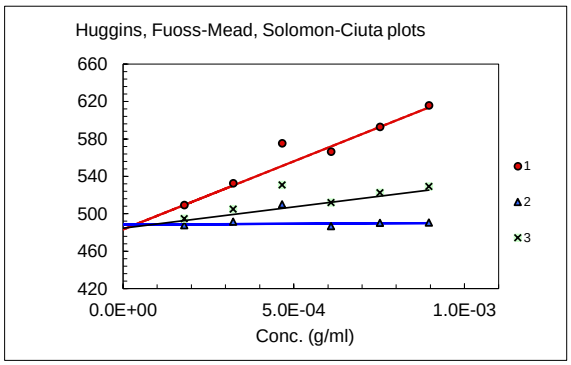

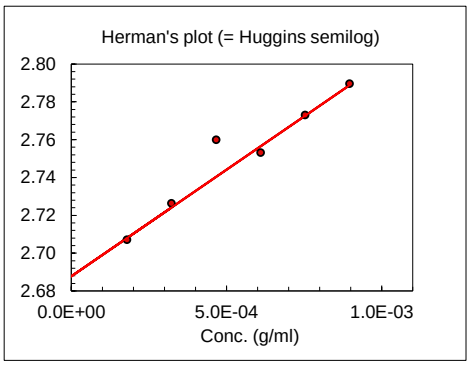

Calculations of the intrinsic viscosity

Fit type.	Fitted data		Linear 1-3 [h] (ml/g)	SD (ml/g)	k'	SD
1	h_{sp}/c vs. c	(Huggins)	**483.3**		0.62	
2	$(\ln h_r)/c$ vs. c	(Fuoss-Mead)	**488.4**		0.51	
3	$[2(h_{sp}-\ln h_r)]^{1/2}/c$	(Solomon-Ciuta)	**487.5**		0.52	
4	$\log h_{sp}/c$ vs. c	(Herman)	**487.2**			
Average			**486.6**	2.2	0.55	0.06
Avg. w/o Huggins			**487.7**	0.6	0.52	0.01

Raw data

Conc. (mg/ml)	t (sec)	t(sec)*	h_r	h_{sp}/c (ml/g)	Accepted in regression
0 (solvent)	201.49	200.73			
0.896		311.50	1.55	616	Yes
0.752		290.30	1.45	593	Yes
0.609		270.01	1.35	567	Yes
0.466		254.54	1.27	576	-
0.322		235.20	1.17	533	Yes
0.179		219.05	1.09	510	Yes

*) Hagenbach corrected

Dried *in vacuo* over P_2O_5:	Yes	Corrected for water content	Yes
Assumed water content	10.43%	Filter type (porosity (µm))	5
Measured water content:	10.43%		

Sample: MXm6 **Temp. (°C):** 20
Solvent: 0.15 M NaNO3/0.01 M EDTA, pH 6.0 **Analyst:** CH

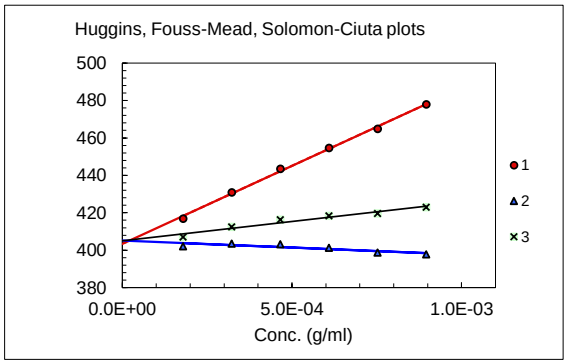

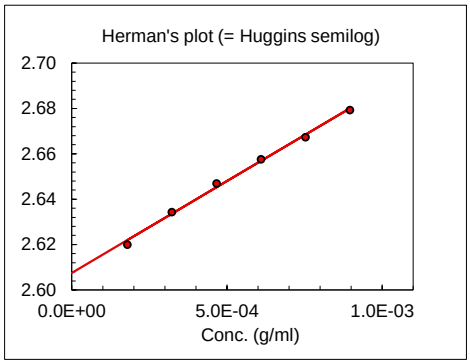

Calculations of the intrinsic viscosity

Fit type.	Fitted data		Linear 1-3 [h] (ml/g)	SD (ml/g)	k'	SD
1	h_{sp}/c vs. c	(Huggins)	**403.4**		0.51	
2	$(\ln h_r)/c$ vs. c	(Mead-Fuoss)	**405.2**		0.45	
3	$[2(h_{sp}-\ln h_r)]^{1/2}/c$	(Solomon-Ciuta)	**405.0**		0.46	
4	log h_{sp}/c vs. c	(Herman)	**405.0**			
Average			**404.6**	0.9	0.48	0.03
Avg. w/o Huggins			**405.1**	0.1	0.46	0.00

Raw data

Conc. (mg/ml)	t (sec)	t(sec)*	h_r	h_{sp}/c (ml/g)	Accepted in regression
0 (solvent)	201.49	200.73			
0.896		286.66	1.43	478	Yes
0.752		270.95	1.35	465	Yes
0.609		256.31	1.28	455	Yes
0.466		242.20	1.21	444	Yes
0.322		228.62	1.14	431	Yes
0.179		215.72	1.07	417	Yes

*) Hagenbach corrected

Dried *in vacuo* over P_2O_5:	Yes	Corrected for water content	Yes
Assumed water content	10.43%	Filter type (porosity (µm))	5
Measured water content:	10.43%		

Sample: MXm10 **Temp. (°C):** 20
Solvent: 0.15 M NaNO3/0.01 M EDTA, pH 6.0 **Analyst:** CH

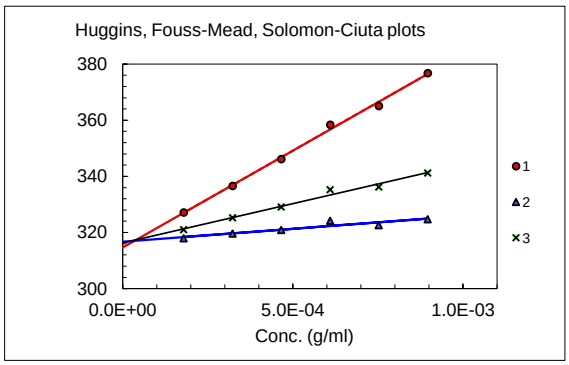

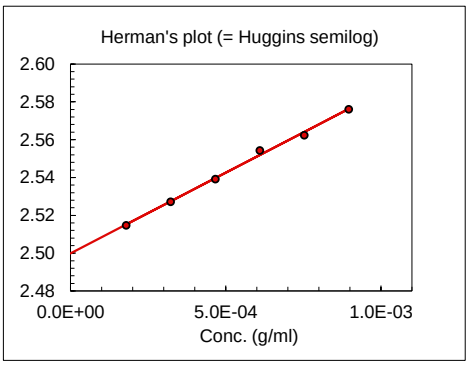

Calculations of the intrinsic viscosity

Fit type.	Fitted data		Linear 1-3 [h] (ml/g)	SD (ml/g)	k'	SD
1	h_{sp}/c vs. c	(Huggins)	**314.6**		0.70	
2	$(\ln h_r)/c$ vs. c	(Fuoss-Mead)	**316.7**		0.59	
3	$[2(h_{sp}-\ln h_r)]^{1/2}/c$	(Solomon-Ciuta)	**316.3**		0.61	
4	log h_{sp}/c vs. c	(Herman)	**316.1**			
Average			**315.9**	0.9	0.63	0.06
Avg. w/o Huggins			**316.4**	0.3	0.60	0.01

Raw data

Conc. (mg/ml)	t (sec)	t(sec)*	h_r	h_{sp}/c (ml/g)	Accepted in regression
0 (solvent)	181.51	180.58			
0.896		241.53	1.34	377	Yes
0.752		230.18	1.27	365	Yes
0.609		220.00	1.22	358	Yes
0.466		209.69	1.16	346	Yes
0.322		200.18	1.11	337	Yes
0.179		191.16	1.06	327	Yes

*) Hagenbach corrected

Dried *in vacuo* over P_2O_5:	Yes	Corrected for water content	Yes
Assumed water content	10.43%	Filter type (porosity (µm))	5
Measured water content:	10.43%		

B.2 Mechanically Degraded XCD

The following pages present reports about each sample belonging to the series of mechanically degraded XCD (see Table 4.3 in Section 4.2.1).

Sample: XCDm0 **Temp. (°C):** 20
Solvent: 0.15 M NaNO3/0.01 M EDTA, pH 6.0 **Analyst:** CH

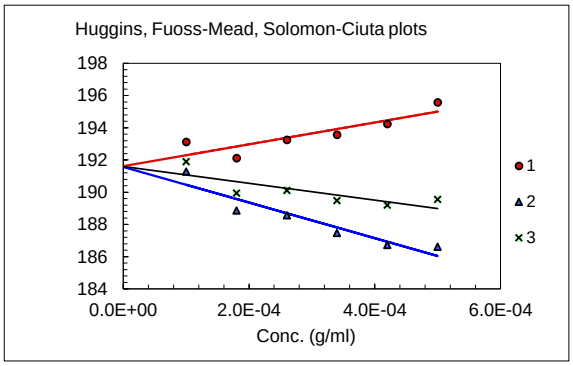

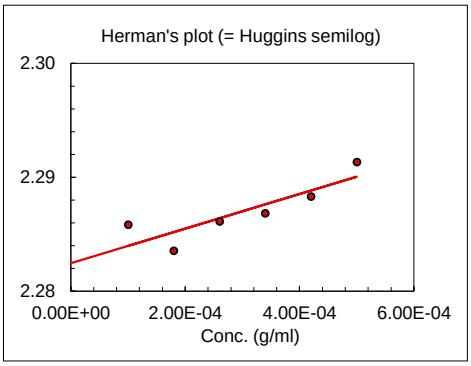

Calculations of the intrinsic viscosity

Fit type.	Fitted data		Linear 1-3 [h] (ml/g)	SD (ml/g)	k'	SD
1	h_{sp}/c vs. c	(Huggins)	**191.62**		0.18	
2	$(\ln h_r)/c$ vs. c	(Fuoss-Mead)	**191.57**		0.20	
3	$[2(h_{sp}-\ln h_r)]^{1/2}/c$	(Solomon-Ciuta)	**191.60**		0.19	
4	$\log h_{sp}/c$ vs. c	(Herman)	**191.63**			
Average			**191.60**	0.03	0.19	0.01
Avg. w/o Huggins			**191.60**	0.03	0.19	0.01

Raw data

Conc. (mg/ml)	t (sec)	t(sec)*	h_r	h_{sp}/c (ml/g)	Accepted in regression
0 (solvent)	201.19	200.43			
0.500		220.03	1.10	196	Yes
0.420		216.78	1.08	194	Yes
0.340		213.62	1.07	194	Yes
0.260		210.50	1.05	193	Yes
0.180		207.36	1.03	192	Yes
0.100		204.30	1.02	193	Yes

*) Hagenbach corrected

Dried *in vacuo* over P_2O_5:	No	Corrected for water content	No
Assumed water content	N/A	Filter type (porosity (µm))	5
Measured water content:	No		

Sample: XCDm1 **Temp. (°C):** 20
Solvent: 0.15 M NaNO3/0.01 M EDTA, pH 6.0 **Analyst:** CH

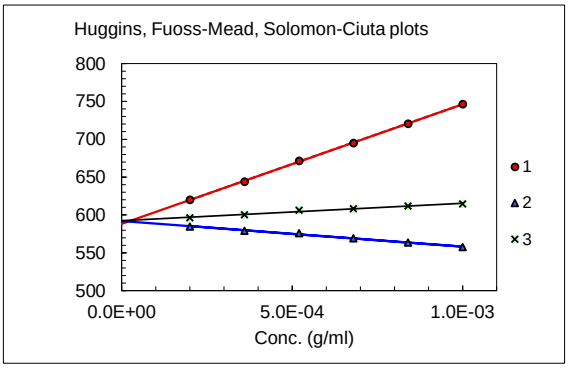

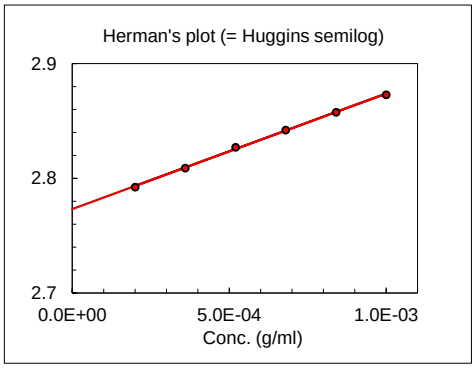

Calculations of the intrinsic viscosity

Fit type.	Fitted data		Linear 1-3 [h] (ml/g)	SD (ml/g)	k'	SD
1	h_{sp}/c vs. c	(Huggins)	**588.2**		0.46	
2	$(\ln h_r)/c$ vs. c	(Fuoss-Mead)	**592.0**		0.40	
3	$[2(h_{sp}-\ln h_r)]^{1/2}/c$	(Solomon-Ciuta)	**592.4**		0.40	
4	$\log h_{sp}/c$ vs. c	(Herman)	**593.1**			
Average			**591**	2	0.42	0.032
Avg. w/o Huggins			**592.5**	0.6	0.401	0.004

Raw data

Conc. (mg/ml)	t (sec)	t(sec)*	h_r	h_{sp}/c (ml/g)	Accepted in regression
0 (solvent)	201.19	200.43			
1.000		350.04	1.75	746	Yes
0.840		321.76	1.61	721	Yes
0.680		295.16	1.47	695	Yes
0.520		270.43	1.35	672	Yes
0.360		246.90	1.23	644	Yes
0.200		225.29	1.12	620	Yes

*) Hagenbach corrected

Dried *in vacuo* over P_2O_5:	No	Corrected for water content	No
Assumed water content	N/A	Filter type (porosity (µm))	5
Measured water content:	No		

Sample: XCDm2 **Temp. (°C):** 20
Solvent: 0.15 M NaNO3/0.01 M EDTA, pH 6.0 **Analyst:** CH

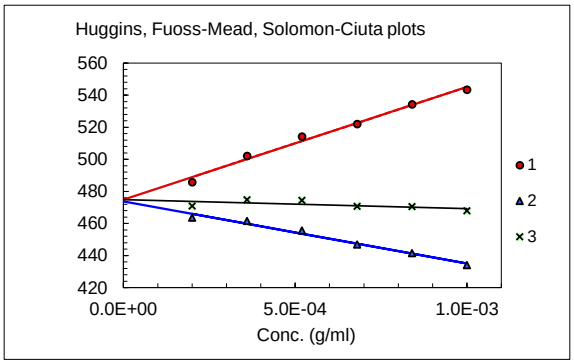

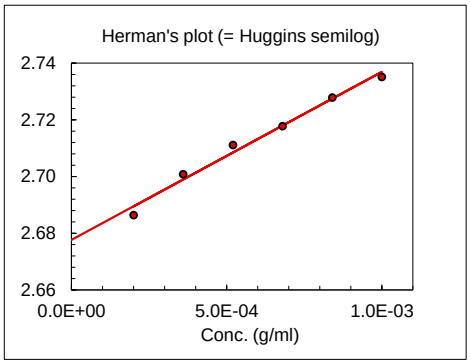

Calculations of the intrinsic viscosity

Fit type.	Fitted data		Linear 1-3 [h] (ml/g)	SD (ml/g)	k'	SD
1	h_{sp}/c vs. c	(Huggins)	**474.8**		0.31	
2	$(\ln h_r)/c$ vs. c	(Fuoss-Mead)	**473.8**		0.33	
3	$[2(h_{sp}-\ln h_r)]^{1/2}/c$	(Solomon-Ciuta)	**474.8**		0.31	
4	$\log h_{sp}/c$ vs. c	(Herman)	**476.0**			
Average			**474.9**	0.9	0.32	0.01
Avg. w/o Huggins			**474.9**	1.1	0.32	0.01

Raw data

Conc. (mg/ml)	t (sec)	t(sec)*	h_r	h_{sp}/c (ml/g)	Accepted in regression
0 (solvent)	201.19	200.43			
1.000		309.36	1.54	543	Yes
0.840		290.40	1.45	534	Yes
0.680		271.59	1.36	522	Yes
0.520		254.02	1.27	514	Yes
0.360		236.66	1.18	502	Yes
0.200		219.90	1.10	486	Yes

*) Hagenbach corrected

Dried *in vacuo* over P_2O_5:	No	Corrected for water content	No
Assumed water content	N/A	Filter type (porosity (µm))	5
Measured water content:	No		

Sample: XCDm3 **Temp. (°C):** 20
Solvent: 0.15 M NaNO3/0.01 M EDTA, pH 6.0 **Analyst:** CH

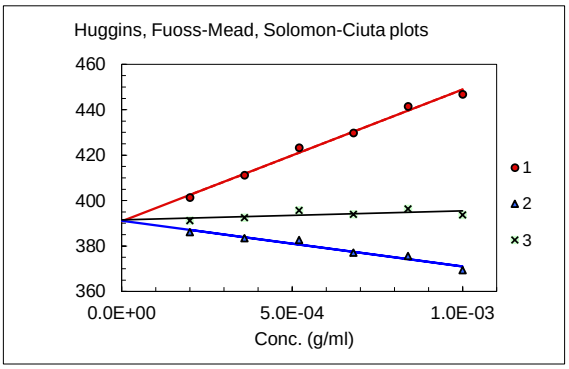

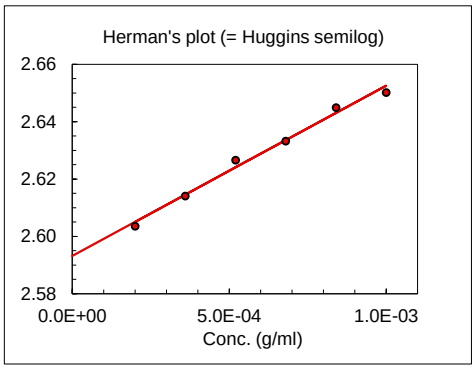

Calculations of the intrinsic viscosity

Fit type.	Fitted data		Linear 1-3 [h] (ml/g)	SD (ml/g)	k'	SD
1	h_{sp}/c vs. c	(Huggins)	**390.9**		0.38	
2	$(\ln h_r)/c$ vs. c	(Fuoss-Mead)	**391.1**		0.37	
3	$[2(h_{sp}-\ln h_r)]^{1/2}/c$	(Solomon-Ciuta)	**391.5**		0.36	
4	$\log h_{sp}/c$ vs. c	(Herman)	**391.9**			
Average			**391.4**	0.4	0.37	0.01
Avg. w/o Huggins			**391.5**	0.4	0.36	0.01

Raw data

Conc. (mg/ml)	t (sec)	t(sec)*	h_r	h_{sp}/c (ml/g)	Accepted in regression
0 (solvent)	201.19	200.43			
1.000		290.00	1.45	447	Yes
0.840		274.77	1.37	442	Yes
0.680		259.01	1.29	430	Yes
0.520		244.55	1.22	423	Yes
0.360		230.10	1.15	411	Yes
0.200		216.52	1.08	401	Yes

*) Hagenbach corrected

Dried *in vacuo* over P_2O_5:	No	Corrected for water content	No
Assumed water content	N/A	Filter type (porosity (µm))	5
Measured water content:	No		

Sample: XCDm4 **Temp. (°C):** 20
Solvent: 0.15 M NaNO3/0.01 M EDTA, pH 6.0 **Analyst:** CH

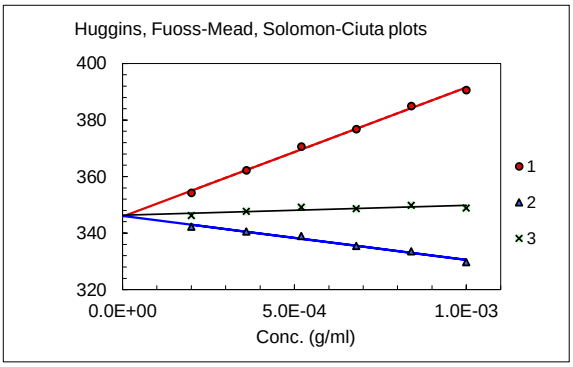

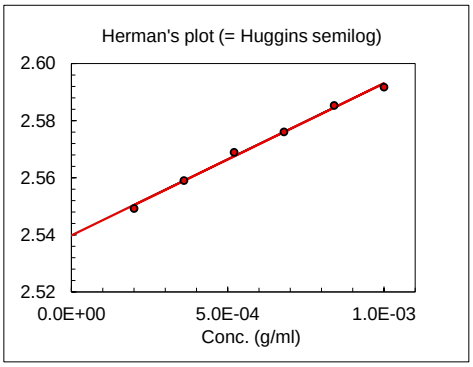

Calculations of the intrinsic viscosity

Fit type.	Fitted data		Linear 1-3 [h] (ml/g)	SD (ml/g)	k'	SD
1	h_{sp}/c vs. c	(Huggins)	**345.8**		0.38	
2	$(\ln h_r)/c$ vs. c	(Fuoss-Mead)	**346.1**		0.37	
3	$[2(h_{sp}-\ln h_r)]^{1/2}/c$	(Solomon-Ciuta)	**346.3**		0.36	
4	log h_{sp}/c vs. c	(Herman)	**346.6**			
Average			**346.2**	0.3	0.37	0.01
Avg. w/o Huggins			**346.3**	0.2	0.37	0.01

Raw data

Conc. (mg/ml)	t (sec)	t(sec)*	h_r	h_{sp}/c (ml/g)	Accepted in regression
0 (solvent)	201.19	200.43			
1.000		278.72	1.39	391	Yes
0.840		265.24	1.32	385	Yes
0.680		251.78	1.26	377	Yes
0.520		239.06	1.19	371	Yes
0.360		226.57	1.13	362	Yes
0.200		214.63	1.07	354	Yes

*) Hagenbach corrected

Dried *in vacuo* over P_2O_5:	No	Corrected for water content	No
Assumed water content	N/A	Filter type (porosity (µm))	5
Measured water content:	No		

Sample: XCDm6 **Temp. (°C):** 20
Solvent: 0.15 M NaNO3/0.01 M EDTA, pH 6.0 **Analyst:** CH

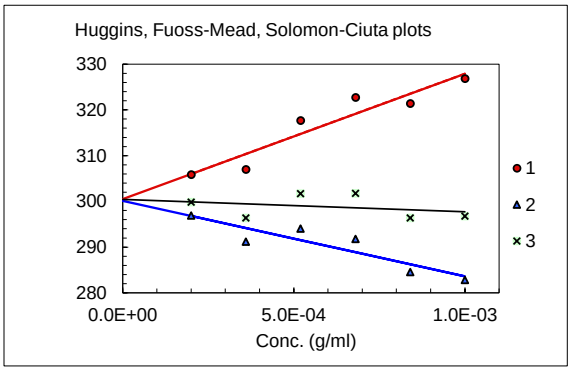

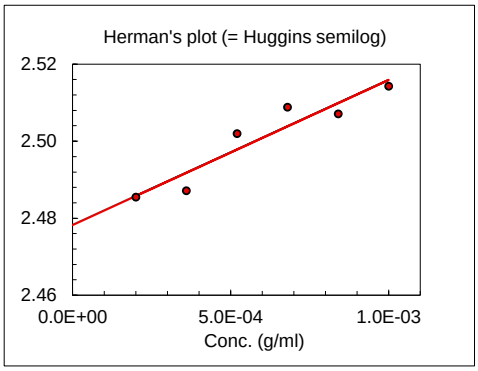

Calculations of the intrinsic viscosity

Fit type.	Fitted data		Linear 1-3 [h] (ml/g)	SD (ml/g)	k'	SD
1	h_{sp}/c vs. c	(Huggins)	**300.5**		0.30	
2	$(\ln h_r)/c$ vs. c	(Fuoss-Mead)	**300.1**		0.32	
3	$[2(h_{sp}-\ln h_r)]^{1/2}/c$	(Solomon-Ciuta)	**300.4**		0.30	
4	$\log h_{sp}/c$ vs. c	(Herman)	**300.8**			
Average			**300.5**	0.3	0.31	0.01
Avg. w/o Huggins			**300.4**	0.3	0.31	0.01

Raw data

Conc. (mg/ml)	t (sec)	t(sec)*	h_r	h_{sp}/c (ml/g)	Accepted in regression
0 (solvent)	201.19	200.43			
1.000		265.94	1.33	327	Yes
0.840		254.55	1.27	321	Yes
0.680		244.42	1.22	323	Yes
0.520		233.54	1.17	318	Yes
0.360		222.58	1.11	307	Yes
0.200		212.69	1.06	306	Yes

*) Hagenbach corrected

Dried *in vacuo* over P_2O_5:	No	Corrected for water content	No
Assumed water content	N/A	Filter type (porosity (µm))	5
Measured water content:	No		

Sample: XCDm10 **Temp. (°C):** 20
Solvent: 0.15 M NaNO3/0.01 M EDTA, pH 6.0 **Analyst:** CH

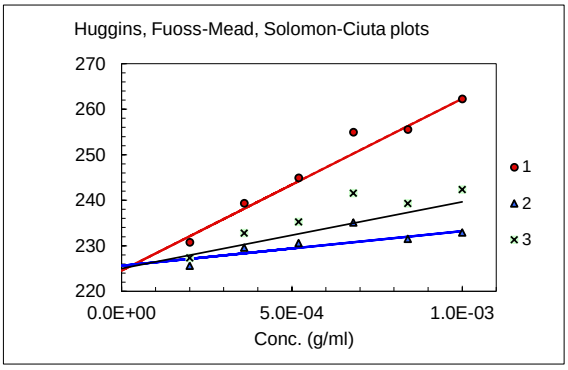

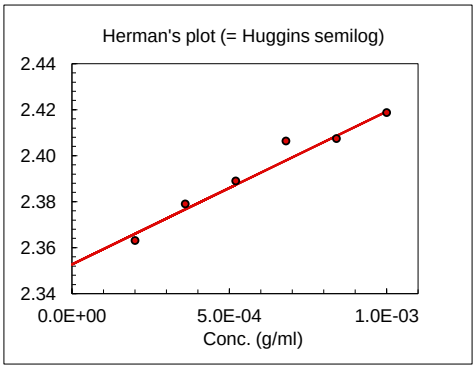

Calculations of the intrinsic viscosity

Fit type.	Fitted data		Linear 1-3 [h] (ml/g)	SD (ml/g)	k'	SD
1	h_{sp}/c vs. c	(Huggins)	**224.5**		0.75	
2	$(\ln h_r)/c$ vs. c	(Fuoss-Mead)	**225.6**		0.65	
3	$[2(h_{sp}-\ln h_r)]^{1/2}/c$	(Solomon-Ciuta)	**225.4**		0.67	
4	$\log h_{sp}/c$ vs. c	(Herman)	**225.3**			
Average			**225.2**	0.5	0.69	0.05
Avg. w/o Huggins			**225.4**	0.2	0.66	0.02

Raw data

Conc. (mg/ml)	t (sec)	t(sec)*	h_r	h_{sp}/c (ml/g)	Accepted in regression
0 (solvent)	201.19	200.43			
1.000		253.00	1.26	262	Yes
0.840		243.46	1.21	256	Yes
0.680		235.18	1.17	255	-
0.520		225.96	1.13	245	Yes
0.360		217.70	1.09	239	Yes
0.200		209.68	1.05	231	Yes

*) Hagenbach corrected

Dried *in vacuo* over P_2O_5:	No	Corrected for water content	No
Assumed water content	N/A	Filter type (porosity (µm))	5
Measured water content:	No		

B.3 XCDp and xan0614-3

The following pages present reports for the samples in Table 4.4, Section 4.2.1.2.

Sample: XCDp-m0 **Temp. (°C):** 20
Solvent: 0.15 M NaNO3/0.01 M EDTA, pH 6.0 **Analyst:** CH

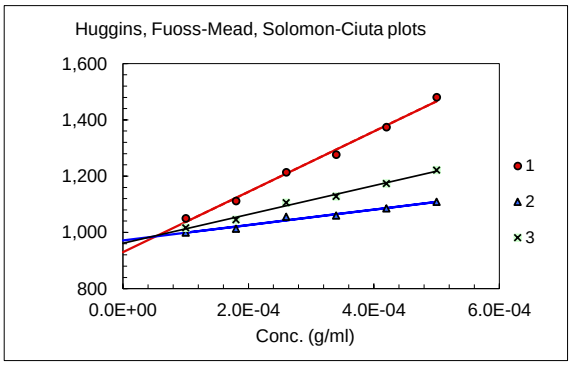

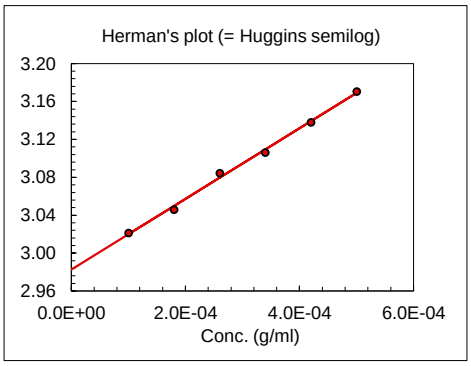

Calculations of the intrinsic viscosity

Fit type.	Fitted data		Linear 1-3 [h] (ml/g)	SD (ml/g)	k'	SD
1	h_{sp}/c vs. c	(Huggins)	**930**		1.24	
2	$(\ln h_r)/c$ vs. c	(Fuoss-Mead)	**971**		0.79	
3	$[2(h_{sp}-\ln h_r)]^{1/2}/c$	(Solomon-Ciuta)	**961**		0.89	
4	$\log h_{sp}/c$ vs. c	(Herman)	**961**			
Average			**956**	18	0.97	0.24
Avg. w/o Huggins			**964**	6	0.84	0.07

Raw data

Conc. (mg/ml)	t (sec)	t(sec)*	h_r	h_{sp}/c (ml/g)	Accepted in regression
0 (solvent)	201.36	200.60			
0.500		349.18	1.74	1,481	Yes
0.420		316.41	1.58	1,374	Yes
0.340		287.68	1.43	1,277	Yes
0.260		263.94	1.32	1,214	Yes
0.180		240.75	1.20	1,112	Yes
0.100		221.68	1.11	1,051	Yes

*) Hagenbach corrected

Dried *in vacuo* over P_2O_5:	Yes	Corrected for water content	Yes
Assumed water content	5.70%	Filter type (porosity (µm))	N/A
Measured water content:	No		

Sample: xan0614-3m0 **Temp. (°C):** 20
Solvent: 0.15 M NaNO3/0.01 M EDTA, pH 6.0 **Analyst:** CH

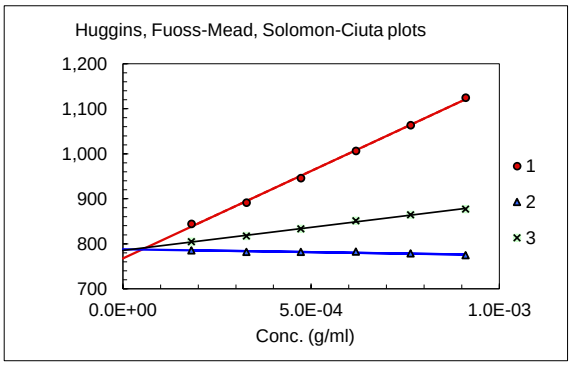

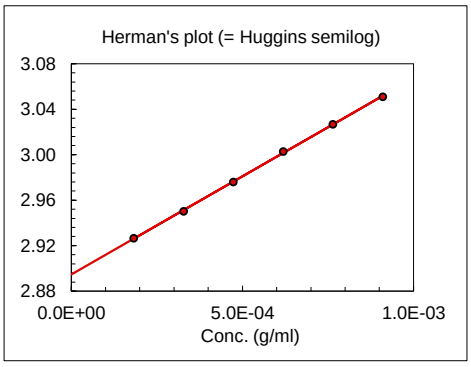

Calculations of the intrinsic viscosity

Fit type.	Fitted data		Linear 1-3 [h] (ml/g)	SD (ml/g)	k'	SD
1	h_{sp}/c vs. c	(Huggins)	**767.5**		0.66	
2	$(\ln h_r)/c$ vs. c	(Fuoss-Mead)	**787.8**		0.48	
3	$[2(h_{sp}-\ln h_r)]^{1/2}/c$	(Solomon-Ciuta)	**785.3**		0.50	
4	log h_{sp}/c vs. c	(Herman)	**784.6**			
Average			**781.3**	9.3	0.55	0.10
Avg. w/o Huggins			**785.9**	1.7	0.49	0.01

Raw data

Conc. (mg/ml)	t (sec)	t(sec)*	h_r	h_{sp}/c (ml/g)	Accepted in regression
0 (solvent)	201.36	200.60			
0.910		405.92	2.02	1,125	Yes
0.764		363.67	1.81	1,064	Yes
0.619		325.61	1.62	1,007	Yes
0.473		290.39	1.45	946	Yes
0.328		259.28	1.29	892	Yes
0.182		231.43	1.15	844	Yes

*) Hagenbach corrected

Dried *in vacuo* over P_2O_5:	Yes	Corrected for water content	Yes
Assumed water content	11.30%	Filter type (porosity (µm))	5
Measured water content:	No		

Sample: xan0614-3m10 **Temp. (°C):** 20
Solvent: 0.15 M NaNO3/0.01 M EDTA, pH 6.0 **Analyst:** CH

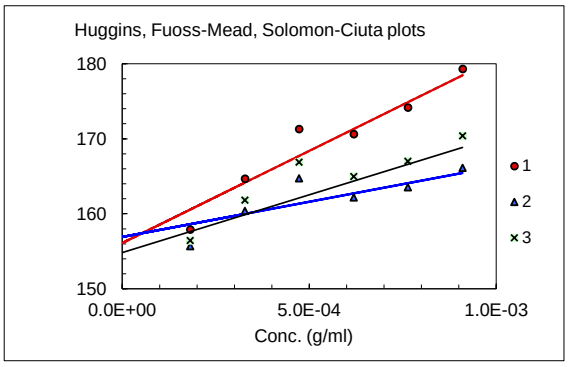

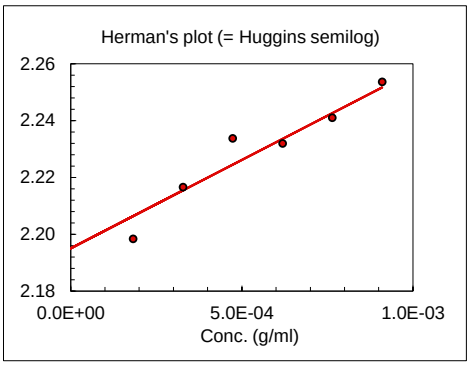

Calculations of the intrinsic viscosity

Fit type.	Fitted data		Linear 1-3 [h] (ml/g)	SD (ml/g)	k'	SD
1	h_{sp}/c vs. c	(Huggins)	**156.1**		1.01	
2	$(\ln h_r)/c$ vs. c	(Fuoss-Mead)	**156.9**		0.88	
3	$[2(h_{sp}-\ln h_r)]^{1/2}/c$	(Solomon-Ciuta)	**156.7**		0.91	
4	log h_{sp}/c vs. c	(Herman)	**156.7**			
Average			**156.6**	0.3	0.93	0.07
Avg. w/o Huggins			**156.8**	0.1	0.90	0.02

Raw data

Conc. (mg/ml)	t (sec)	t(sec)*	h_r	h_{sp}/c (ml/g)	Accepted in regression
0 (solvent)	201.36	200.60			
0.910		233.34	1.16	179	Yes
0.764		227.30	1.13	174	Yes
0.619		221.79	1.11	171	Yes
0.473		216.86	1.08	171	-
0.328		211.44	1.05	165	Yes
0.182		206.37	1.03	158	-

*) Hagenbach corrected

Dried *in vacuo* over P_2O_5:	Yes	Corrected for water content	Yes
Assumed water content	11.30%	Filter type (porosity (µm))	5
Measured water content:	No		

B.4 XCD and MX in $NaHCO_3$/NaOH

The following pages present reports for the MX and XCD samples in Table 4.5, Section 4.2.1.3 that were analysed using $NaHCO_3$/NaOH as solvent.

Sample: XCDm0 **Temp. (°C):** 25
Solvent: 25 mM NaHCO3/19.1 mM NaOH, pH 10.8 **Analyst:** CH

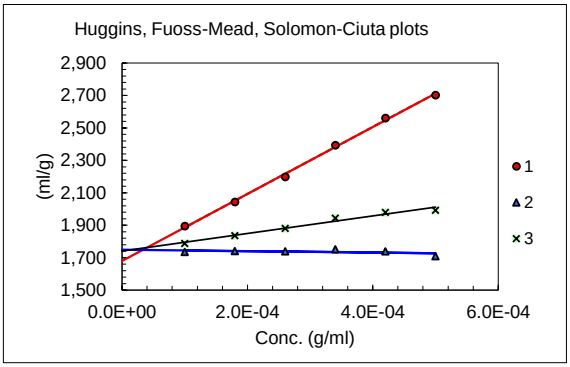

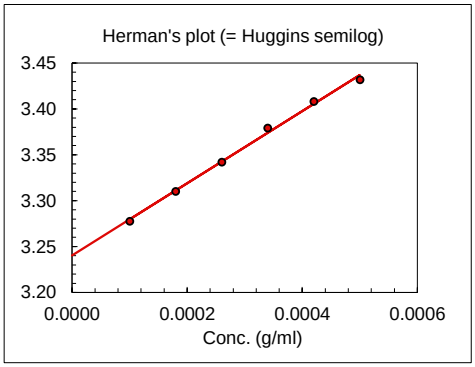

Calculations of the intrinsic viscosity

Fit type.	Fitted data		Linear 1-3 [h] (ml/g)	SD (ml/g)	k'	SD
1	h_{sp}/c vs. c	(Huggins)	**1,680**		0.73	
2	$(\ln h_r)/c$ vs. c	(Mead-Fuoss)	**1,749**		0.49	
3	$[2(h_{sp}-\ln h_r)]^{1/2}/c$	(Solomon-Ciuta)	**1,741**		0.51	
4	$\log h_{sp}/c$ vs. c	(Herman)	**1,739**			
Average			**1,727**	32	0.58	0.14
Avg. w/o Huggins			**1,743**	5	0.50	0.02

Raw data

Conc. (mg/ml)	t (sec)	t(sec)*	h_r	h_{sp}/c (ml/g)	Accepted in regression
0 (solvent)	180.86	179.92			
0.500		423.05	2.35	2,703	Yes
0.420		373.42	2.08	2,561	Yes
0.340		326.38	1.81	2,394	Yes
0.260		282.75	1.57	2,198	Yes
0.180		246.10	1.37	2,044	Yes
0.100		214.03	1.19	1,896	Yes

*) Hagenbach corrected

Dried *in vacuo* over P_2O_5:	No	Corrected for water content	No
Assumed water content	N/A	Filter type (porosity (µm))	5
Measured water content:	No		

Sample: MXm0 **Temp. (°C):** 25
Solvent: 25 mM NaHCO3/19.1 mM NaOH, pH 10.8 **Analyst:** CH

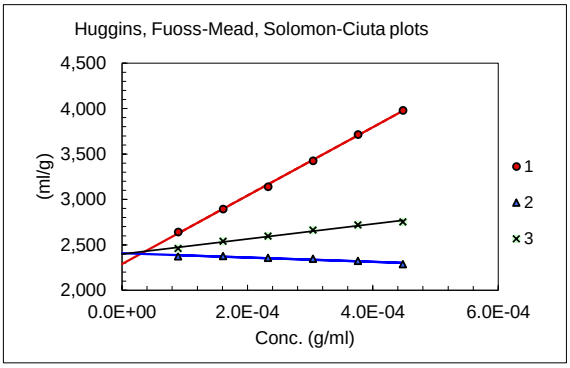

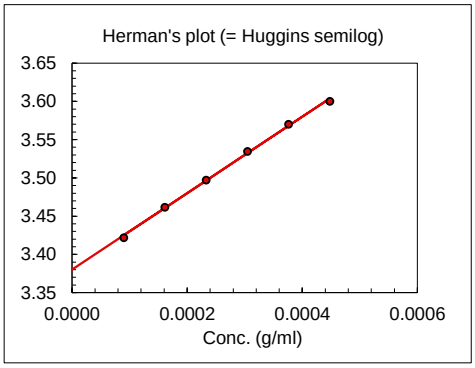

Calculations of the intrinsic viscosity

Fit type.	Fitted data		Linear 1-3 [h] (ml/g)	SD (ml/g)	k'	SD
1	h_{sp}/c vs. c	(Huggins)	**2,289**		0.72	
2	$(\ln h_r)/c$ vs. c	(Mead-Fuoss)	**2,408**		0.46	
3	$[2(h_{sp}-\ln h_r)]^{1/2}/c$	(Solomon-Ciuta)	**2,399**		0.48	
4	$\log h_{sp}/c$ vs. c	(Herman)	**2,399**			
Average			**2,374**	57	0.55	0.14
Avg. w/o Huggins			**2,402**	5	0.47	0.01

Raw data

Conc. (mg/ml)	t (sec)	t(sec)*	h_r	h_{sp}/c (ml/g)	Accepted in regression
0 (solvent)	180.86	179.92			
0.448		500.80	2.78	3,982	Yes
0.376		431.44	2.40	3,716	Yes
0.305		367.65	2.04	3,426	Yes
0.233		311.55	1.73	3,142	Yes
0.161		263.92	1.47	2,896	Yes
0.090		222.51	1.24	2,643	Yes

*) Hagenbach corrected

Dried *in vacuo* over P_2O_5:	Yes	Corrected for water content	Yes
Assumed water content	10.43 %	Filter type (porosity (µm))	5
Measured water content:	10.43%		

Appendix C

SEC-MALLS

This appendix contains supplementary diagrams and data of samples analysed with SEC-MALLS. Complete experimental data are included in the digital attachment under "Supplementary files/SEC-MALLS/ASTRA 6 Experiments/" (requires the software ASTRA by Wyatt Technology).

C.1 Example of Regression Analysis

Fig. C.1 shows an example of how the Berry model was used to fit light scattering data during processing in the software ASTRA.

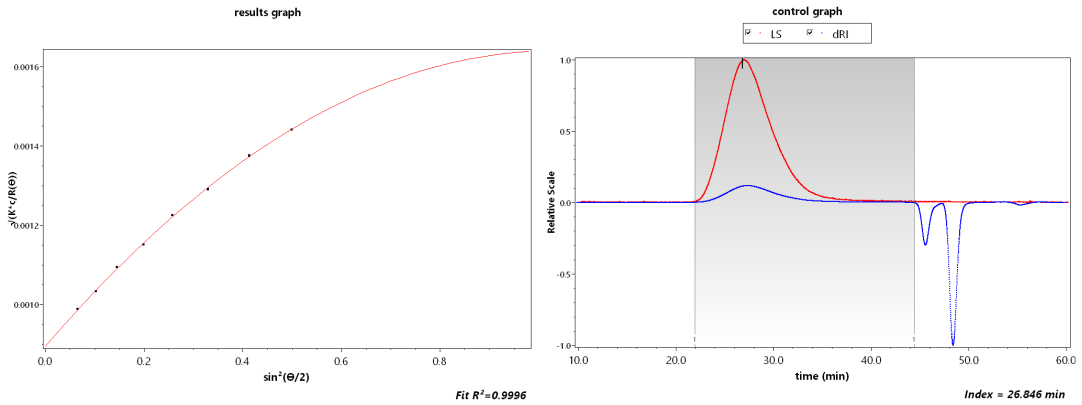

Figure C.1: Example of how a second order polynomial expansion was used to fit light scattering data plotted according to the Berry fit method for extrapolation towards $\theta = 0$. These data have been obtained by analysis of MXm1b (see Section 4.2.2.1) in ASTRA. Only LS detectors 4-11 were included. Data shown in the results graph are those obtained for a specific slice as indicated by the vertical line close to the apex of the red LS curve in the control graph.

C.2 SEC-MALLS of MX

Fig C.2 displays chromatograms and molecular weight distributions for injections *a* and *b*, respectively, for all samples from the series of mechanically degraded MX. Supplementary data are presented in Tables C.1 and C.2. Columns titled "Uncrt" refer to the statistical uncertainties of the quantities in the neighbouring column to the left. These were calculated with ASTRA[41].

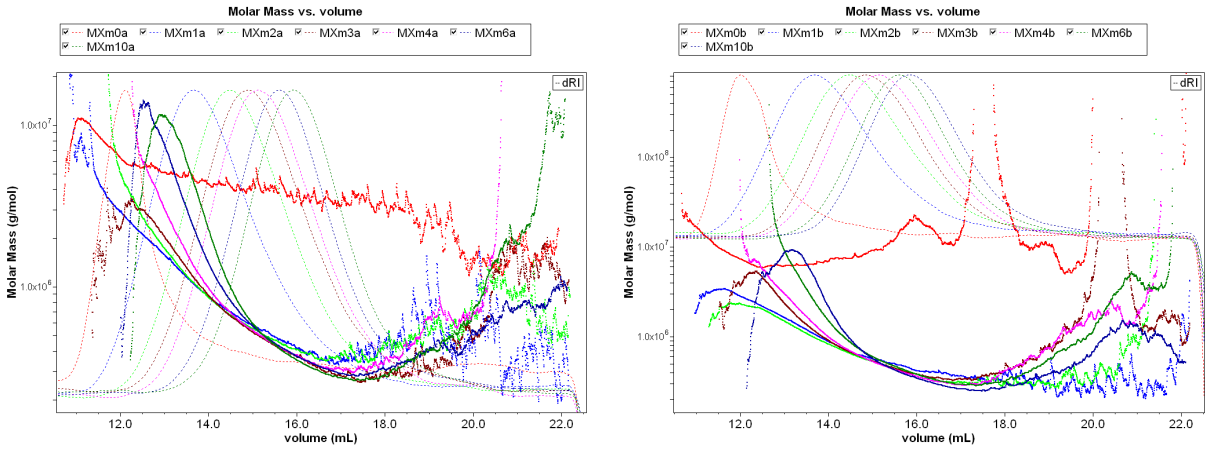

(a) MX - Injection *a*

(b) MX - Injection *b*

Figure C.2: Chromatograms and molecular weight distributions for injections *a* and *b* of all samples belonging to the series of mechanically degraded MX. Dashed lines with thinner line widths correspond to the differential refractive index signals, scaled relatively against their respective magnitudes. Data plotted as squares correspond to molecular weights. The SEC columns used were TSK G6000 + G5000 PWXL, and the buffer used was 150 mM $NaNO_3$/10 mM EDTA.

Table C.1: Part I of data obtained by SEC-MALLS analyses of the undegraded and the series of mechanically degraded MX samples.

Sample	Mn (kDa)	Uncrt	Mw (kDa)	Uncrt	Polydispersity (Mw/Mn)	Uncrt
MXm0a	4175.4	16.00%	5249.1	9.40%	1.257	18.57%
MXm0b	7289.1	7.10%	7779.1	7.60%	1.067	10.36%
MXm1a	784.8	7.10%	1083.3	3.70%	1.380	8.06%
MXm1b	752.9	5.20%	1076.9	2.40%	1.430	5.78%
MXm2a	607.2	3.00%	778.4	2.30%	1.282	3.75%
MXm2b	559.5	3.10%	716.5	2.10%	1.281	3.75%
MXm3a	486.4	3.30%	639.6	2.50%	1.315	4.09%
MXm3b	534.5	1.50%	690.9	1.60%	1.293	2.21%
MXm4a	483.1	1.40%	628.4	1.20%	1.301	1.84%
MXm4b	476.9	1.30%	635.5	1.30%	1.333	1.81%
MXm6a	431.6	1.00%	583.2	0.90%	1.351	1.36%
MXm6b	444.6	0.70%	610.2	0.70%	1.373	1.00%
MXm10a	380.8	0.80%	549.3	0.90%	1.443	1.20%
MXm10b	374.4	1.20%	542.2	1.20%	1.448	1.69%

Table C.2: Part II of data obtained by SEC-MALLS analyses of the undegraded and the series of mechanically degraded MX samples.

Sample	Rw (nm)	Uncrt	Injected mass (µg)	Calculated mass (µg)	Mass recovery (%)
MXm0a	299.2	3.90%	25	25.39	101.6
MXm0b	307.7	2.40%	25	16.22	64.9
MXm1a	115.6	6.70%	50	46.11	92.2
MXm1b	116.3	4.90%	50	46.32	92.6
MXm2a	75.0	8.30%	50	43.67	87.3
MXm2b	78.3	7.10%	50	46.79	93.6
MXm3a	61.0	12.60%	50	48.39	96.8
MXm3b	62.3	7.30%	50	43.55	87.1
MXm4a	51.7	6.40%	50	45.87	91.7
MXm4b	52.3	6.50%	50	45.28	90.6
MXm6a	43.6	5.50%	50	92.35	184.7
MXm6b	45.6	3.50%	50	88.14	176.3
MXm10a	39.0	6.10%	50	91.44	182.9
MXm10b	37.8	9.40%	50	46.77	93.5

C.3 SEC-MALLS of XCD

Fig C.3 displays chromatograms and molecular weight distributions for all samples from the series of mechanically degraded XCD. Supplementary data are presented in Tables C.3 and C.4. Columns titled "Uncrt" refer to the statistical uncertainties of the quantities in the neighbouring column to the left. These were calculated with ASTRA[41].

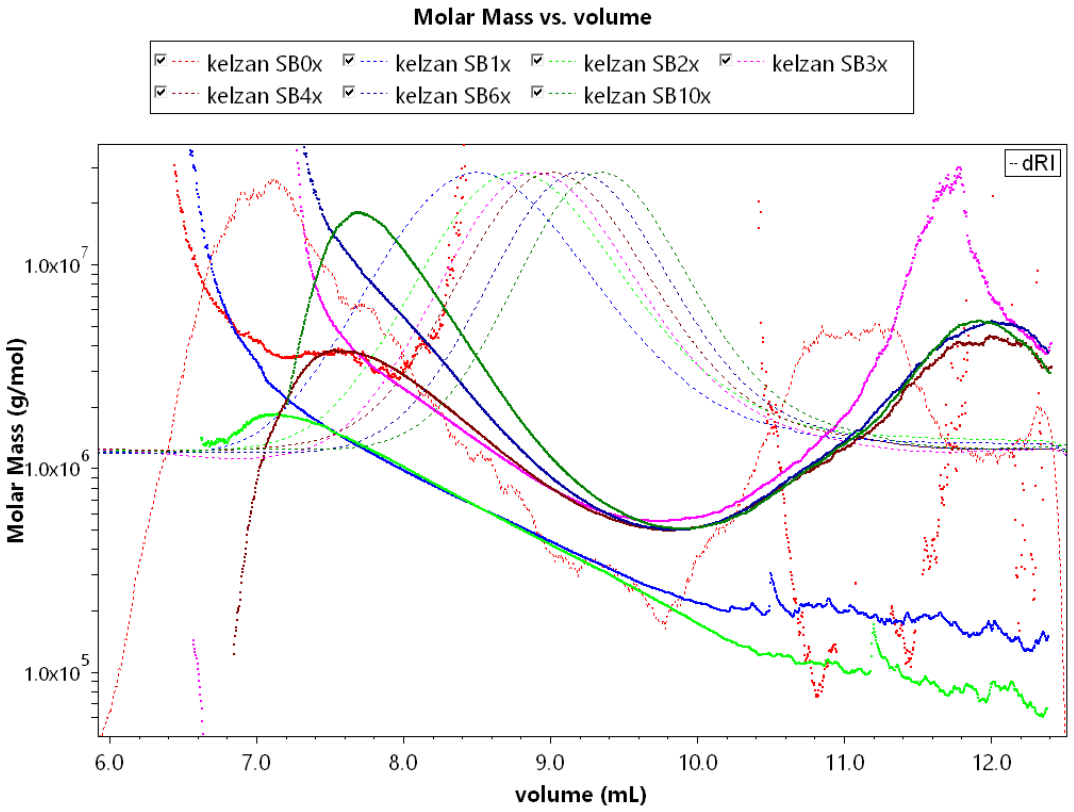

Figure C.3: Chromatograms and molecular weight distributions of all samples belonging to the series of mechanically degraded XCD. Dashed lines with thinner line widths correspond to the differential refractive index signals, scaled relatively against their respective magnitudes. Data plotted as squares correspond to molecular weights. The SEC column used was TSK G6000PW, and the buffer was 150 mM $NaNO_3$/10 mM EDTA.

Table C.3: Part I of data obtained by SEC-MALLS analyses of the undegraded and the series of mechanically degraded XCD samples.

Sample	**Mn (kDa)**	**Uncrt**	**Mw (kDa)**	**Uncrt**	**Polydispersity (Mw/Mn)**	**Uncrt**
XCDm0	3846.8	12.60%	4923.0	7.10%	1.280	14.46%
XCDm1	480.3	1.50%	720.6	1.20%	1.500	1.92%
XCDm2	333.9	2.70%	542.2	0.80%	1.624	2.84%
XCDm3	874.2	0.30%	1166.6	0.40%	1.334	0.46%
XCDm4	812.2	0.50%	1113.1	0.50%	1.370	0.71%
XCDm6	793.8	0.30%	1242.3	0.40%	1.565	0.49%
XCDm10	798.7	0.30%	1414.3	0.30%	1.771	0.44%

Table C.4: Part II of data obtained by SEC-MALLS analyses of the undegraded and the series of mechanically degraded XCD samples.

Sample	**Rw (nm)**	**Uncrt**	**Injected mass (µg)**	**Calculated mass (µg)**	**Mass recovery (%)**
XCDm0	244.5	3.10%	6	0.15	2.6
XCDm1	88.1	2.90%	50	36.82	73.6
XCDm2	70.1	3.20%	50	39.64	79.3
XCDm3	53.5	1.40%	50	34.00	68.0
XCDm4	50.9	2.00%	50	37.73	75.5
XCDm6	47.7	1.60%	100	73.96	74.0
XCDm10	44.9	1.70%	100	75.49	75.5

Appendix D

Rotational Rheometry

Fig. D.1 on the next page shows the complete viscosity-shear rate curves for MX and XCD, where data for concentrations of 500 ug/mL and less have been included in addition to those previously shown in Figs. 4.8a and 4.8b of Section 4.3. Data for shear rates lower than 10^{-2} s^{-1} were not obtained for 1.0 mg/mL and lower. Raw data have been included in the digital attachment under "Supplementary files/Rotational Rheometry/" (some files require the software rSpace by Malvern Instruments).

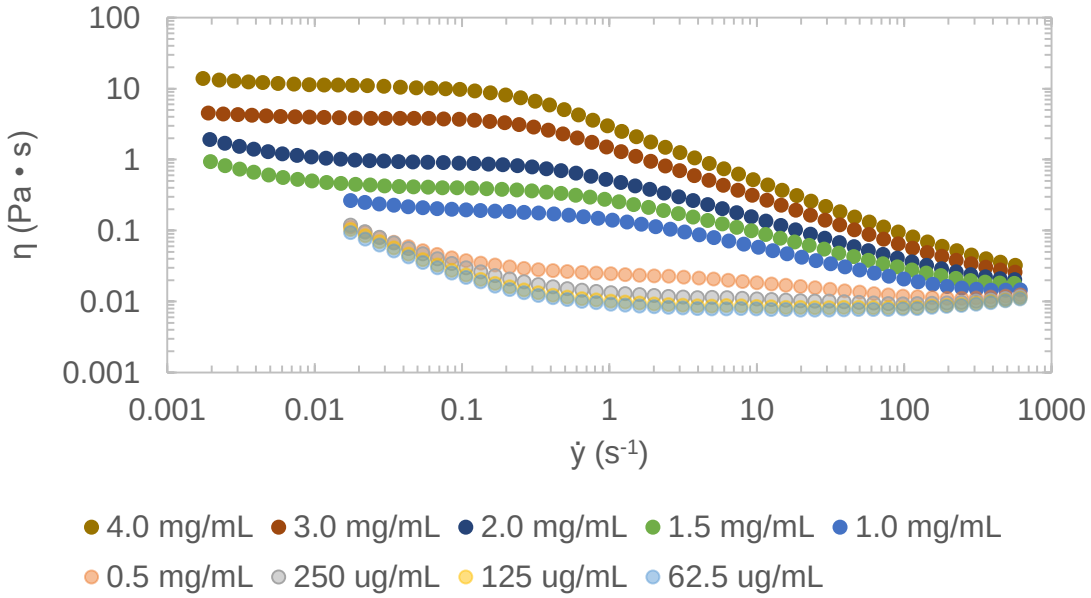

(a) Results for MX.

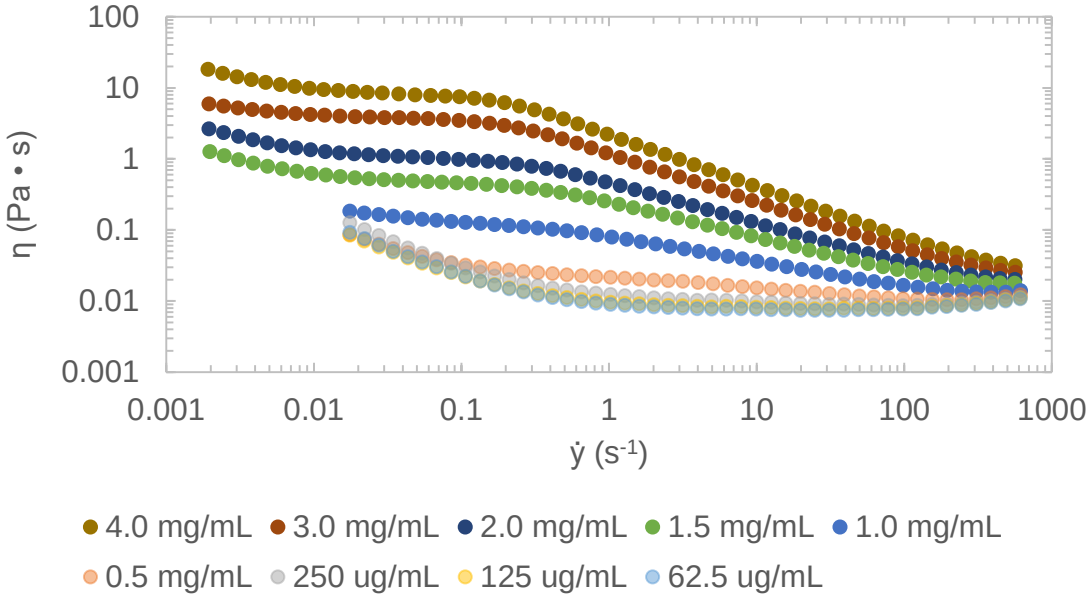

(b) Results for XCD.

Figure D.1: Viscosity-shear rate curves for MX and XCD obtained with the Kinexus ultra+ rotational rheometer (Malvern Panalytical). Data are averages from three parallels of measurements. All concentrations have been included. $T = 25\,°C$.

Appendix E

BCA Assay & Spectrophotometry

E.1 D-Glucose Standard Curves

Standard curves for relating optical density of 560 nm light, OD_{560}, to the molar concentration of reducing ends are given in Figures E.1 and E.2. The curves were established through linear regression of results from D-glucose standards. Each curve is based on results from a separate BCA assay experiment. Reducing end concentrations of xanthan samples were therefore found using the corresponding standard curve from the same analysis. For each sample it has been specified which curve that was used. As the light path of the semi-micro cuvettes was $l = 1$ cm, values for molar absorbtivity (ϵ) have been calculated from the slope of the regression lines according to Eq. 2.23 in Section 2.6.1.

The curve in Fig. E.1b is actually a modification of the one in Fig. E.1a. When performing the BCA assay for most of the xanthan samples (see Tables 4.8 and 4.9 in Section 4.4.1), only three parallels of the 3 µg/mL glucose standard were included as it was assumed that there would not be any significant differences in absorption for the standards. However, the avg. OD_{560} appeared to be 1.35 times larger than for the corresponding 3 µg/mL standard in Fig. E.1a. By assuming that the OD_{560} of the other standards would have increased with the same factor of 1.35, the curve in Fig. E.1b was obtained through scaling of the results in **(a)**. Thus, the expressions for the second linear regression curve became practically identical to the first one. However, this assumption makes the standard curve in Fig. **(b)** more uncertain than the other curves presented here, as it is not known if the other standards really would have had different absorption values.

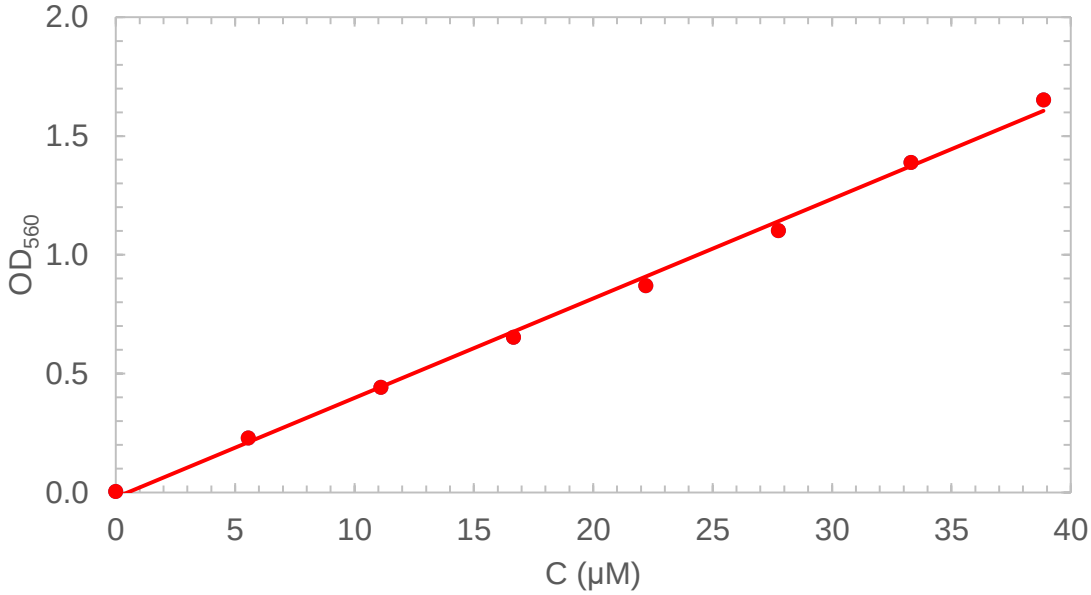

(a) Standard curve used for MX and XCD samples in Table E.1. Trendline: y = 0.0564x - 0.0278, $R^2 = 0.997$. Molar absorptivity: $\epsilon = 56\,400\,M^{-1}\,cm^{-1}$.

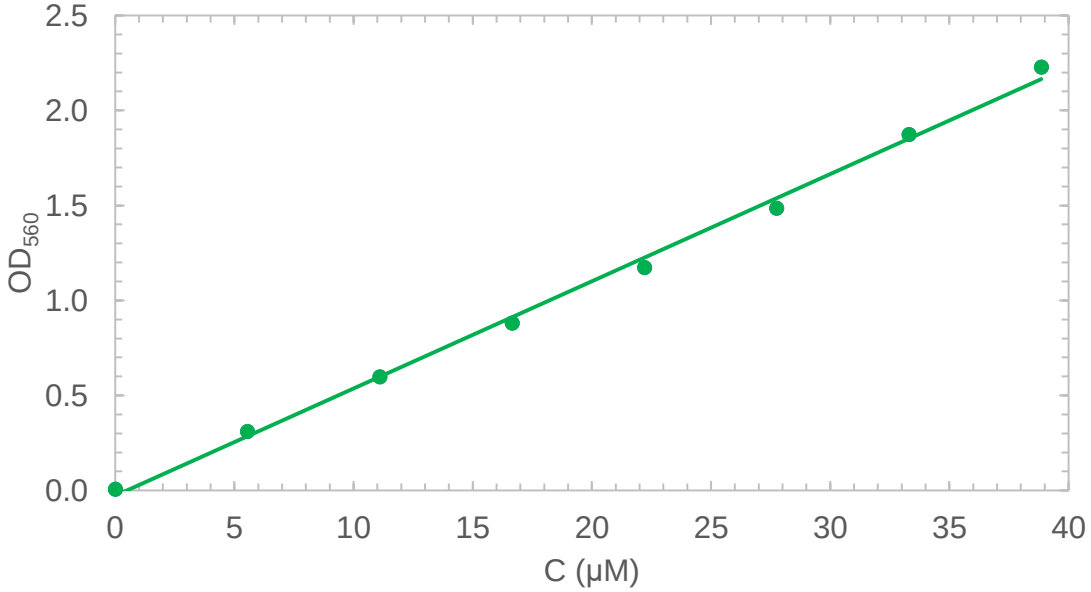

(b) Standard curve used for MX and XCD samples in Table E.2. Obtained by scaling the OD_{560} values of standards in (a) with factor 1.35. Trendline: y = 0.0564x - 0.0278, $R^2 = 0.997$. Molar absorptivity: $\epsilon = 56\,400\,M^{-1}\,cm^{-1}$.

Figure E.1: Standard curves displaying the optical density of 560 nm light for D-glucose standards as a function of reducing end concentration. Used for MX and XCD samples.

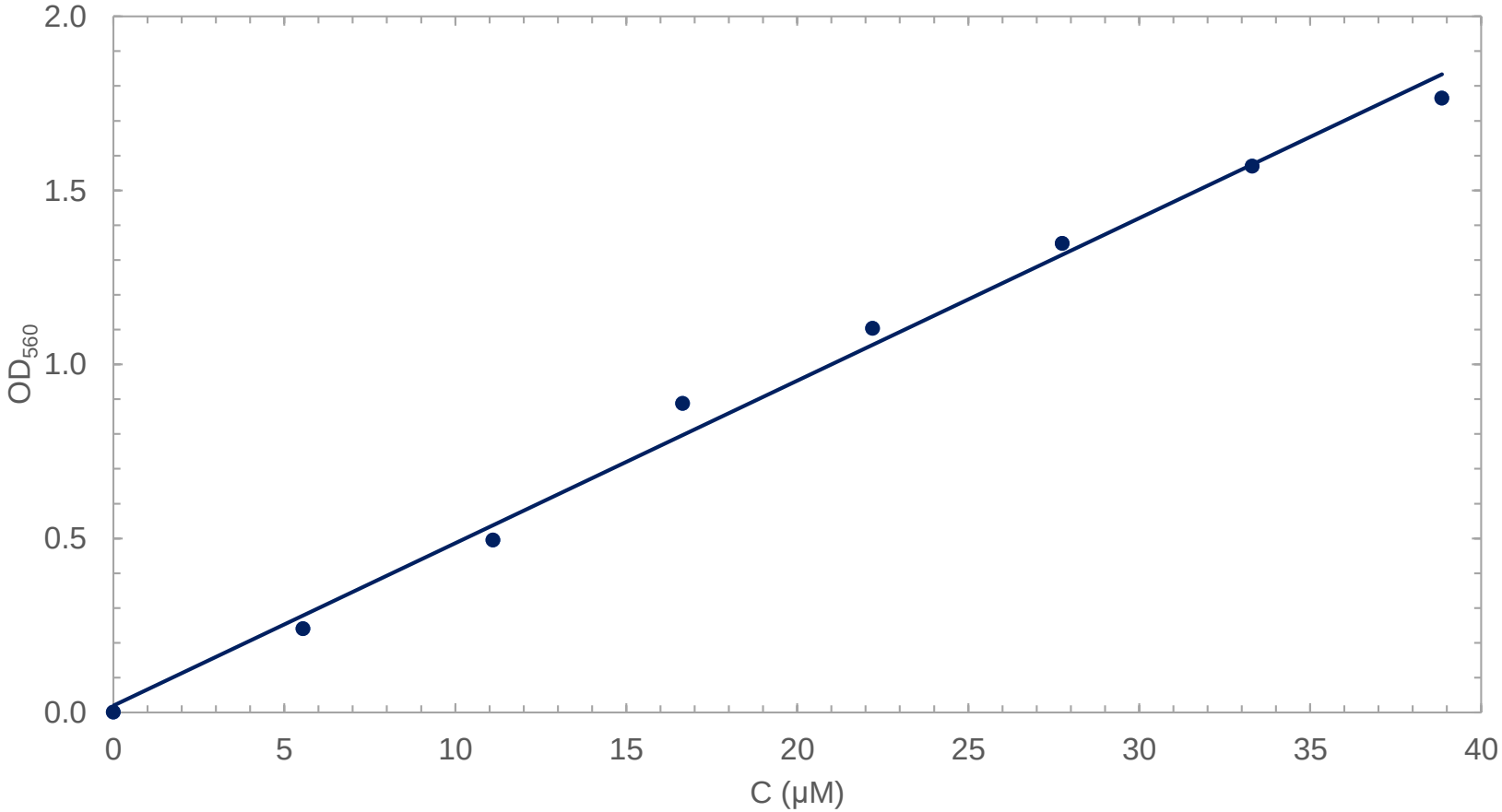

Figure E.2: Standard curve displaying the optical density of 560 nm light for D-glucose standards as a function of reducing end concentration. Used for xan0614-3 samples (see Table E.3). Trendline: y = 0.0467x + 0.0196, $R^2 = 0.993$. Molar absorptivity: $\epsilon = 46\,700\,M^{-1}\,cm^{-1}$.

E.2 Raw Data

Raw data from BCA & spectrophotometry can be found in the following three tables. They have been sorted according to the date of experiment, and thus also according to which standard curve that was used when performing the calculations.

Table E.1: Raw data from the BCA assay experiment on March 8 2018. Obtained using standard curve 1 (Fig. E.1a.

		P1	P2	P3
Sample	**c** (µg/mL)	**OD_{560}**	**OD_{560}**	**OD_{560}**
Glc	0	0.014	−0.005	0.004
	1	0.227	0.235	0.227
	2	0.441	0.445	0.442
	3	0.659	0.653	0.647
	4	0.876	0.558	0.864
	5	1.093	1.098	1.113
	6	1.410	1.386	1.370
	7	1.650	1.653	1.652
MX*	100	3.348	3.380	N/A
XCD*	100	3.540	3.496	N/A
MX†	5000	1.160	1.244	N/A
XCD‡	5000	4.235	4.415	N/A

* Degraded with H_2O_2/NaOH for 1 hour at 80 °C.
† Calculated $DP_n = 177$.
‡ Calculated $DP_n = 50$.
None of the samples were dialysed.

Table E.2: Raw data from the BCA assay experiment on April 15 2018. Obtained using standard curve 2 (Fig. E.1b).

				P1	P2	P3
Sample	**Treatment**	**Time (h)**	**c (µg/mL)**	**OD_{560}**	**OD_{560}**	**OD_{560}**
Glc	N/A	N/A	3	0.874	0.896	0.871
MX	N/A	N/A	500	0.162	0.158	0.158
XCD	N/A	N/A	500	1.596	1.632	1.808
MX	H_2O_2/NaOH and	1	500	0.874	0.886	0.884
XCD	dialysed	1	500	1.476	1.504	1.498
MX	BGI (1:100)	0	250	0.153	0.160	0.157
		1	100	0.061	0.069	0.070
		3	50	0.032	0.037	0.037
		24	25	0.026	0.033	0.027
		48	25	0.029	0.032	0.027
MX	EG (1:1000)	0	250	0.050	0.055	0.052
		1	100	0.039	0.035	0.071
		3	50	0.013	0.017	0.025
		24	25	0.011	0.005	0.004
		48	25	0.006	0.011	0.002
MX	BGI (1:1000)	0	250	0.051	0.048	0.048
		1	100	0.049	0.039	0.036
		3	50	0.018	0.009	0.017
		24	25	0.029	0.010	0.005
		48	25	0.002	0.006	0.001
XCD	BGI (1:100)	0	250	3.880	3.948	3.888
		1	100	3.312	3.340	3.328
		3	50	1.464	1.464	1.452
		24	25	0.686	0.686	0.681
		48	25	1.015	1.021	1.004
XCD	EG (1:1000)	0	250	0.989	0.994	1.031
		1	100	0.468	0.467	0.479
		3	50	0.290	0.293	0.290
		24	25	0.243	0.243	0.235
		48	25	0.408	0.406	0.392
XCD	BGI (1:1000)	0	250	1.224	1.226	1.254
		1	100	1.001	0.993	0.989
		3	50	0.653	0.648	0.641
		24	25	0.797	0.787	0.795
		48	25	0.910	0.906	0.877

Table E.3: Raw data from the BCA assay experiment on April 25 2018. Obtained using standard curve 3 (Fig. E.2).

			P1	P2	P3
Sample	**Time (h)**	**c** (µg/mL)	**OD_{560}**	**OD_{560}**	**OD_{560}**
Glc	N/A	0	−0.001	0.006	−0.001
		1	0.243	0.244	0.236
		2	0.495	0.502	0.489
		3	0.869	0.906	0.888
		4	1.102	1.120	1.090
		5	1.366	1.356	1.322
		6	1.596	1.578	1.536
		7	1.776	1.758	1.762
xan0614-3	0	250	0.155	0.154	0.154
xan0614-3 w/	0	250	0.887	0.884	0.859
BGI (1:100)	1	100	1.374	1.420	1.388
	3	50	1.094	1.097	1.092
	24	25	0.612	0.609	0.611
	44	25	0.563	0.563	0.563

Appendix F

^{1}H-NMR

Additional data such as mass concentration, pD and integrals for ^{1}H-NMR samples can be found in Table F.1. All ^{1}H-NMR spectra are found on the following pages. Raw and processed NMR data can be found in the digital attachment under "Supplementary files/NMR/" (requires the software TopSpin by Bruker).

Table F.1: Additional data about samples analysed with ^{1}H-NMR. The three last columns display the integrals for each peak relative to H-1 α-man for each spectrum.

Sample	**Treatment**	**Dialysed**	**c (mg/mL)**	**pD***	**Bound acetyl**	**Free acetate**	**Bound pyruvyl**
MX	BGI (1:100), 24h	No	10	7.3	4.09	0.15	3.11
	H_2O_2/NaOH	No	8	7.0	0.99	3.65	3.83
	H_2O_2/NaOH	Yes	12	5.8	1.43	0.15	4.60
XCD	BGI (1:1000), 0h	No	3	6.2	3.42	0.03	3.03
	BGI (1:1000), 24h	No	16	5.6	2.81	0.09	1.88
	H_2O_2/NaOH	No	8	7.3	0.57	2.35	1.64
	H_2O_2/NaOH	Yes	12	5.0	1.01	0.07	1.95
xan0614-3	BGI (1:100), 0h	No	8	5.9	2.35	0.01	1.61
	BGI (1:100), 24h	No	8	6.0	2.73	0.02	1.87

* Obtained by measuring with pH micro electrode and adding 0.4 to the resulting value.

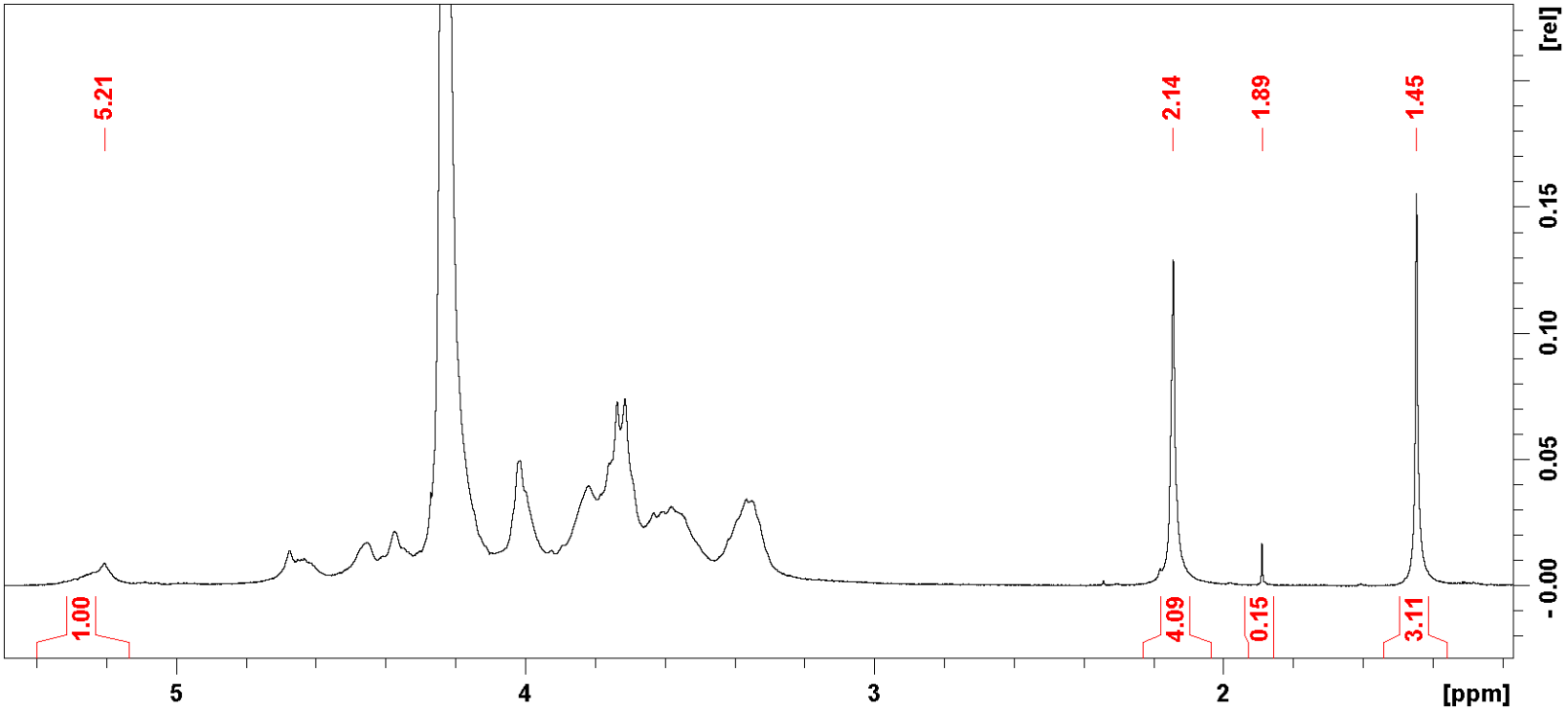

Figure F.1: ^{1}H-NMR spectrum for MX degraded with BGI (1:100) for 24 hours of incubation at 60 °C. Analysed with a Bruker Avance III HD 400 MHz at 80 °C using a 5 mm SmartProbe.

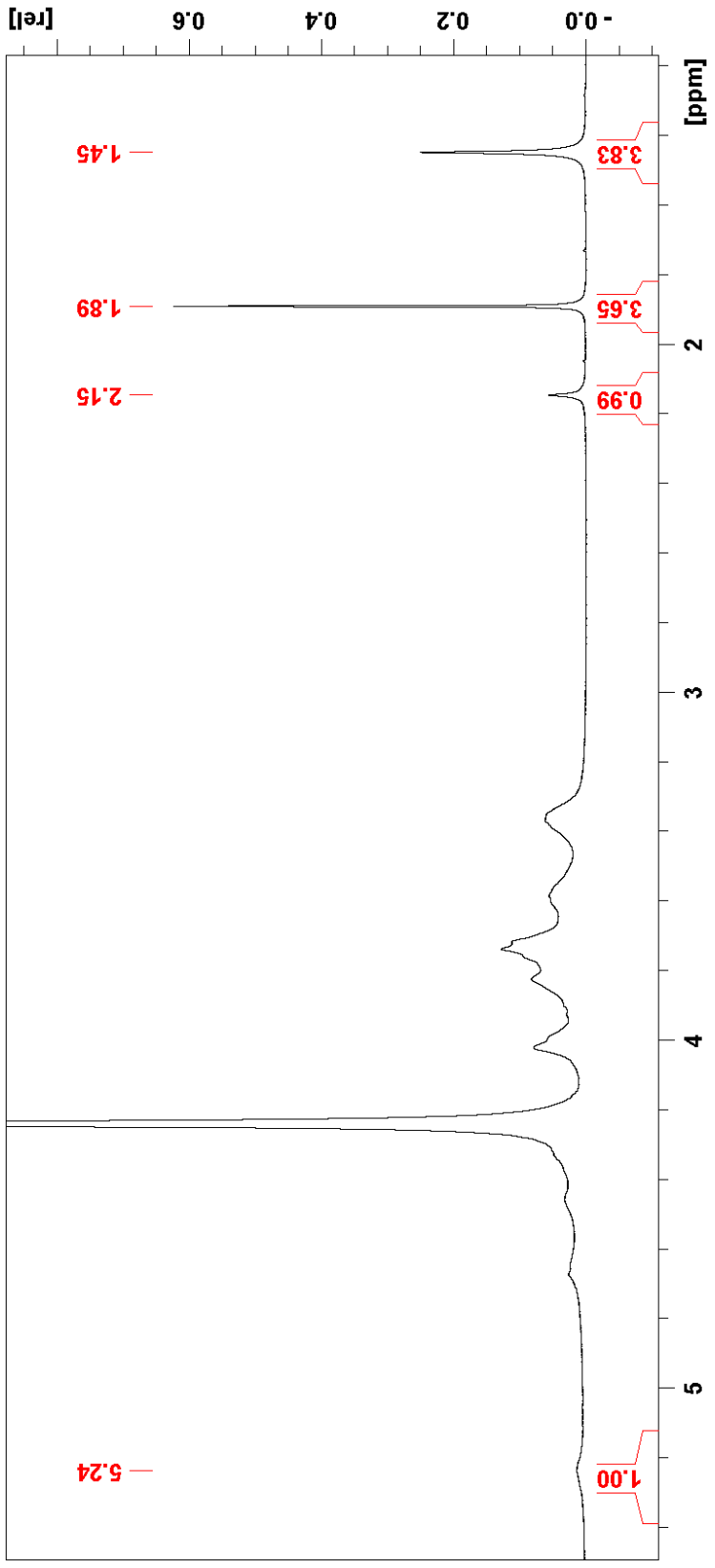

Figure F.2: ^{1}H-NMR spectrum for MX degraded with H_2O_2/NaOH for 1 hour of incubation at 80 °C. Analysed with a Bruker Avance III HD 400 MHz at 80 °C using a 5 mm SmartProbe.

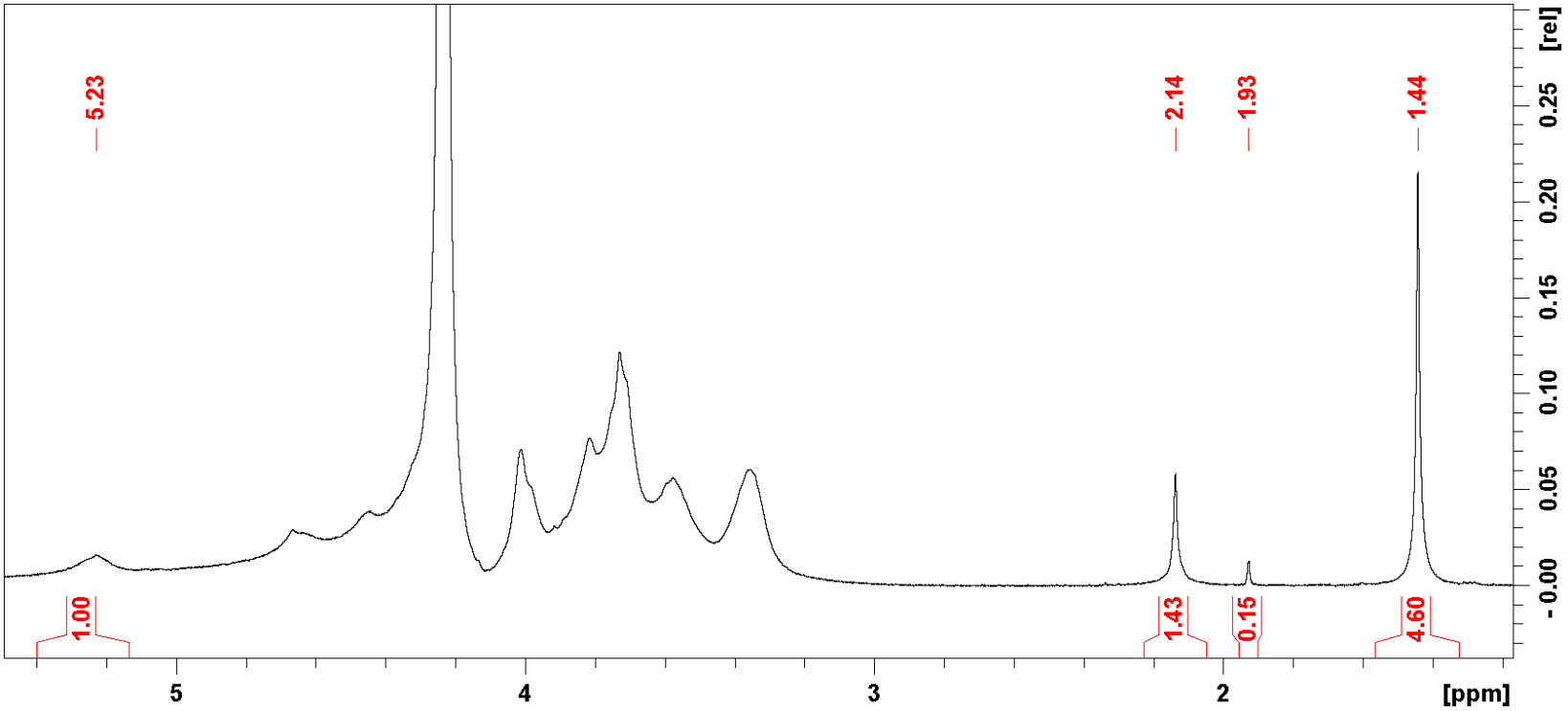

Figure F.3: ^{1}H-NMR spectrum for MX degraded with H_2O_2/NaOH for 1 hour of incubation at 80 °C followed by dialysis against MQ water. Analysed with a Bruker Avance III HD 400 MHz at 80 °C using a 5 mm SmartProbe.

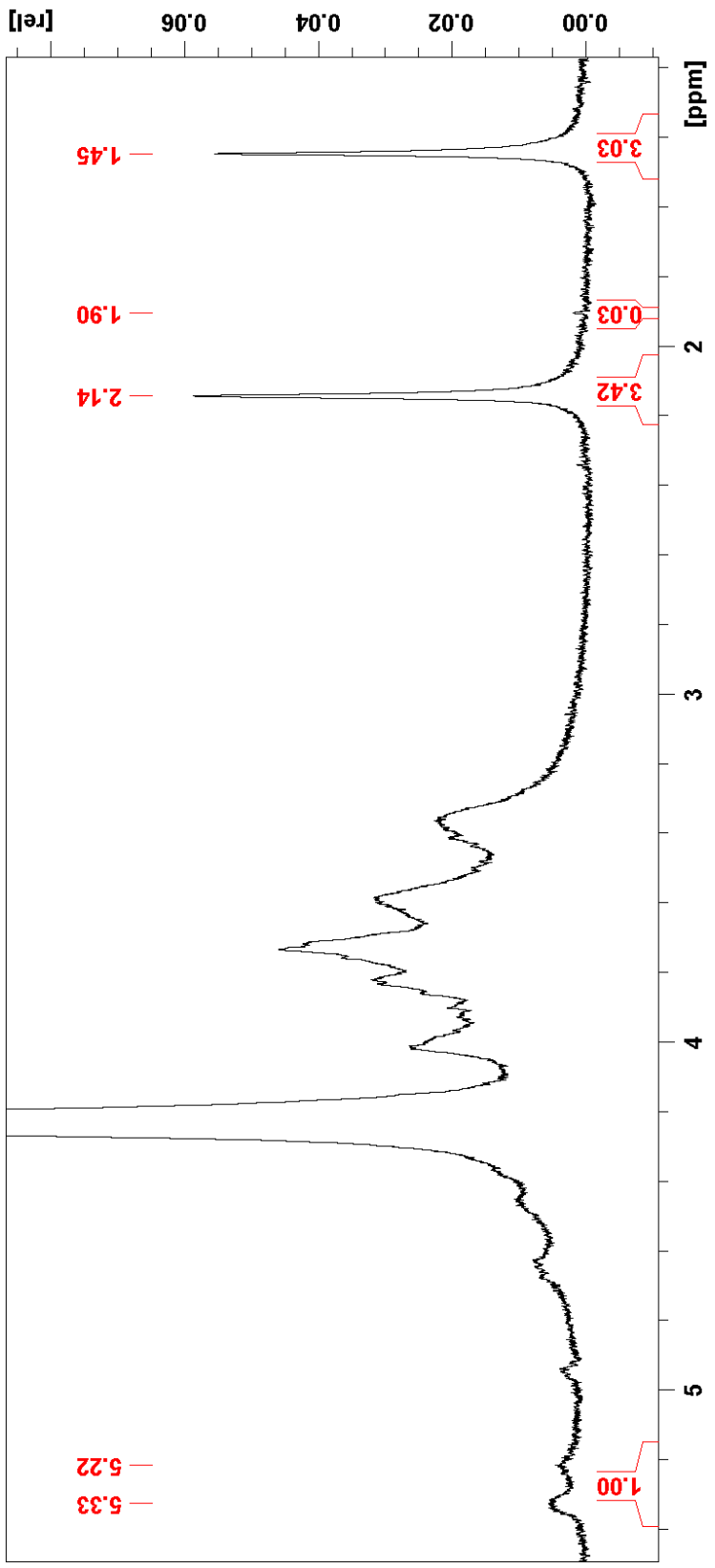

Figure F.4: ^{1}H-NMR spectrum for XCD degraded with BGI (1:1000) for 0 hours of incubation at 60 °C. Analysed with a Bruker Avance III HD 400 MHz at 80 °C using a 5 mm SmartProbe.

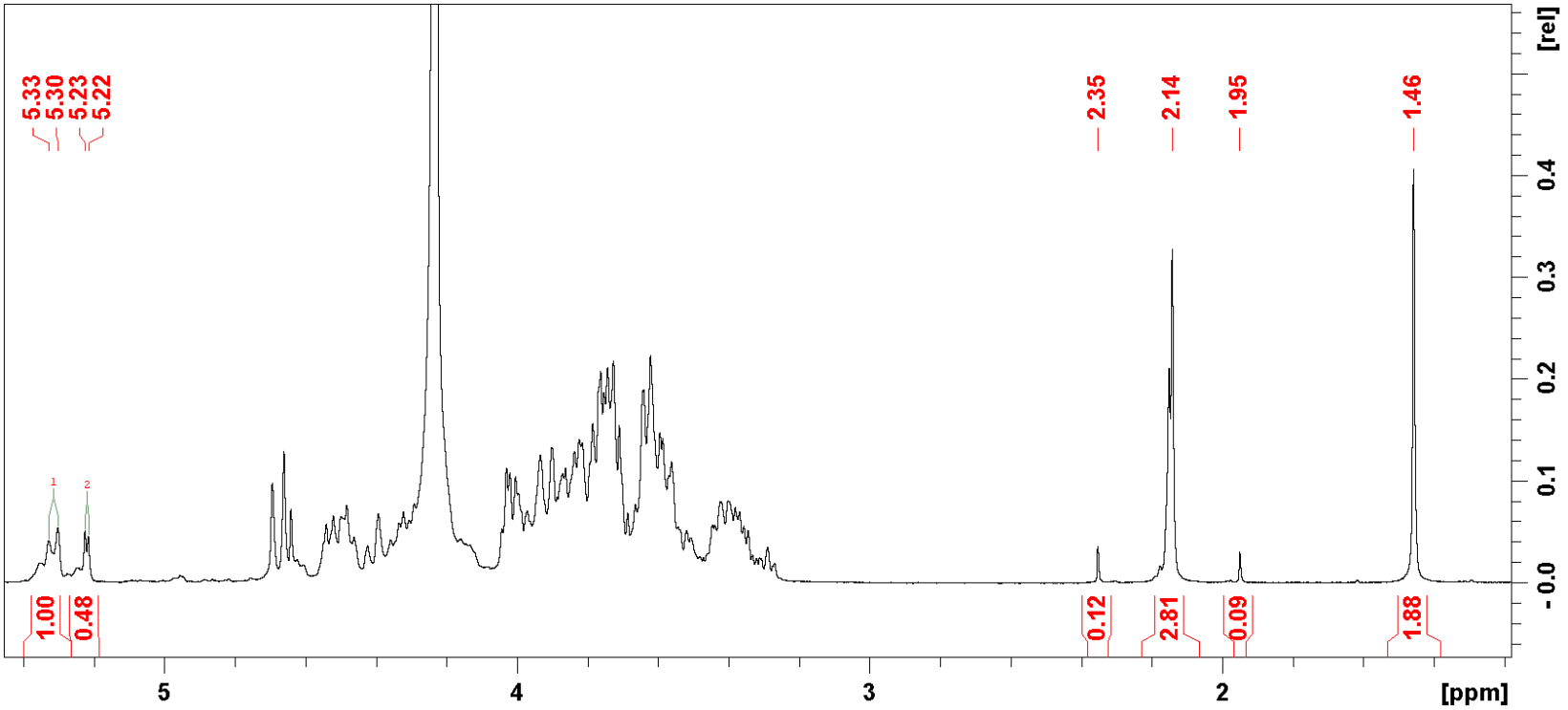

Figure F.5: ^{1}H-NMR spectrum for XCD degraded with BGI (1:1000) for 24 hours of incubation at 60 °C. Analysed with a Bruker Avance III HD 400 MHz at 80 °C using a 5 mm SmartProbe.

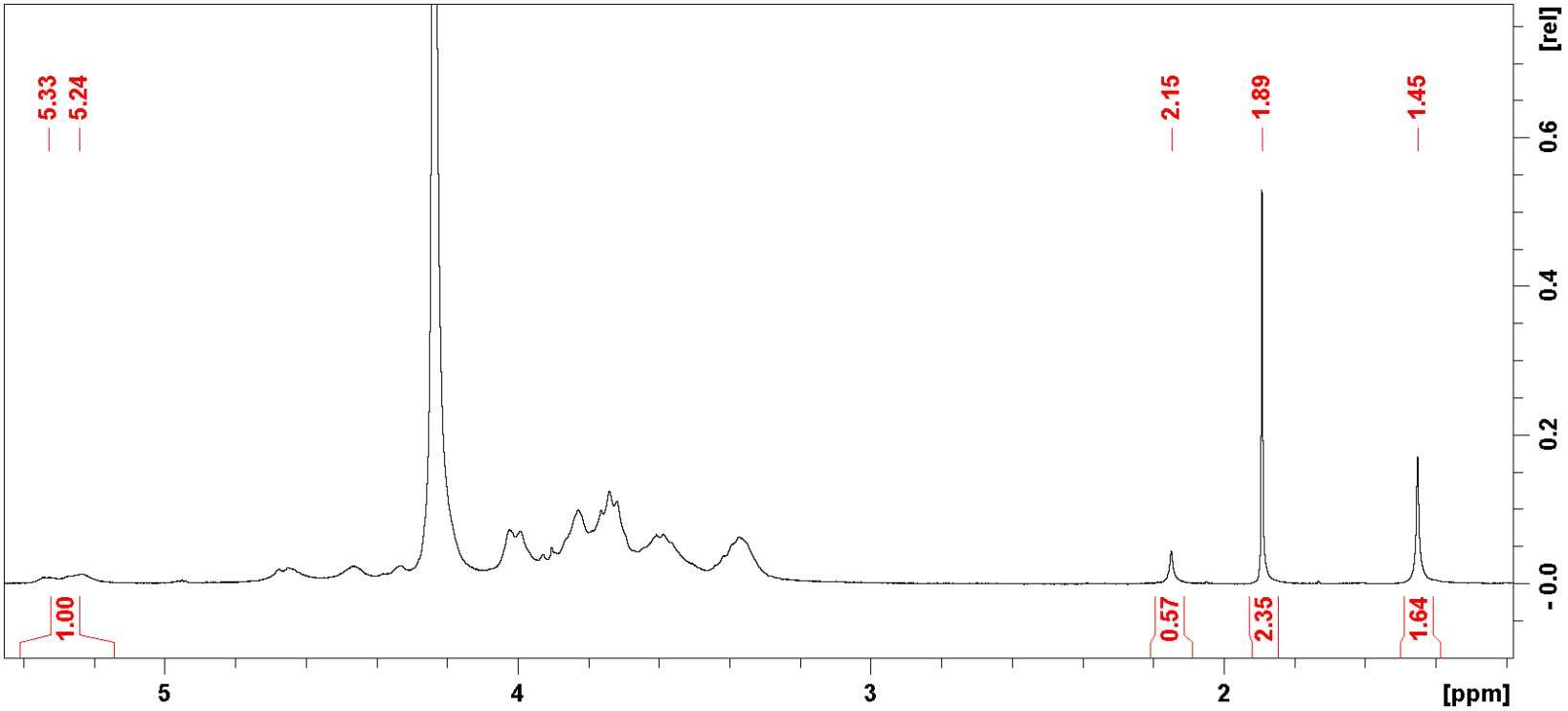

Figure F.6: ^{1}H-NMR spectrum for XCD degraded with H_2O_2/NaOH for 1 hour of incubation at 80 °C. Analysed with a Bruker Avance III HD 400 MHz at 80 °C using a 5 mm SmartProbe.

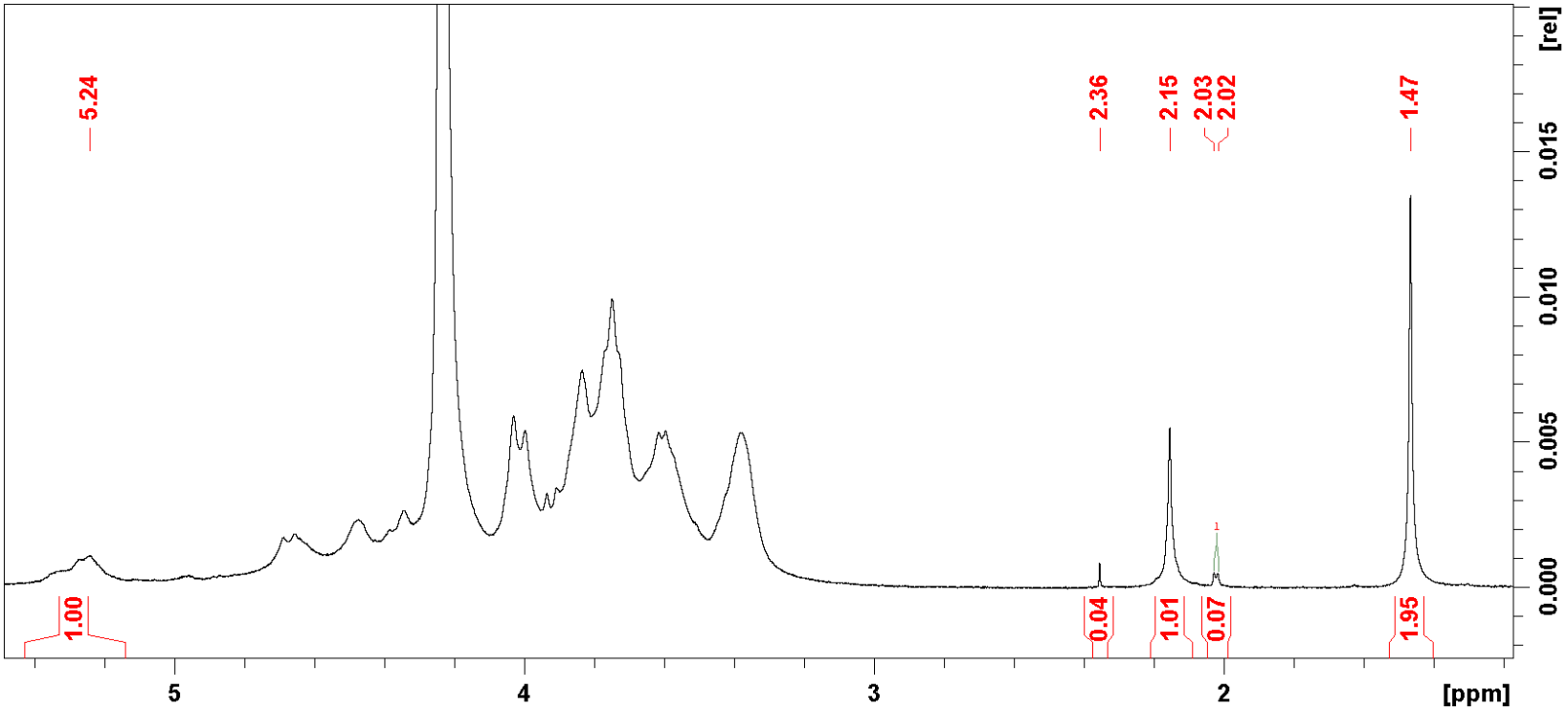

Figure F.7: ^{1}H-NMR spectrum for XCD degraded with H_2O_2/NaOH for 1 hour of incubation at 80 °C followed by dialysis against MQ water. Analysed with a Bruker Avance III HD 400 MHz at 80 °C using a 5 mm SmartProbe.

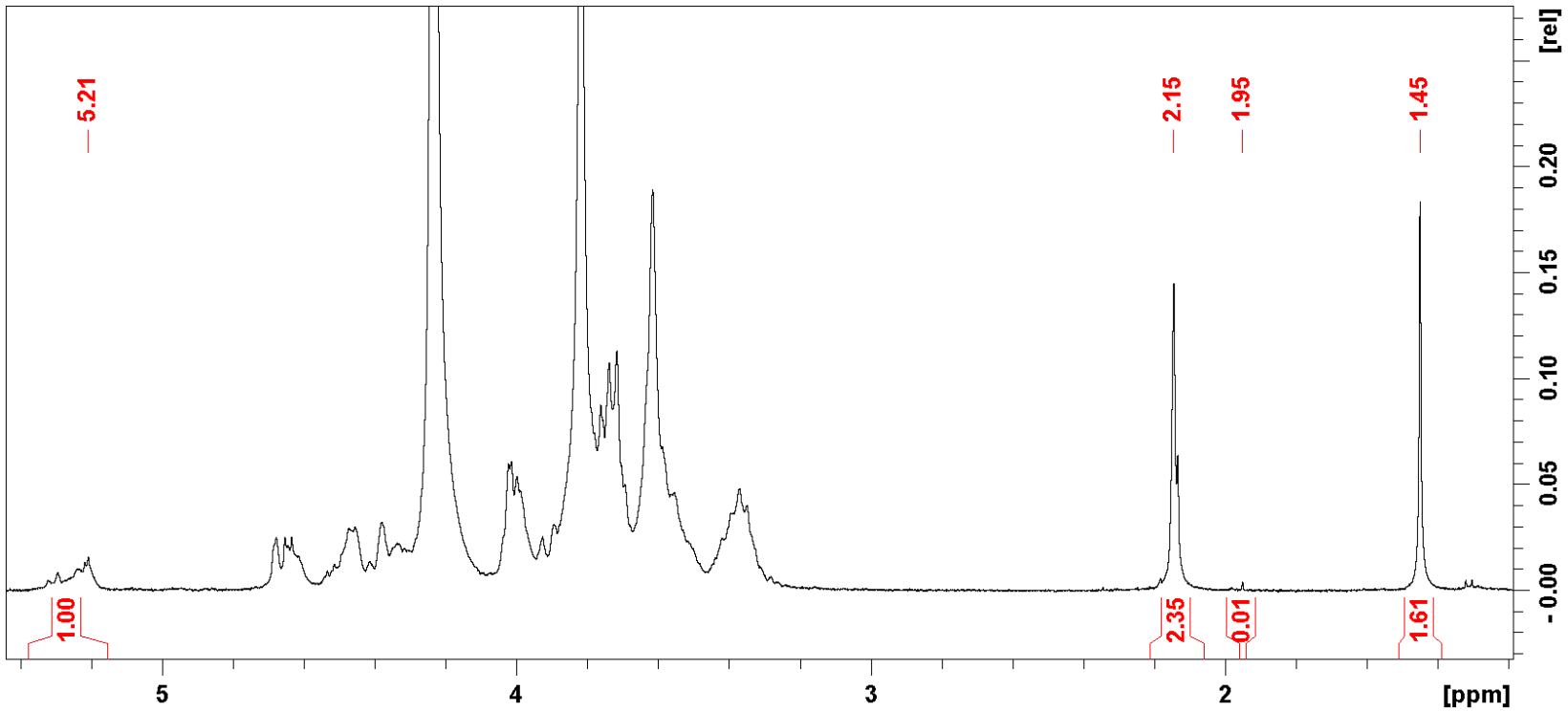

Figure F.8: ^{1}H-NMR spectrum for xan0614-3 degraded with BGI (1:100) for 0 hours of incubation at 60 °C. Analysed with a Bruker Avance III HD 400 MHz at 80 °C using a 5 mm SmartProbe.

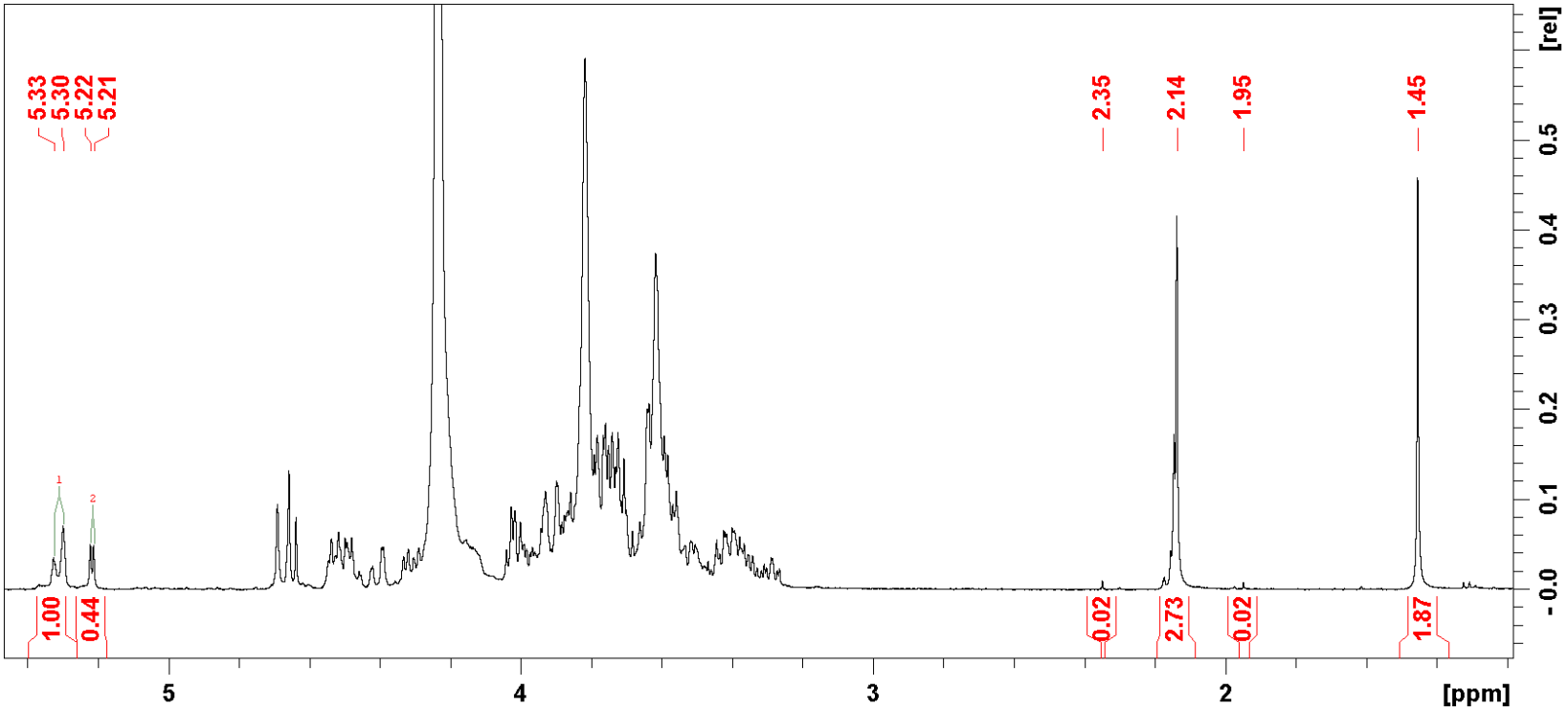

Figure F.9: ^{1}H-NMR spectrum for xan0614-3 degraded with BGI (1:100) for 24 hours of incubation at 60 °C. Analysed with a Bruker Avance III HD 400 MHz at 80 °C using a 5 mm SmartProbe.